2021

Resting-State Cerebral Perfusion Patterns: An Exploratory Factor Analysis of Single-Photon Emission Computed Tomography Clinical Data

Scott Harcourt

Resting-State Cerebral Perfusion Patterns: An Exploratory Factor Analysis of Single-Photon Emission Computed Tomography Clinical Data

by

Scott C. Harcourt

A Dissertation Presented to the
College of Psychology at Nova Southeastern University
in Partial Fulfillment of the Requirements
for the Degree of Doctor of Philosophy

NOVA SOUTHEASTERN UNIVERSITY

2021

DISSERTATION APPROVAL SHEET

This Dissertation was submitted by Scott Harcourt under the direction of the Chairperson of the Dissertation committed listed below. It was submitted to the College of Psychology and approved in partial fulfillment of the requirements for the degree of Doctor of Philosophy in Clinical Psychology at Nova Southeastern University.

Approved:

__6/22/2021_____
Date of Defense

DocuSigned by:
Charles J. Golden, Ph.D., Chair
69AB71735A914B4...

DocuSigned by:
Tom Kennedy, Ph.D.
344F7054C9544C1...
Tom Kennedy, Ph.D.

Lisa Lashley
Lisa Lashley, Ph.D.

DocuSigned by:
69AB71735A914B4...
___6/22/2021_____
Date of Final Approval

Charles J. Golden, Ph.D., Chair

Statement of Original Work

I declare the following:

I have read the Code of Student Conduct and Academic Responsibility as described in the *Student Handbook* of Nova Southeastern University. This dissertation represents my original work, except where I have acknowledged the ideas, words, or material of other authors.

Where another author's ideas have been presented in this dissertation, I have acknowledged the author's ideas by citing them in the required style.

Where another author's words have been presented in this dissertation, I have acknowledged the author's words by using appropriate quotation devices and citations in the required style.

I have obtained permission from the author or publisher—in accordance with the required guidelines—to include any copyrighted material (e.g., tables, figures, survey instruments, large portions of text) in this dissertation manuscript.

Scott Harcourt

Name

June 22, 2021

Date

Acknowledgements

I would like to thank my committee, Dr. Charles Golden, Dr. Lisa Lashley, and Dr. Tom Kennedy, for making this possible. Special thanks to Dr. Golden for suggesting the dataset, to Dr. Kennedy for his statistical checks, and to Dr. Lashley for her mentorship.

TABLE OF CONTENTS

LIST OF TABLES

LIST OF FIGURES

ABSTRACT

Resting-state (RS) networks (neural regions demonstrating a temporal correlation when a person is not engaged in deliberate activity) are a new topic in neuroscience and neuropsychology, not gaining significant traction in the literature until 2005. Few studies have used single-photon emission computed tomography (SPECT) regional cerebral blood flow (rCBF) to analyze RS. The omission is critical because SPECT RS networks have a different structure and statistical representation than functional magnetic resonance imaging (fMRI) RS networks. Moreover, recent fMRI research has explored RS differences in persons with psychopathology but have not studied brain-behavior assessment with the potential of application of neuropsychological assessment of psychopathology. SPECT may offer a cheaper, faster, and more accessible option for detecting psychopathology, increasing public access to mental healthcare, and enhancing treatment efficacy research. The principal objective of this study was to describe human RS rCBF patterns in persons with clinical neuropathologies and psychopathologies using SPECT. A robust exploratory factor analysis (EFA) of 12,217 clinical participants was implemented with techniques to increase reliability and replicability, such as parallel and bootstrapped analysis, multiple extraction and rotation comparisons, minimum covariance determinant (MCD) control for outliers, multiple imputation for missing data, and oblique rotation with higher-order factor extraction. This study reliably established eight first-order and four second-order latent constructs explanatory of 66% of the total variance in RS rCBF in 12,217 participants with clinical psychopathology and neuropathology. These factors were interpreted based on functional contributions from 67 structural regions of the brain, and informed by previous fMRI RS research. Results of

the second-order interpretation included factors of Spontaneous Cognition, Control, Visuoperception, and Homeostasis. The derived latent constructs may be used in a future confirmatory analysis of RS rCBF models, or alternately, in the design of other follow-up studies to clarify interpretation. This research supplements existing publications using fMRI that have already reliably characterized RS networks (e.g., the default mode network, salience network, and dorsal attention network.) This study is a unique and substantial supplement to the basic neuropsychological understanding of brain-behavior relationships and provides an opportunity for follow-up into RS rCBF relationships with specific pathological signs and symptoms.

CHAPTER I: STATEMENT OF THE PROBLEM

The thesis of this paper is based on the combination of four key elements: resting-state cerebral perfusion; single-photon emission computed tomography (SPECT) neuroimaging; clinical neuropsychiatric and neuropsychological pathologies; and the use of exploratory factor analytic techniques to distill these three items into interpretable patterns. In the evidence presented herein, we show why the study of resting-state perfusion is important; why SPECT is an appropriate neuroimaging technique for this task; why it is important to examine a sample that includes clinical psychopathology; and, why and how venerable statistical analysis techniques such as exploratory factor analysis are reliable in reducing unmanageable data into interpretable results.

The convergent focus of these elements is on uncovering regional blood flow patterns related to clinical psychopathology and neuropathology. Statistical analysis of at-rest relative cerebral blood flow (rCBF) in this clinical population may show patterns that are consistent throughout pathologies. SPECT imaging is an economical modality with which to demonstrate these findings. It remains a task for future researchers to determine how these common patterns across pathological outpatients relate to patterns in healthy normal brains, and how they are differentiated across unique disorders.

The necessity of this study stems from the lack of published literature on SPECT resting-state blood flow patterns in clinical samples given the potential benefits. Separately, the discrete elements of the study are well studied, but when combined, there is little published research. This paper's contribution to the state of the science is to provide a first effort at this combined approach, featuring the use of a large clinical sample. In addition, there is a clinical need: Between functional magnetic resonance

imaging (fMRI), positron emission tomography (PET), and SPECT, SPECT is the most economical to purchase, install, and operate. Demonstrating the utility of SPECT resting-state imaging in neuropsychiatric or neuropsychological outpatient clinical applications may increase healthcare access for the underserved.

Study of resting-state perfusion patterns in outpatients may also allow the identification, differentiation, and treatment outcome assessment of neuropsychiatric and neuropsychological disorders that would otherwise escape diagnostic clarity. By obtaining a mapping of the underlying latent constructs of brain perfusion in an outpatient, and then quantitatively comparing to a template garnered from many subjects of varying pathologies, a clinician could compare scores (essentially, factor scores to be obtained through subsequent empirical confirmation of results in replication studies). Then, the clinician could quantify the likelihood of inclusion in a certain class of disorders, or even classification as a specific disorder, as well as assessment of severity. This at-rest perfusion data may then be used as a baseline in assessing progress of that individual through treatment using psychopharmaceuticals, psychotherapy, transcranial magnetic stimulation, deep brain stimulation, or other modalities.

In the text, *psychopathology* refers to an emotional, behavioral, or mental health disorder, i.e. depression, anxiety, or ADHD. *Neuropathology* refers to a disorder of the central nervous system, i.e. dementia, Parkinson's disease, or epilepsy. *Neuropsychiatric disorder* is used to refer to psychopathologies arising from the central nervous system, while *neuropsychological disorder* refers to maladaptive relationships between brain and behavior, such as behavioral and cognitive changes resulting from central nervous system disease or injury. *Neurological disorder* refers to diseases of the central nervous system.

CHAPTER II: LITERATURE REVIEW

As previously stated, this study explores the convergence of four major components: neuroimaging and SPECT; regional cerebral blood flow; psychopathology and neuropathology; and exploratory factor analytic determination of latent constructs. We therefore focus our investigation into the published literature describing these areas as follows. First, we review a brief history of neuroimaging to describe why SPECT is a viable alternative to other methods and the limitations and benefits of SPECT over other methods; this is essentially a review of the experimental apparatus. Second, we review neuroanatomical structure and function as it applies to the regions under study, as this is essential to the interpretation of results since the implication is that function drives regional blood flow. Third, we review the biological underpinnings of blood flow, or how and why the functional neuronal activity in cerebral regions governs perfusion response. Fourth, we briefly review the experimental designs applicable to our project. Finally, we look at the peer-reviewed investigations supporting the above topics. We begin with a short overview of each of the study components before proceeding to in-depth reviews.

Neuroimaging: State of the Science

Overview. The advent of modern and accessible neuroimaging began with X-ray computed tomography (CT) in the 1970s, followed by positron-emission tomography (PET) and single-photon emission computed tomography (SPECT) in the late 1970s to early 1980s. Functional magnetic resonance imaging (fMRI) began clinical implementation in the 1980s and was extensively explored in the 1990s (Huettel, Song, & McCarthy, 2014). These technologies provided the ability to image structural features of the brain, measure perfusion and metabolism, and gauge cerebral activation.

In the long debate between localization and functional specialization versus global functioning and equipotentiality, these neuroimaging developments gave credence to a combined theory of specialization and functional connectivity. Functional imaging showed activation in specific anatomical regions related to a specific activity, while perfusion, metabolism, and connectivity imaging demonstrated relationships between specific activated areas that formed distributed networks. Functional connectivity, defined as the correlated activity of multiple contiguous areas of the brain during a behavior (or absence of behavior), is shown through the spatial covariance structure of neural anatomy (Bijsterbosch, Smith, & Beckmann, 2017).

Neuroimaging data management. Neuroimaging gathers data at a fundamental level of measurement of the pixel (two-dimensional) or voxel (three-dimensional), each a box or cube of cerebral tissue measuring from 1 mm to 10 mm on each side. In fMRI, a temporal dimension is added since data collection is repetitive over time (Ashby, 2015).

One statistical approach to dealing with this mass of data (with around 1.2 million voxels in the brain) is to compare each voxel to every other using direct correlations, t-tests, or analysis of variance (ANOVA), and then dealing with the sequelae of reliability problems due to family-wise error (FWE). For example, statistical parametric mapping (SPM) is a common approach that uses the general linear model (GLM) to make voxel-based statistical comparisons and random field theory (RFT) to handle the problem of multiple comparisons (Bijsterbosch, Smith, & Beckmann, 2017).

An alternative approach is to use data reduction techniques to reduce hundreds of thousands of voxels to their principal components based on their interrelatedness, then comparing the components. Principal components analysis (PCA) and modifications of it,

such as independent component analysis (ICA) or partial least squares (PLS) correlation, are frequently used for this purpose in connectivity approaches. An example is the scaled sub-profile model (SSM), which first normalizes data, and then conducts a PCA analysis, followed by assignment of factor scores to each participant on each component for comparison purposes (Ashby, 2015). This method is closest to the current study.

Clinical applications. Along with the clinical benefits offered by neuroimaging in the localization, diagnosis, and assessment of treatment outcomes, there is the unfulfilled promise of similar benefits to neuropsychiatry and neuropsychology; specifically, improvements in the differentiation, diagnosis, and assessment of the outcome of disorders (Amen et al., 2011; Camargo, 2001).

Numerous metabolic and functional activation studies have addressed human psychopathology and neuropathology using PET and fMRI (Broyd et al., 2008; Whitfield-Gabrieli & Ford, 2012; Leech & Sharpe, 2014). SPECT studies are fewer in number, partially because SPECT technology had poorer resolution than PET until recent hardware developments closed that gap (Camargo, 2001). fMRI also became more widely available as universities and teaching hospitals invested in equipment, and it became a favorite tool of researchers and grant funders. Once fMRI equipment is installed, maintenance costs are fixed, so many fMRI plants are used 24 hours a day (Huettel, Song, & McCarthy, 2014).

On the other hand, SPECT is cheaper and has other prominent advantages, which we discuss in detail below. As Camargo opined in 2001, "brain SPECT in psychiatric disorders is still investigational. Despite considerable research interest in this area, specific perfusion patterns of the various diseases have not been definitely recognized"

(p. 619.) The situation has changed little almost two decades later. By not using SPECT in neuropsychological and neuropsychiatric research, we continue to neglect a neuroimaging resource that may answer many basic research questions in a more economical manner (Amen et al., 2011; Camargo, 2001).

Furthermore, resting-state connectivity imaging has the potential to reveal commonalities between diagnostic groups. Potentially, there is an underlying neurobiological phenotype in psychopathology that explains comorbidity, overlapping symptoms, and similarities between disorders (Kaczkurkin et al., 2018). The underlying dimensionality of mental illness is a concept that is gaining momentum, with initiatives afoot to replace the current categorical approach (i.e., the Research Domain Criteria project launched in 2009 by the National Institute of Mental Health.) rCBF may be one of several biological markers that could be used in delineating such a continuum.

Resting-state patterns of connectivity. In addition to the use of SPECT in the detection, diagnosis, and assessment of neuropsychiatric and neuropsychological disorders, the role of interconnected regions of interest (ROI) has not been explored extensively using SPECT. ROI are the brain's anatomical divisions made using common brain atlases, usually based on histology and cytoarchitecture (such as the 52 Brodmann areas named by Korbinian Brodmann in 1909) and are used throughout the various neuroimaging methods. Research beginning in the mid-1990s using PET and fMRI re-discovered a concept first noted in the 1970s, now called the resting-state or DMN. Researchers identified interconnected systems of ROI that are more activated in the resting state, with limited sensory input, than under an activation task (Bijsterbosch, Smith, & Beckmann, 2017).

There are no published studies regarding the resting-state network using SPECT. This modality would serve well in such a task; within this paper, we discuss the complementary differences between the SPECT method and PET and fMRI methods. Multimethod replication and concurrent support across different modalities are fundamentals of scientific validation, which would be well served by SPECT replications of fMRI and PET observations of cerebral activations (Harris, 2001).

SPECT. Besides the lack of at-rest perfusion pattern studies in SPECT, there is also a lack of exploration into the underlying factors related to perfusion and cerebral activation in SPECT. Few studies present a factor analytic approach to PET results, and no studies do so with SPECT data. As a result, these modalities have not been fully explored for interconnected networks, as in fMRI research.

A factor analysis of SPECT perfusion data is a notorious omission from the literature. It limits the concurrent validation of PET and fMRI DMN findings using multimethod research. This multimethod analysis is essential because each imaging method has its own methodological and statistical limitations, i.e., fMRI studies of DMNs have had to accommodate large amounts of noise in the data over very short temporal intervals of less than half a second that confound results. SPECT imaging and analysis overcomes these obstacles and therefore is in the position to supplement and lend validity to fMRI findings.

Summary. The state of the science has two shortcomings. First, neuroimaging has not sufficiently addressed the identification and specification of neuropathology, including neuropsychiatric and neuropsychological disorders. Second, neuroimaging has not adequately explored the interconnectedness of isolated brain regions or the cerebral

state at rest, using perfusion imaging modalities, limiting the potential multimethod concurrence with findings in functional imaging.

In this paper, we study the second point in detail using SPECT perfusion imaging and a large clinical database consisting of persons of all pathology levels. Concerning the first point, we do not intend on differentiating pathologies with respect to their relative perfusion, as this is too broad a task for one study; this is left for future research.

Neuroimaging: General

Tomography is a method of using penetrating imaging techniques to view a slice, or cross-section, of the brain; computed tomography is the addition of computational hardware to adjust for the rotation of the imaging camera and to stack imaging slices into a three-dimensional representation (Van Heertum, Tikofsky, & Ichise, 2010). The most common imaging methods in medical use are positron-emission tomography (PET), functional magnetic resonance imaging (fMRI), and single-photon emission computed tomography (SPECT).

Early blood flow and activation research. In the 1870s, an Italian psychologist, Angelo Mosso, measured blood flow variations in head-injured patients using a plethysmograph device that translated the cerebral vasculature pulsations onto a paper roll via stylus. He showed that increased cognition and other functional changes caused related increases in local blood pulsation. Although limited to measurement in injured patients and to the area of the cortex that was exposed by the injury, the Mosso method was the first experimental measure of the neuronal activation coupling hypothesis (Sandrone et al., 2014).

In 1928, John Fulton observed variance in audible bruits (vascular murmurs) over

a patient's exposed visual cortex, dependent on the degree of visual attention and complexity of the visual task. For instance, eyes-open caused more bruit than eyes-closed, and reading produced much more bruit than the other two conditions (Raichle, 1998).

Whole-brain CBF. The first quantitative measurement of blood flow in the human brain concerning neural activity was by Kety and Schmidt in 1945. They adapted the Fick principle used to measure cardiac output, using inhaled nitrous oxide, which is not metabolized and diffuses across the blood-brain barrier quickly. Volume and concentration of the nitrous oxide mixture were measured, and cannula at the femoral arteries and jugular veins measured the input and output of nitrous concentrations in the blood. The patient inhaled the gas until equilibrium was reached, then cerebral blood flow (CBF) was calculated from the results.

CBF is typically measured in units of fluid volume per unit time per unit brain mass (ml/min/100g); the results of Katy's initial nitrous oxide methods indicated that global (whole brain) blood flow averaged 54 ml/min/100g (*SD* = 12) in 14 young, healthy males. This value has been replicated using modern techniques (Traystman, 2004; Kety & Schmidt, 1945).

Regional CBF. The first measurement of functional regional blood flow was by David Ingvar and Neils Lassen around 1965. It was made using four scintillation detectors, one each per lobe over the left hemisphere, and showed that under task (reversing digit span), the blood flow was reapportioned into the temporal lobe and to more central and post-central areas. Overall, CBF increased in the task condition. Lassen later expanded Ingvar's scintillator to 254 probes, yielding varied regional CBF (rCBF)

patterns for an assortment of tasks (Knezevic, 1988).

Neuroimaging development. Although CT was the first widely available neuroimaging modality, PET and SPECT have also been available to researchers for about the same period. MRI was a later development. All methodologies are currently widely used clinically and in research, and each has its strong and weak points. Following are brief descriptions to inform the subsequent discussion of the imaging literature.

CT. X-ray computed tomography was modified from the existing x-ray technology of a basic, fixed, wide-focus image to a rotating x-ray emitter in 1973 by Godfrey Hounsfield. CT focuses a narrow beam to image the brain in cross-sectional slices processed through tomography to produce a three-dimensional brain image that is generally limited to structural findings in black and white. CT also is used to perform in vivo radiography using radiopharmaceuticals, which was the genesis of PET; intravenously injected contrast agents emphasize tissues or blood vessels of interest in a process referred to CT with contrast or fluoroscopy. CT fluoroscopic agents that cross the blood-brain barrier are used in accentuating vasculature in neoplasms or cerebrovascular disorders (Lusic & Grinstaff, 2014; van Heertum, Tikofsky, & Ichise, 2010).

PET. In PET, a radiopharmaceutical is swallowed, injected, or inhaled, absorbed by tissue in relation to cellular metabolic rate; emitted positrons then annihilate electrons in the tissue, releasing two photons; gamma waves from the energy release of the tissues are then photographed. PET can be used to measure metabolic change using glucose or blood flow change using radiopharmaceutical oxygen. The underlying principle is that neuronal activity is coupled to local blood flow changes. Use of radiotracers such as oxygen-15, absorbed like water, yields rCBF with a spatial resolution of 8 mm and a

temporal resolution of 2 min; fluorodeoxyglucose labeled with fluorine-18, absorbed as glucose, gives regional glucose metabolism rate with a 4 mm/30 min resolution (van Heertum, Tikofsky, & Ichise, 2010).

MRI. MRI is based on the underlying behavior of protons of hydrogen atoms in an induced magnetic field and derives from Felix Block and Edward Purcell's work in 1946 and Paul Lauterbur in 1973. MRI was initially used only for anatomical imaging until Ogawa adapted it to detect in vivo changes in oxygen content of the blood caused by disturbances in the magnetic field due to net oxygen content of hemoglobin. Next, the recognition that neuronal activity was tied to changes in the oxygenation of blood localized to the neurons was applied to create fMRI (Raichle, 1998).

fMRI. A form of MRI known as fMRI-BOLD (or T2*) measures the blood-oxygen-level-dependent contrast hemodynamic response due to neuronal activation coupling. The coupling response is triggered by increased cellular activity; the response signals for an increase in blood flow and vasodilation to bring additional glucose as fuel for the neurons and oxygen for oxidation of that fuel. A small amount of oxygen is depleted as it is oxidized, and the MRI measures this reduction in oxygen concentration carried by hemoglobin within the blood vessel (Raichle, 1998).

In fMRI BOLD, the measured magnetization is from the used and deoxygenated hemoglobin. The actual blood flow increase is larger than necessary, and there is a net overshoot of blood flow during activation (Raichle, 1998).

Unique properties of fMRI over PET and SPECT are temporal repetition, noise, and brevity of the image capture period. fMRI scans can record neural events as brief as 50 ms in length, but the hemodynamic response to the event may take 6-10 s to appear,

giving poor temporal resolution and making real-time data collection impossible. Typical scan slices or repetitions are at 2 s intervals (Lindquist, 2008).

fMRI is highly sensitive to movement, respiration, and heartbeat, which cause distortion. MR signal fluctuation due to electrons' thermal motion creates random noise; the more powerful the scanner, the greater the noise. Calibration drift over time is typical. Also, the proportion of deoxygenated hemoglobin to the rest of the brain mass is tiny, and the fMRI signal very weak. The challenge with fMRI is to statistically differentiate the signal from the noise, while with PET and SPECT, the issue is to prevent a strong signal from attenuating due to tissue and bone or decaying over time (Lindquist, 2008).

CASL. Continuous arterial spin labeling (CASL) MRI is a specialized form of magnetic resonance used to measure rCBF. CASL traces arterial blood water content by applying a magnetic label. Due to the low signal-to-noise ratios and poor sensitivity, CASL has a limited clinical role but is used in research (Hermes et al., 2007).

SPECT. SPECT imaging begins with injection (typically through an intravenous port) of a radioisotope such as technetium-99m (T-99m) or Xenon-133 (Xe-133), which is bound to a radiotracer such as hexamethyl propylene amine oxime (HMPAO) or ethylcysteinate dimer (ECD). This injection occurs at the time of clinical or experimental interest; in the case of cerebral SPECT, two conditions are typically imaged: at-rest (baseline) and activation (under task). These injections are typically made on separate days to avoid contamination due to residual tracer (van Heertum, Tikofsky, & Ichise, 2010).

Radioisotopes. Xenon-133 is preferred as a tracer in quantitative measurements of absolute CBF but has a short 5 min window of acquisition and is a gas that must be

inhaled (Catafau, 2001). The radioisotope T-99m is not metabolized in the brain; when combined with the appropriate radiotracer ligand, the tracer remains pure and stable, has standard and reliable dosing, does not interfere with the thyroid, and issues low radioactivity of less than 1 rad (van Dyck et al., 1996). T-99m has a half-life of 6 hr, so there would be 50% of pure radioisotope remaining after 6 hr, 25% after 12 hr, and so on. To increase shelf life, the isotope is shipped as molybdenum-99, which decays into T-99 and has a half-life of 66 hr. Thus, using a so-called generator package supplies radiotracer for up to a week or more (at nine days, there would be 10% of the molybdenum left after decay). The concentration of tracer loading to the brain tissue is dependent on the gradient between the arterial supply concentration and the tissue concentration and the perfusion of blood (Devous, 2005).

Radiotracers. ECD and HMPAO have different absorption mechanisms, and the choice of radiotracer is dependent on the clinical question (Asenbaum, Brucke, Pirker, Pietrzyk, & Podreka, 1998). HMPAO is lipophilic (dissolved by fats), and about 2-4% of the injected radioligand crosses the blood-brain barrier. Uptake peaks within 2 min from injection, and the ligand becomes hydrophilic, binding with glutathione in the tissue, making travel back across the blood-brain barrier impossible, and locking in a stable concentration of radiotracer in the brain tissue for up to six hours. Distribution of HMPAO is mainly to the gray matter at about 3:1 versus white matter (Catafau, 2001; Bushnell, Eastman, & Barnes, 1991).

Because of the 2 min injection-to-peak time for T-99m-HMPAO, the radioligand can be injected during an at-rest state or while under task without interruption or knowledge of the experimental participant (when performed with an intravenous

catheter). Because of a 40 min to 6 hr window for imaging (90 min is optimal), the participant can then be taken to the SPECT equipment at leisure (van Heertum, Tikofsky, & Ichise, 2010). This allows standard experimental apparatus to be used, such as computers and dimmed quiet rooms; this is not possible with fMRI, which is noisy, cold, and prevents the use of magnetic metals. Even PET requires that the experimental protocol occurs within the imaging equipment. Also, both PET and fMRI require that no movement take place during the experimental protocol. Thus, the use of SPECT has a distinct advantage in at-rest versus activation task experimental protocols.

After injection, the tracer quickly crosses the blood-brain barrier and is distributed to tissue in proportion to neural activity. The relatively stable nature of T-99m/HMPAO allows for imaging to take place optimally 90 min after injection, but the available imaging interval ranges from 40 min to 6 hr, much longer than PET. Evidence shows that the distribution of T-99m/HMPAO is linearly related to rCBF (although there is a mild underestimation of rCBF at flows above 80 ml/min/100g that is compensated for in numerical processing; Payne, Trivedi, & Devous, 1996).

Collimation. Photons are emitted from the cerebral tissue in all directions as the tracer decays and are detected by gamma camera(s). A collimator establishes the incident angle of the emitted radiation as the camera collects it, and this data is used to reconstruct the three-dimensional distribution of radiotracer in tissue. The collimator is a constriction that allows only single photons traveling specific trajectories to pass through, at times selecting just 1 of every 10,000 photons (Van Audenhaege et al., 2015). Increasing aperture increases sensitivity at the cost of resolution; limiting the aperture improves resolution but decreases sensitivity. PET systems do not use collimation and exhibit two

to three times better sensitivity (Rahmim & Zaidi, 2008).

Camera. Modern clinical brain SPECT systems are multi-head gamma-camera-based, with a typical array consisting of three cameras at 120-degree intervals around the head. The cameras revolve around the head in a circular motion, taking images at 3-degree intervals for 120 projections for a 128x128 matrix size (Jung et al., 2009). Axial, sagittal, or coronal views are computed tomographically.

Resolution. Although SPECT gives poorer resolution than PET or fMRI, modern equipment can yield from 4 mm-6 mm resolution (at a 128x128 mm acquisition matrix) with a 20-30 s temporal resolution when using ultra-high-resolution fan-beam collimation (by comparison, fMRI resolution can be as low as 2 mm). About 30 min or more may be required to image a complete data package of 120 projections, but this can be reduced to 3-5 min for specific imaging questions and targets and when using multiple cameras. The latest technology (silicon photomultipliers, cadmium zinc telluride detectors, multiple-pinhole collimators, and multiplexed collimator data) allows for resolution under 1 mm (Van Audenhaege et al., 2015). Furthermore, simultaneous SPECT and MRI is a recent development that improves data collection possibilities.

Processing. SPECT imaging can be viewed graphically as reconstructed three-dimensional images with color-coding to indicate hypoperfusion (blue shades) or hyperperfusion (red shades). However, for research purposes, such as exploring the differentiation of psychiatric disorders, differences in perfusion may be subtle; they are better detected using quantitative perfusion data. Quantitative data is then processed and normalized such that it no longer represents a dimensional quantity but instead a relative magnitude (Catafau, 2001).

Utility. The prevalent uses of SPECT in clinical neurological diagnostic imaging are to detect and monitor cerebrovascular disease, dementia, epileptic foci, traumatic brain injury, inflammatory disorders, movement disorders, and assessment of brain death. Perfusion imaging may show functional impairment before there is evidence of structural impairment on MRI or CT; however, since pathological perfusion patterns may appear similar on imaging, specificity is sometimes lacking (Catafau, 2001). There is also limited use in psychiatric practice for diagnosis and treatment (Amen et al., 2011; Camargo, 2001). SPECT is often used in conjunction with other imaging to attempt to corroborate multimodal findings. SPECT is subject to detrimental effects from sedatives administered before scanning (Jung et al., 2009).

Neuroimaging methods comparison. SPECT is competitive with PET and fMRI imaging because of available near-equivalent resolution at a much lower price (Devous, 2005). SPECT equipment can be obtained at lower cost ($95,000 refurbished, $400,000 new), up to one-fifth that of PET (around $300,000 refurbished, $2 million new), and radiotracers used in SPECT have viability for up to 9 days. On the other hand, PET often requires a cyclotron nearby or on site to manufacture the tracers that have half-lives of only seconds to hours (Amen et al., 2011). PET radioligands may also take longer to settle into target tissue than SPECT ligands. A SPECT scan can take place in just 20-30 min (Devous, 2005).

fMRI, in comparison to SPECT and PET, is expensive, especially for higher-powered 7-Tesla scanners. According to sales specialist Block Imaging (www.blockimaging.com), a basic 3 Tesla scanner starts at $400,000 refurbished and $2.2 million new, exclusive of additional coils, magnetically neutral experimental stimuli,

real estate, shielding, and safety protocols. MRI requires ample dedicated space with safety precautions due to magnetic fields, low signal-to-noise ratio, and produces temporal samples that are much shorter than those needed for some imaging questions. Rental time for research begins at $550 per hour.

Perhaps most concerning with MRI is that persons with pacemakers, pins, rods, and plates may not be eligible for scanning due to magnetic interference. Cases are reported of unconscious hospital patients who were CT-scanned before MRI and found to have unknown or undeclared bullet fragments or metal shavings that could have been fatal in a scanner. MRI scanner magnets are always on; people have died in magnetic intrusion accidents and oxygen deprivation due to chemicals used in automated maintenance of the units. The MRI tunnel is much longer than that of SPECT, inducing claustrophobia; magnets are very loud; and scan times are 2-3 times the SPECT length (van Heertum, Tikofsky, & Ichise, 2010).

fMRI has the advantage of no radiotracer usage and related risk, and repeated measures can be conducted without concern for residual half-life. On the other hand, repeated measures are standard in fMRI due to the need to isolate and eliminate the high amount of noise using statistical methods; methods with better signal-to-noise ratios do not demand replication trials. Fast scan times reduce movement artifacts easier than in PET or SPECT (van Heertum, Tikofsky, & Ichise, 2010).

Safety. Beyond the specific precautions necessary in using fMRI magnets previously discussed, patient safety for radiation exposure is a factor in imaging with Xray, CT, PET, and SPECT, as well as MRI when contrasting agents are used. Although the perceived risk is low, radiologists act on the principle of least exposure possible to

complete the task and weigh the value of results versus exposure risk. The average person receives just over three milliSieverts (mSv) annually in ionizing radiation from background sources such as the sun and radon, exclusive of medical radiation. Diagnostic x-rays range from .01 mSv for a skull x-ray to 1.2 mSv for an abdominal scan. An entire procedure for a head CT is about 2.0 mSv, and 10.0 mSv for an abdominal CT set of scans (American Nuclear Society, http://www.ans.org/pi/resources/dosechart/; Health Physics Society, http://hps.org/documents/meddiagimaging.pdf).

In comparison, PET brain scans (O-water) average 1.0 mSv, while SPECT-TC-99-HMPAO brain scans average 6.9 mSv. Specialized contrast scans with gallium-67 for neoplasms may have an effective exposure of 18.5 mSv. A radiology professional is limited to 50 mSv annual exposure (but seldom receives it; American Nuclear Society, http://www.ans.org/pi/resources/dosechart/; Health Physics Society, http://hps.org/documents/meddiagimaging.pdf).

While a single SPECT procedure is double the average annual background exposure, there is little empirical knowledge of the lifetime effects of net radiation exposure. Due to poorly characterized risks, elective exposure is avoided in pregnant women and children. However, the decision is less clear in the instance of neuropathology and psychopathology: if other methods of diagnosis are not available or accessible, the risk of undiagnosed disorders may well outweigh the risk of lifetime radiation exposure.

Relevant Neuroanatomical Descriptions

To interpret the meaning of patterns of rCBF, it is first necessary to have a brief understanding of the anatomical and functional regions of the brain. The primary

structural groups for our purposes are the limbic system and basal ganglia (together referred to as subcortical systems), and the cerebellum, frontal lobe, temporal lobe, motor-sensory area, parietal lobe, and occipital lobe; the current analysis does not address the brainstem area. Below is a topical description of component parts, afferents and efferents, and function, as needed to evaluate interconnectivity in resting-state rCBF.

Limbic system. The limbic system is in the subcortical region extending from the neocortex to the diencephalon (thalamus and hypothalamus). It is ambiguously defined in the literature, with components variously assigned to the frontal lobe, temporal lobe, or basal ganglia, but for our purposes, it includes the amygdala, parahippocampal gyrus and hippocampal formation, and anterior, middle, and posterior cingulate gyri (Table 1; Carpenter, 1985).

Amygdala. The bilateral amygdala and related nuclei (basolateral, corticomedial, and central) are forward and above the hippocampus and the lateral ventricle anterior horn in the temporal lobe. They are connected to the tails of the caudate nuclei. They are often considered to be part of the mesial temporal lobe, along with the hippocampi (Haines, 1995).

Efferents include the stria terminalis to the septal region, the nucleus of the stria terminalis, and the contralateral amygdala; and the ventral amygdalofugal pathway to the entorhinal cortex and hippocampus proximally, and to the cerebral cortex, brainstem, and mediodorsal thalamus, distally. Afferent fibers include sensory inputs from the hypothalamus, basal ganglia, septal region, brainstem autonomic centers, and travel the stria terminalis and the ventral amygdalofugal pathways, as well as through the olfactory stria and via direct connections to the temporal lobe (Blumenfeld, 2010).

Table 1

Limbic System

Region of Interest	Afferents	Efferents
Amygdala	Hypothalamus	Septal region
	Basal ganglia	Nucleus of the stria terminalis
	Septal region	Contralateral amygdala
	Brainstem	Entorhinal cortex
	Temporal lobe	Hippocampus
		Cortex
		Brainstem
		Thalamus
Parahippocampal gyrus	Septal nuclei	Septal nuclei
	Preoptic nuclei	Preoptic nuclei
	Ventral striatum	Ventral striatum
	Orbital cortex	Orbital cortex
	Anterior cingulate cortex	Anterior cingulate cortex
	Thalamus	Thalamus
	Mamillary bodies	Mamillary bodies
	Entorhinal cortex	Entorhinal cortex
Hippocampal formation	Temporal lobe	Temporal lobe
	Amygdala	Amygdala
	Orbital cortex	Orbital cortex
	Olfactory bulb	Olfactory bulb
Cingulate gyrus	Amygdala	Amygdala
	Hypothalamus	Hypothalamus
	Mesial temporal lobe	Mesial temporal lobe
	Ventral prefrontal cortex	Ventral prefrontal cortex

Parahippocampal/hippocampal formation. The hippocampal formation includes the hippocampus, dentate gyrus, entorhinal cortex, subicular cortex, and parahippocampal cortex, and lies to the medial side of the inferior horn of the lateral ventricle. The cortex of the hippocampus is three-layered, transitioning to six layers from the subiculum to the parahippocampal gyrus (Haines, 1995).

Efferents travel to and afferents from the fornix (connecting to the septal nuclei, preoptic nuclei, ventral striatum, orbital cortex, anterior cingulate cortex, thalamus, and mamillary bodies) and entorhinal cortex via the subiculum. Afferents from the hippocampus travel to the temporal lobe, amygdala, orbital cortex, and olfactory bulb. The parahippocampal gyrus has a known role in spatial memory and navigation and is linked to contextual associations. The hippocampal formation is implicated in forming new memories, especially learning and retaining verbal information and episodic memories. Patients with damaged hippocampi can sometimes maintain brief working and short-term memory but typically cannot process short-term engrams into long-term memories (Shepherd, 1994).

Cingulate gyrus. The cingulate lies in the medial temporal lobe above and following the corpus callosum curve and is also known as the limbic cortex. The anterior cingulate cortex (ACC) has extensive afferent and efferent connections to the amygdala and hypothalamus and is believed to help regulate affect, the association of emotions with internal and external stimuli, and the verbalization of desires. It is implicated in autonomic and endocrine regulation, pain perception, and selection and initiation of motor movements. The ACC may also have a role in decision-making and social behavior (Blumenfeld, 2010).

The posterior cingulate cortex (PCC) is associated with cognition and affect, recall of autobiographical and emotional memories, and is active during the absence of external stimuli. It may have a role in selective attention between internal and external events. Afferent and efferent connections are dense but not well documented. Interconnectivity with the remainder of the mesial temporal lobe and the ventromedial PFC is strong, and the PCC appears to function as a hub of cognition. It is active in the dorsal attention network, salience network, and executive control through the frontoparietal control network. Raichle (2001) noted that the PCC and precuneus have approximately 40% higher blood flow than the cerebral hemisphere average (Leech & Sharpe, 2014).

Basal ganglia. The basal ganglia (for our purposes) comprise the caudate nucleus, putamen, pallidum, thalamus, and related subcortical nuclei (Table 2). The primary and most well-studied function of these nuclei is in motor control and motor learning, but they also have executive functioning roles and are activated in conjunction with emotion and specific behavior (Carpenter, 1985; Nolte & Angevine, 2007).

Table 2

Basal Ganglia

Region of Interest	Afferents	Efferents
Caudate nucleus	Cortex	Thalamus
Putamen	Thalamus	Frontal cortex
Pallidum	Substantia nigra	
Thalamus		

Afferent information in the basal ganglia comes from the cortex, thalamus, and substantia nigra, and is input into and processed by the caudate nucleus, putamen, and

accumbens nucleus (collectively known as the striatum). Efferent information goes from the globus pallidus (interior segment) and substantia nigra pars reticulata to the thalamic ventral nuclei and then to the frontal cortex. Information is relayed within the basal ganglia by the globus pallidus external segment, the subthalamic nucleus, and the substantia nigra pars compacta. Dopamine has a crucial governing function inside the input nuclei (Blumenfeld, 2010).

The canonical model of efferent and afferent function in the basal ganglia is that cortical neuronal activation signals the striatum through the globus pallidus-internal and substantia nigra pars reticulata. Signals travel to the thalamus and then to the cortex in two parallel cortex-basal ganglia-thalamus-cortex loops. Current research, however, is expanding on this model to accommodate a more complex network, including internal loops that both inhibit and select (Lanciego, Luquin, & Abeso, 2014).

The new model proposes three functional subsystems: the motor, associative, and limbic/emotional domains. These systems contribute to attention, time estimation, implicit learning, habit formation, and reward-based behavior and emotions. For example, PET studies have shown that the nucleus accumbens is activated in tasks evoking emotional responses (Lanciego, Luquin, & Abeso, 2014).

The basal ganglia structure is multifunctional. First, the goal-directed function helps in the acquisition of novel activities through selective facilitation of PFC-striatal-pallidal activity. Second, the habit system creates habitual motor responses through reinforcement learning. Third, the switching and inhibition system stops an ongoing activity and changes to a new one through the inferior frontal cortico-subthalamic nuclei circuit (Lanciego, Luquin, & Abeso, 2014).

Cerebellum and cerebellar vermis. The cerebellum's surface comprises a gray matter cerebellar cortex with underlying white matter medullary substance and four embedded subcortical pairs of intrinsic nuclei (Table 3).

Table 3

Cerebellum

Region of Interest	Efferents	Afferents
Cerebellar cortex	Red nuclei	Spinocerebellar tract
Cerebellar crus	Thalamus	Pontine nuclei
Cerebellar vermis	Motor cortex	Cortex
	Reticular formation	
	Pons	
	Vestibular nucleus	

The cerebellar hemispheres are overlaid in the center by the cerebellar vermis. Three cerebellar peduncle pairs connect the cerebellum to the pons, spinal cord, brain stem, and upper neural areas. The peduncle's anterior is known as the crus cerebri, and contains motor tracts traveling from the thalamus to the pons and spine (Carpenter, 1985; Nolte & Angevine, 2007).

Afferents. Afferent input enters the cerebellar cortex via the inferior and middle peduncles. In the cortex, the myelinated axons transform into unmyelinated mossy fibers and climbing fibers. Afferent fibers outnumber efferents in a 40:1 ratio (Carpenter, 1985). Fibers synapse through direct connections by climbing fibers or through a mossy fiber-granular cell-parallel fiber relay to the Purkinje cell in the cerebellar cortex. Additional fibers from the locus coeruleus and raphe nucleus innervate the cerebellar cortex, importing excitatory norepinephrine and serotonin. Golgi, stellate, and basket

interneurons support other neurons and exert an inhibitory effect within the cortex. The Purkinje cells, in turn, generate GABA-induced inhibitory efferents into the deep cerebellar nuclei (Haines, 1995). In addition to the Purkinje projections, there is also extracerebellar excitatory afferent input into the deep cerebellar nuclei. The deep cerebral nuclei then generate excitatory efferent signals (Haines, 1995).

Efferents. The bulk of deep cerebellar nuclei efferents exit the dentate, emboliform, and globose nuclei, travel through the superior peduncle, and into the upper pons and tegmentum, then on to the contralateral red nuclei, thalamus, and ventrolateral and ventral posterolateral thalamic nuclei. These project into the motor cortex, then relay to the corticospinal tract to coordinate somatic motor function (Haines, 1995; Carpenter, 1985). Efferents from the deep cerebellum fastigial nucleus travel via the uncinate fasciculus to the contralateral pons, lateral vestibular nucleus, reticular formation, ipsilateral juxtarestiform body, and vestibular nuclei. Inhibitory cerebellar vermis and flocculus efferents connect to the vestibular nucleus (Haines, 1995).

Pathways. The cerebellar efferents' seat is the deep cerebellar nuclei that communicate with the rest of the central nervous system. There are three afferent/efferent pathways from the deep nuclei: the spino-cerebellar, the vestibulo-cerebellar (which is located primarily outside the cerebellum), and the cerebro-cerebellar (Haines, 1995).

In the spino-cerebellar pathway, the fastigial nucleus receives afferent vestibular, proximal somatosensory, auditory, and visual information from the spinocerebellar tract, then projects to the reticular formation, vestibular nuclei, and contralaterally to the medial descending tracts. The interposed nuclei (emboliform nucleus and globose nucleus) receive spinal data and proximal somatosensory, auditory, and visual information.

Interposed nuclei efferents include contralateral projections into the red nucleus at the rubrospinal tract that project via the lateral descending tracts (Shepherd, 1994).

In the cerebral-cerebellum pathway, afferent information travels from the ipsilateral cerebral cortex to the pontine nuclei and then onto the dentate nucleus. Efferent data is projected to the contralateral red nucleus and then to the ventrolateral thalamic nucleus (Shepherd, 1994).

Function. The cerebellum contains about half of the brain's neurons and has classic balance and equilibrium regulation, regulation of muscle tone, and sensorimotor movement coordination. The cerebellum is a higher-level motor system that primarily drives other lower motor systems, as it has no direct connection to the spinal cord. The vermis, vestibular nuclei, and flocculonodular lobes control proximal and trunk muscles and vestibular-ocular control. The interposed nuclei control distal extremity muscles. The dentate nuclei coordinate extremity motor programming. All function is ultimately ipsilateral since all motor pathways from the cerebellum are either direct or double-crossed (Blumenfeld, 2010). The function of the inferior olive of the medulla bidirectional connection to the cerebellar nuclei is not fully understood but may function as a master RAS clock producing and regulating a timing sequence or oscillatory signal for the rest of the brain.

Cerebellar neurons exhibit plasticity and the ability to maintain states of long-term potentiation and depression, indicating that the cerebellum has a learning function that is not well-explored (Shepherd, 1994). PET studies have indicated that lateral cerebellar activity increases during the naming of functional words (*dig*, *fly*) versus object words (*shovel*, *airplane*; Blumenfeld, 2010). Lesion studies have indicated a cerebellar

role in attention, processing speed, and visuospatial processing, although whether the cerebellum is the processing center, or a relay, is unknown (Blumenfeld, 2010).

Feed-forward design. The cerebellum uses a feed-forward system, unlike most other brain functions. It collects proprioceptive, sensory, and perceptual data in advance of action to calculate the best approximation of potential motoric responses and their possible results; it is predictive rather than reactive. The cerebellum appears to maintain a trove of afferent data that is overwritten if not used (Blumenfeld, 2010; Haines, 1995). The cerebellum signals gradual muscle tension and contraction changes to maintain posture, equilibrium, and skilled voluntary movements (Blumenfeld, 2010).

Continuous neural activity. A person at rest (even under visual and auditory deprivation) collects large amounts of data in a continuous cycle of collect, store, and overwrite. The exclusive inhibitory output of the cerebellar Purkinje cells presents a 'button-down' mode of operation, with an inhibitory signal always present and preventing an action unless a command releases the 'button.' In the at-rest state, the cerebellum is continuously collecting information, even while not maintaining equilibrium or movement control (Haines, 1995). The cerebellar cortex exerts inhibitive control on lower motor circuits based on regulation from the PFC and basal ganglia, while automatic cerebellar systems maintain equilibrium, balance, and sensory data collection for the ongoing feed-forward analysis (Carpenter, 1985).

Frontal lobes. The frontal lobes include the discrete regions of the olfactory cortex on the ventral surface; the superior, middle, and inferior frontal gyri, from rostral to caudal on the dorsal medial to the lateral; gyrus rectus; supplementary motor area, precentral gyrus, and the paracentral lobule (Table 4; Shepherd, 1994).

Table 4

Frontal Lobes

Region of Interest	Efferents	Afferents
Olfactory cortex	Hippocampus/Parahippocampal	Hippocampus/Parahippocampal
Frontal gyri: superior, mid, inferior	Amygdala	Amygdala
Gyrus rectus	Cingulate gyrus	Cingulate gyrus
Supplementary motor area	Thalamus	Thalamus
Precentral gyrus	Basal ganglia	Basal ganglia
Paracentral lobule	Hypothalamus	Hypothalamus
	Septal region	Septal region
	Subthalamic region	Subthalamic region
	Cerebellum	Cerebellum
	Midbrain	Midbrain

The prominent feature of the frontal lobe is the PFC or frontal heteromodal association cortex, with bidirectional cortical and subcortical connections to and from the sensory and motor unimodal association cortices for auditory, visual, motor, and sensory as well as the limbic cortex. The interconnectivity is indicative of the role of the PFC as the highest-order system in the brain, controlling and regulating lower-order systems. Emotional and motivational input from the limbic cortex mediates and moderates sensorimotor input from the motor and somatosensory cortices. Input from hearing, vision, and language modify planning and programming of actions in a feed-forward (using already collected sensory data) and a feedback design (using data collected after actions have started; Carpenter, 1985; Nolte & Angevine, 2007).

Topography. The frontal lobes include the area posterior to the PFC, forward of the central sulcus, and above the Sylvian fissure. The posterior frontal lobe includes

(lateral to medial) Broca's area (dominant hemisphere), the primary and premotor cortices and the frontal eye fields, and the supplementary motor area. The medial surfaces include the anterior cingulate gyrus and the posteromedial orbitofrontal cortex. The orbitofrontal olfactory area appears on the posterior ventral aspect of the lobes (Haines, 1995).

The inferior frontal gyrus (Broca's area) occupies the lower frontal lateral part of the frontal lobe, just below the middle frontal gyrus. The middle frontal gyrus contains the supplementary motor area on its posterior end. The superior frontal gyrus extends from the PFC pole back to the precentral gyrus at the motor strip. The gyrus rectus lies on the frontal lobe inferior medial surface, above the eye orbits forward of the optic chiasm. The paracentral lobule on the medial surface spans from the frontal lobe to the parietal lobe and is the medial terminus of the motor and sensory strips (Nolte & Angevine, 2007).

Connections. The subcortical uncinate fasciculus connects the amygdala region and limbic system to the orbital and medial PFC. Dense projections also issue from the PFC to the mediodorsal thalamic nucleus, medial pulvinar, and interlaminar nuclei. Projections also issue from the caudate head to the basal ganglia and from the PFC to the hypothalamus, septal region, subthalamic region, cerebellum, and midbrain. Primary neurotransmitter modulation occurs through connections from the brainstem and subcortical areas that provide dopamine, acetylcholine, serotonin, norepinephrine, orexin, and histamine (Blumenfeld, 2010).

Functions. The frontal lobes are implicated either before, during, or after most behaviors regardless of where the behavior is initiated. Functions unique to the human frontal lobes include restraint (including judgment, foresight, perseverance, delayed

gratification, inhibition, self-governance, and concentration); initiative (including curiosity, spontaneity, motivation, drive, creativity, cognitive set, mental flexibility, and personality); and order (abstract reasoning, working memory, perspective, planning, insight, organization, sequencing, and temporal order; Blumenfeld, 2010).

The dorsolateral PFC is implicated in working memory (the ability to maintain a limited amount of information in memory while performing cognitive operations upon it); the same area in conjunction with the medial temporal lobes is associated with novel learning, with some evidence that verbal learning takes place on the dominant hemisphere and nonverbal learning in the nondominant. The dorsolateral PFC is correlated with shifting of cognitive set and mental flexibility. Maintaining selective attention is also attributed to the PFC (Blumenfeld, 2010; Shepherd, 1994).

The laterality of PFC function is tentative. Some evidence supports a relationship between depression and left- and mania with right-sided lesions. Also, in about 90% of right-handers and 60-70% of left-handers, language dominance in Broca's area is in the left hemisphere, although many exceptions are known (Blumenfeld, 2010; Shepherd, 1994).

Olfactory cortex. The olfactory cortex receives input from the olfactory bulb and functions in odor discrimination, perception, memory, and habituation. The olfactory cortex connects to the orbital cortex, mediodorsal thalamic nucleus, hypothalamus, amygdala, and hippocampus (Haines, 1995).

Superior frontal gyrus. The superior frontal gyrus lies in the frontal lobe's superior and medial aspects and includes the supplementary motor area. It functions in planning complex movements (mostly contralateral, but some ipsilateral), higher

cognitive function including control and execution, working memory, spatial processing, and impulse control. The front and medial portions are implicated in DMN studies, possibly related to interconnectivity with the cingulate cortex in maintaining cognitive control. Other connections are the middle and inferior gyri, precentral gyrus, caudate, thalamus, and frontal operculum (motor circuits). The dorsal (spatial) stream of the visual pathway from the occipital lobe terminates at the superior frontal gyrus and the inferior gyrus (Haines, 1995).

Middle frontal gyrus. The middle frontal gyrus includes the frontal eye fields at its posterior end, which cross over into the precentral gyrus. It also includes the dorsolateral prefrontal cortex (DLPFC) in its midsection and the anterior prefrontal cortex (PFC) at the front (also called the frontopolar or rostral prefrontal cortex). Bidirectional connections are found with the orbitofrontal cortex, thalamus, dorsal caudate nucleus, hippocampus, and the primary and secondary association areas of the temporal, parietal, and occipital intersection. The middle gyrus is engaged in executive functioning, including working memory, memory retrieval, memory for source and context, and prospective memory; cognitive flexibility and planning; reallocation of attention and multiple task coordination or cognitive branching; motor planning and organization; inhibition; and abstract reasoning. It may also have contributory roles in deception, conflict, deductive reasoning, threat-induced anxiety, and social cognition (Shepherd, 1994).

Inferior frontal gyrus. The inferior frontal gyrus lies on the frontal lobe's lateral and inferior surfaces from the frontal pole back to the precentral gyrus. It is subdivided into the cytoarchitecturally unique pars opercularis, pars triangularis, and pars orbitalis.

It contains Broca's area, associated with expressive speech, in the opercular and triangle areas. It also functions in executive control, particularly response inhibition and attention; autobiographical memory retrieval; phonological and semantic verbal fluency; language processing and comprehension; and empathy. It has strong connections with the middle frontal gyrus. It is at the anterior end of the dorsal and ventral vision processing streams and may have a role in integration (Shepherd, 1994).

Gyrus rectus. The gyrus rectus (or straight gyrus) is a continuation of the superior frontal gyrus as it wraps around the inferior medial surface of the frontal lobe and is a part of the orbitofrontal cortex along with the orbital gyri. Its putative function is in higher cognition and possibly personality. There is not much empirical insight into function since lesions typically involve other areas of the ventromedial PFC, which typically cause alterations to emotional experience, expression, social functioning, observance of social conventions, deciding advantageously on personal matters, impulse control, inhibition, and antisocial behavior (Shepherd, 1994).

Supplementary motor area. The supplementary motor area functions in the translation of cognition into action. The area lies immediately anterior to the precentral gyrus on the frontal lobe's superior and medial aspects in the dorsomedial frontal cortex and is also considered a part of the motor-sensory area. The supplementary motor cortex resembles the PFC's cytoarchitecture in its anterior portion and the precentral gyrus's cytoarchitecture in its posterior. The supplementary area is involved in movement and action that requires prediction and outcome planning and in self-initiated actions with movement sequences, switching between actions, inhibiting actions, or novel actions (Shepherd, 1994).

Paracentral lobule. The paracentral lobule is the continuation of the precentral and postcentral gyri onto the medial surface and functions in both contralateral motor and sensory capacities for the lower limbs and excretory functions. It is also a part of the parietal lobe and the motor-sensory area (Shepherd, 1994; Blumenfeld, 2010).

Temporal Lobes. The temporal lobes are composed of the superior, middle, and inferior temporal gyri; superior and mid pole; amygdala; parahippocampal/hippocampal formation; fusiform gyrus; and Heschl's gyrus (Table 5). The amygdala, parahippocampal/hippocampal formation, and fusiform gyrus are also included for current purposes. The lateral temporal lobe holds the primary auditory cortex, and the medial structures are associated with emotion and memory (Carpenter, 1985; Nolte & Angevine, 2007; Shepherd, 1994).

Table 5

Temporal Lobes

Region of Interest	Efferents	Afferent
Temporal gyri: superior, middle, inferior	Cerebral cortex	Olfactory cortex
Temporal poles: superior & mid	Hypothalamus	Visual association cortex
Parahippocampal/hippocampal formation	Septal area	Auditory association cortex
Fusiform gyrus	Stria terminalis	Somatosensory cortex
Heschl’s gyrus	Brainstem	Thalamus
	Thalamus	Hypothalamus
	Prefrontal cortex	Amygdala

Superior temporal gyrus/ Heschl’s gyrus. The superior temporal gyrus lies on the temporal lobe's superior surface next to the lateral sulcus, covering Heschl's gyrus on the insular cortex within the opercular window. It consists of the primary auditory cortex at

the posterior end, the secondary auditory cortex, and Wernicke's (dominant hemisphere only) area. While the superior gyrus's anterior and posterior sections are involved only in speech processing, the mid-superior temporal gyrus appears to process both speech and sounds. Processing is in a complexity gradient from posterior to anterior, with simpler (phonemes) at the posterior and words and phrases in the mid-regions (Haines, 1995).

Middle/inferior temporal gyrus. The middle temporal gyrus lies on the lobe's lateral surface between the superior and inferior gyri and has a role in lexical-semantic and conceptual-semantic relationships. The superior, middle, and temporal gyri function to process language, semantic memory, visual perception, and multimodal sensory integration (Shepherd, 1994).

Fusiform gyrus. The occipitotemporal sulcus separates the inferior temporal gyrus from the fusiform gyrus, where temporal and occipital lobes meet. The fusiform gyrus plays a role in facial recognition and familiar categorical visual recognition. The inferior temporal gyrus and fusiform gyrus may also be involved in the semantic association of visual images, as lesions cause visual agnosia. Pure alexia can also result from injuries to this juncture (Shepherd, 1994).

Superior/ mid-temporal pole. The temporal pole is the lobe's anterior tip formed by the superior, middle, and inferior temporal gyri. It has numerous connections with the amygdala and the orbital PFC. Current thinking is that the pole is an association cortex for social and emotional multimodal analysis and processing. The dominant pole is associated with semantic memory, while the nondominant is linked to personal, episodic, socially relevant, and emotional memory (Blumenfeld, 2010).

Efferent/afferent connections. The hippocampus is interconnected with the

parahippocampal gyrus through the subiculum and the dentate gyrus, and from there has bidirectional pathways to the cerebral cortex. The largest efferent projection from the hippocampus is to the hypothalamus. The amygdala projects to the septal area, bed nucleus of the stria terminalis, brainstem, thalamus, hypothalamus, PFC, and other cortex. It mediates the response to emotional stimuli. Afferent connections to the amygdala come from the cerebral cortex's sensory areas (the visual, auditory, and somatosensory association cortices) and the olfactory cortex. The temporal poles take afferents from the amygdala and the thalamus medial geniculate body. The temporal gyri receive afferent information via Meyer's loop from the visual cortex through the thalamus (Kiernan, 2012).

Motor-sensory area. The motor-sensory area includes the precentral gyrus, postcentral gyrus, Rolandic operculum, paracentral lobule, and supplementary motor area (Table 6). Descriptions for the paracentral lobule are found in the frontal lobe description (Carpenter, 1985; Nolte & Angevine, 2007).

Table 6

Motor-Sensory Area

Region of Interest	Efferents	Afferents
Precentral gyrus	Basal ganglia	Thalamus
Postcentral gyrus	Thalamus	Cerebellum
Rolandic operculum	Corticospinal/corticobulbar	Sensory association cortex
Paracentral lobule	Brainstem	Basal ganglia via thalamus
Supplementary motor area		

Precentral gyrus. The precentral gyrus (also primary motor cortex or motor strip) is the central sulcus's anterior bank and the frontal lobe's posterior boundary. It contains a

somatic mapping of the human body and is the cortical substrate for motor control, and is highly dependent on descending and ascending tracts to govern movement and action. Efferent fibers from the precentral gyrus cross contralaterally to the appropriate motor nuclei in the basal ganglia, thalamus, the spine through the corticospinal tract, and the cranial nerves through the corticobulbar tract. Afferents come from the cerebral cortex (premotor and sensory areas) and the thalamus's ventrolateral nucleus. Interconnection with the neighboring supplemental motor area and premotor cortex allow management of higher-level operations. The precentral gyrus meets the postcentral gyrus at the medial paracentral lobule and lateral Rolandic operculum (Haines, 1995).

Postcentral gyrus. Also known as the sensory strip or the primary sensory cortex, the postcentral gyrus is the central sulcus's posterior bank and the anterior delineation of the parietal lobe. It contains a contralateral somatic mapping of the body and is the cortical substrate for sensory input. Afferent connections from the thalamic nuclei via the corona radiata bring sensory data (touch, temperature, and pain) from the ascending spinal and trigeminal lemniscal tracts and proprioceptive information through the cerebellum (Haines, 1995).

Rolandic operculum. The Rolandic operculum, also known as the central operculum or subcentral gyrus, is the lateral cortex where the precentral and postcentral gyri meet and separate the inferior frontal gyrus-pars opercularis from the supramarginal gyrus of the parietal lobe. The Rolandic operculum's function is not clearly defined: It is anterior to the gustatory cortex, posterior to the auditory cortex, and may influence each. An early case lesion study indicated that damage causes articulation problems (Tonkonogy & Goodglass, 1981). It was recently investigated as the substrate of bodily

self-consciousness and integrator of exteroceptive–interoceptive signals by Blefari et al. (2017).

Parietal lobes. The parietal lobe comprises the supramarginal gyrus, angular gyrus, precuneus, postcentral gyrus, paracentral lobule, and the superior and inferior parietal gyri (Table 7). The paracentral lobule and postcentral gyrus are described previously in sections devoted to the frontal lobe and motor-sensory area. It lies behind the central sulcus, above the Sylvian fissure, and anterior to the parieto-occipital sulcus. Visual processing areas surround the parietal lobe at the posterior border with the occipital cortex, in addition to auditory processing areas and somatosensory information. It includes areas for the primary and secondary sensory information processing, specification of spatial targets for the motor system, generation of attention, and visual and spatial motion analysis (Carpenter, 1985; Nolte & Angevine, 2007).

Table 7

Parietal Lobes

Region of Interest	Efferents	Afferents
Supramarginal gyrus	Primary motor cortex	Auditory association cortex
Angular gyrus	Secondary motor cortex	Visual association cortex
Precuneus	Superior temporal gyrus	Somatosensory cortex
Postcentral gyrus	Amygdala	Thalamus
Paracentral lobule	Entorhinal cortex	Brain stem
Parietal gyri: superior & inferior	Hippocampus	
	Insula	

Efferents/afferents. The parietal areas receive afferent information from the sensory cortices, ventral posterior nucleus of the thalamus, and brain stem via the thalamus. Efferents are sent to the primary and supplementary motor cortex, superior

temporal gyrus, amygdala, entorhinal cortex, hippocampus, and insula (Cavanna & Trimble, 2006).

Precuneus. The precuneus is on the posterior medial aspect of the parietal lobe. It is linked to visuospatial imagery, episodic memory retrieval, self-processing, first-person perspective-taking, and experience of agency. In resting-state studies of the DMN, the precuneus is highly active at rest, and research suggests that it has a role in self-consciousness or other self-related mental representations during rest (Cavanna & Trimble, 2006).

Supramarginal gyrus. The supramarginal gyrus is an inverted U-shaped gyrus around the posterior termination of the lateral fissure. It is involved with phonological and articulatory processing. Along with the angular gyrus, this area is tied to calculation (Haines, 1995).

Angular gyrus. The angular gyrus is located immediately posterior to the supramarginal gyrus and is involved in semantic processing with the posterior cingulate. The nondominant angular gyrus is implicated in emotional processing. The angular and supramarginal areas receive auditory, visual, and somatosensory input and process the sensory data into phonological and semantic language information (Haines, 1995).

Superior parietal gyri. This area spans from the postcentral gyrus to the inferior parietal lobule and medially to the precuneus. The superior lobule is engaged in action processes, visuomotor functions, visual perception, spatial cognition, reasoning, working memory, and attention (Wang et al., 2015).

Inferior parietal gyri. The inferior parietal gyri (lobule) are associated with maintaining attention on current goals, selectively responding to salient novel

information, and responding to environmental stimuli (Shepherd, 1994).

Occipital lobes. The occipital lobe, occupying the area behind the parietal-occipital sulcus to the occipital pole, is the smallest lobe at about 20% of the brain's total volume (Table 8). Structurally, the occipital lobe contains the calcarine cortex, cuneus, lingual gyrus, superior, middle, and inferior occipital gyri (Carpenter, 1985; Haines, 1995).

Calcarine cortex. The calcarine cortex surrounds the calcarine fissure, also called the primary visual cortex, striate cortex, or area V1. The calcarine fissure separates the cuneus above from the fusiform and lingual gyri below and contains the calcarine artery. Afferents come from the lateral geniculate nucleus of the thalamus by way of the optic radiation. Efferents go to the visual association area. The primary visual cortex is also involved in the summoning of visual mental images (Blumenfeld, 2010).

Table 8

Occipital Lobes

Region of Interest	Efferents	Afferents
Calcarine cortex	Dorsal & ventral streams:	Thalamus
Cuneus	Mesial & inferior temporal lobe	
Lingual gyrus	Parietal lobe	
Occipital gyri (superior, mid, inferior)	Frontal lobe	

Cuneus. At the medial surface of the anterior occipital lobe, the cuneus lies aft of the precuneus in the posterior parietal lobe. It processes visual information from retinotopic mappings of the visual fields. Pyramidal cells in the striate cortex project to the inferior occipital gyrus (the extrastriate cortices). Afferent information associated with attention, working memory, and rewards loads into the cuneus for mid-level visual

processing (Shepherd, 1994).

Lingual gyrus. The lingual gyrus is on the medial surface of the occipital lobe along the tentorial surface. The lingual gyrus engages in visual processing, especially letters, encoding visual memories, and logical ordering (Shepherd, 1994).

Occipital gyri. The inferior, middle, and superior occipital gyri contain extrastriate visual processing areas, also called the secondary visual cortex or visual association area (V2-V5). They receive afferent data from the calcarine cortex for processing. In some individuals, the gyri are not distinct structurally or functionally (Shepherd, 1994).

Multiple cortical modules process and analyze visual information received at the primary visual cortex in the occipital lobe from the optic nerves via the thalamus, and the information is projected via two primary streams. The dorsal (*where*) stream processes motion and spatial relationships and constitutes the spatial vision, motion, and positioning stream. It connects V1 and V2 in the primary and secondary visual cortices to V5 and the middle temporal and parietal lobes. The ventral (*what*) stream analyzes form, color, faces, and letters and governs object recognition, color perception, and higher-resolution perception. It connects the calcarine cortex (V1) to V2 and V4 in the secondary visual cortex and projects into the inferior temporal lobe (Blumenfeld, 2010; Shepherd, 1994).

Brainstem nuclei. Although not part of this experiment's data, the following areas are described with respect to the ROI variables' afferents and efferents (Carpenter, 1985; Haines, 1995; Nolte & Angevine, 2007).

Reticular nucleus. The reticular nucleus is distributed through the pons and

medulla and is part of the distributed reticular activating system (RAS) that maintains arousal and cortical tone. It is directly involved in spinal movement and control, such as in walking and standing. Afferents include the deep cerebellar nuclei and other sensory pathways; efferents are to the spinal column and the thalamic areas (Nolte & Angevine, 2007).

Vestibular nucleus. The vestibular nucleus is closely associated with the RAS, and takes afferents from the deep cerebellar nuclei and vestibular canal. The lateral vestibular nucleus generates efferent fibers that compose the vestibulospinal tract that continues down the spinal cord. It transmits extensor muscle tone control signals from the cerebellum to the limbs and is integral in standing. The medial vestibular nucleus generates fibers that travel the medial longitudinal fasciculus pathway and play a role in eye movement. The medial vestibular and inferior vestibular nuclei also send efferent information to the cerebellum (Nolte & Angevine, 2007).

Red nucleus. The red nucleus projects to the brainstem and spinal cord and has a role in limb flexion. It takes afferent information from the deep cerebellar nuclei (Nolte & Angevine, 2007).

The neural substrate of consciousness. Because of the nature of at-rest cerebral processing, awareness, arousal, and consciousness are default activities during the brain's awake state. Therefore, a discussion of consciousness's neural underpinnings provides a foundation for understanding and interpreting at-rest rCBF.

The level of consciousness is described as alertness, attention, and awareness. Essentially, all three qualities are maintained at some default level of operation in the brain's resting state (minimal sensory activity and no intentional task being executed).

These processes involve the upper brainstem, thalamus, hypothalamus, basal forebrain, medial and lateral frontoparietal association cortex, and cingulate gyrus areas, especially the areas known as the RAS (Blumenfeld, 2010).

Alertness. Specific neural substrates of alertness and wakefulness in the upper brainstem include the pedunculopontine and laterodorsal tegmental nuclei with cholinergic output, and the pontomesencephalic reticular formation with non-cholinergic (glutamatergic) output, project to the thalamus, hypothalamus, and basal forebrain. Locus coeruleus and lateral tegmental areas with noradrenergic output and dorsal and medial raphe with serotonergic output project to the cortex and other structures. The substantia nigra pars reticulata and ventral tegmental area project dopaminergic output to the striatum, limbic cortex, and PFC (Blumenfeld, 2010).

Arousal is supported by thalamic systems, including the intralaminar, midline, and ventromedial thalamic nuclei, which relay the upper brainstem neurotransmitter signals to the cerebral cortex. The thalamic reticular nucleus receives input from the cortex, thalamus, and brainstem, and in turn, sends inhibitory GABAergic signals to the thalamus and brainstem to regulate information transfer (Blumenfeld, 2010).

In the hypothalamus, arousal is supported by the orexinergic and histaminergic output of the posterior lateral hypothalamic (tuberomammillary) nucleus, as regulated by the anterior hypothalamic and brainstem inputs, and then projected to the thalamus and cortex (Blumenfeld, 2010).

The basal forebrain systems supporting arousal include the nucleus basalis, diagonal band, and medial septal neurons and their GABAergic and cholinergic neurotransmitters, with inputs from the brainstem and projections to the cortex and

thalamus (Blumenfeld, 2010).

Attention. Attention includes selective or directed attention (focusing on several competing stimuli) and sustained attention, composed of vigilance, concentration, and freedom from distraction. Selective attention to a specific somatosensory stimulus activates the corresponding somatotopic region of the parietal lobe. Selective attention towards a visual stimulus activates the corresponding retinotopic areas of the visual cortex. There may also be an excitatory valence attached to the stimuli under attention in selective attention, while an inhibitory valence is assigned to all competing stimuli by the PFC. The anterior cingulate cortex and limbic pathways, tectum and pretectal areas, pulvinar, cerebellum, and basal ganglia may also play a role. These areas are activated in fMRI studies of general alertness and selected and sustained attention; attention networks tend to be more lateralized to the dominant hemisphere than generalized awareness networks (Blumenfeld, 2010).

Attention requires heteromodal integration, including spatial representations from the parietal association cortex for attention objects in space and auditory, visual, and somatosensory representations from the overlapping temporal, occipital, and parietal association areas near the lateral parietal cortex. Likewise, the frontal heteromodal association cortex (or PFC) integrates information from the frontal eye fields for the direction of visual focus on the object of attention and target following, and motor movement in following the target is planned and executed through the PFC and dopaminergic signals to the striatum. The PFC also determines the relevance of stimuli and makes comparisons to re-evaluate and redirect attention as needed. fMRI studies have shown PFC activity in sustaining attention and reducing distractibility, presumably

through respective excitatory and inhibitory mechanisms (Blumenfeld, 2010).

The anterior cingulate cortex governs motivational aspects of attention with the amygdala, medial orbitofrontal cortex, thalamic mediodorsal nucleus, and other limbic structures. The visual focus of attention is coordinated by the superior colliculi, pretectal area, and pulvinar, together with the parietal-temporal-occipital cortex and frontal eye fields, which direct eye movement and possibly auditory monitoring as well (Blumenfeld, 2010).

Awareness. Conscious awareness is a term used to describe the summarization of sensory, motor, emotional, and memory information into a description of real-time mental activity that can be recalled at a future date. This binding process is assumed to take place over a distributed area, with theories of temporal-parietal-occipital junction association area involvement, widespread connections between regions within the cortical layers, and synchronized activity between regions in accord with oscillations detected in the binding regions (Blumenfeld, 2010).

It is reasonable to assume that consciousness relies on declarative memory to form the episodic sequence of real-time events so that it can form a storable engram of memory. Declarative memory is processed in the medial temporal and diencephalic regions. The generation of the engram of conscious experience may also require the generation of visual images to provide encodable material for memory, thus likely involving the visual primary and association cortex. The PFC is recruited to process working memory and functions in chronological sequencing and self-monitoring.

Cerebral Perfusion, Hemodynamics, and Metabolic Processes

In discussing the measurement of rCBF using SPECT, it is helpful to have a brief

understanding of what biological mechanisms govern blood flow. Therefore, we review blood flow, how neuronal activity generates and manages blood flow through neurovascular coupling mechanism, then the fuel and oxidants needed for neuronal activity, leading to a synopsis of resting-state rCBF theory.

General patterns of perfusion. In the medically normal, at-rest brain, SPECT imaging generally shows symmetrical perfusion between hemispheres. The temporal, parietal, and occipital cortices and basal ganglia show higher rCBF than other subcortical white matter. Eye opening or closure at injection results in up to 30% higher rCBF in the occipital cortex. Motor and sensory stimuli, in general, may show asymmetrical flow patterns (Prior, 2016).

Total cerebral perfusion. In the absolute sense, cerebral perfusion is the total volume of blood available to the brain, as carried by the bilateral carotid and vertebral arteries. Total cerebral perfusion is monitored and adjusted by the homeostatic mechanism of autoregulation that sets the mean arterial blood pressure. The four cerebral supply arteries are joined in the circle of Willis at the basilar artery to provide a pooled supply of blood sufficient to meet all cerebral metabolism and waste removal needs. This design allows redundancy, adjustment, and reversal of flow to balance supplies in limited obstruction to one or more of the component vessels.

However, in some individuals, the Circle of Willis is incomplete, or the communicating arteries that interconnect the component arteries are diminutive or prematurely terminate, thus limiting blood transfer to balance the artery flows. Furthermore, in otherwise typical brains, an obstruction will cause ischemic stroke due to hypoperfusion. Conversely, extreme hyperperfusion (hyperemia) is possible in

pathologies such as diabetic ketoacidosis, resulting in cerebral edema and accompanying cerebral pressure and tissue damage due to a transient dysfunction in blood flow autoregulation (Roberts et al., 2006).

Relative perfusion. In the relative sense, cerebral perfusion is the locally and temporally variant pattern of regional blood flows, which are labeled as hypoperfused when below the average expected value, and hyperperfused if above the average expected value. Neural activity demands determine the intra-individual patterns of hyperperfusion. Hypoperfusion patterns may be determined by pathology.

When increasing blood flow into hyperperfused regions, there is not corresponding hypoperfusion in neighboring regions. Blood never leaves the vasculature, so there is no direct compensatory effect that requires blood at other regions' expense. Instead, there is enough buffering capacity available from the supply arteries to supply all regions while maintaining a roughly constant total cerebral blood volume. Neurovascular coupling works to change local blood supplies by constricting or dilating arterioles and arteries as needed (Fantini, Sassaroli, Tgavalekos, & Kornbluth, 2016).

Although inter-individual patterns of rCBF can be averaged to determine the regional expected rCBF for comparison purposes, this method typically presents a great deal of error due to between-subject natural variance and works best with very pronounced patterns of change. Since inter-individual differences in rCBF are common and pronounced, many times, a determination of rCBF is made in an at-rest state as a baseline measurement per individual; this is then subtracted or otherwise compared to rCBF under active states of mental or motor activity to determine hyper- or hypoperfusion.

Neurovascular coupling. Neurovascular coupling (also functional hyperemia or hemodynamic response) is the explanatory mechanism for the adjustment of cerebral blood flow through vasodilation and vasoconstriction to meet localized cell groups' needs. The energy needs of neurons are primarily excitatory; inhibitory neurons represent only about 10% of total neurons. Excitatory processes are chiefly glutamatergic, and energy is consumed to generate and propagate action potentials, move ionic gradients, cycle synaptic vesicles through endocytosis and exocytosis, and uptake and recycle glutamate and calcium ions (Lourenço et al., 2014).

Blood transports glucose and oxygen in a just-in-time supply system because these fuels, for the most part, cannot be stored in reserve in the brain. The mechanical parts of this hypothetical model are the neurons; arteries, arterioles (smooth muscle lined sub-vessels ranking between arteries and capillaries in diameter), and capillaries; endothelial cells, pericytes, and smooth muscle cells of the blood vessels; and astrocytes and microglia that compose the glial cells (Roberts et al., 2006). In addition to mechanical actors, known vasodilators such as adenosine, nitric oxide, hydrogen ions, potassium ions, calcium ions, and lactate are hypothesized to play a role (Venkat, Chopp, & Chen, 2016).

The blood flow to the brain represents 20% of the whole-body blood volume, for 2% of the body mass (Venkat, Chopp, & Chen, 2016). Due to the lack of storage mechanisms, the heterogeneous needs of different brain regions, the limited volume of the cranium and blood vessels, and the resulting need for efficient programming of supplies, neurovascular coupling is of vital biological importance. Some have hypothesized that cognitive processes are limited by glucose availability as transported

by the blood vessels (Harris, Jolivet, & Attwell, 2012).

Hemodynamic response. The underlying assumption of SPECT, PET, and fMRI is that mental activity and external behavior require large groups of simultaneously firing neurons, thus consuming energy supplied by glucose and oxidized by oxygen. The energy supply is used to establish and overcome electrical potentials in the neuron that enable it to fire (excitation) or, conversely, not fire (inhibition).

Modern fMRI studies have allowed the temporal patterns of the hemodynamic response to be better understood. As observed in fMRI, it generally takes 6 ms until the hemodynamic response peak, which ends after about 20 ms in the absence of the stimulus. Of course, multiple and rapid presentations of the stimulus, multiple stimuli, and multiple ROI activations cause additive responses. It is rare that in an experimental paradigm, much less a natural state, a single hemodynamic response can be observed independently. Moreover, the hemodynamic response varies somewhat inter-individually as well as intra-individually.

Heterogeneous distributions. The principal indirect source of metabolism in the brain is the glucose and oxygen transported by the bloodstream. In the most straightforward process, glucose transporter proteins, primarily Glut1 and Glut3 residing in brain cell membranes, mediate *facilitated diffusion* to bring the glucose into the cell from the blood. There it is oxidized to form ATP and NADH, both of which provide energy for cellular processes. Glucose is the primary fuel for neurons, although ketones can substitute if available in quantity (Duelli & Kuschinsky, 2001).

Research has demonstrated that neither capillaries (the primary transporter to cells) nor glucose transporters (in the cell membranes) are distributed homogenously;

they tend to be denser in cerebral areas that customarily have higher blood perfusion (Duelli & Kuschinsky, 2001). It appears that local glucose consumption determines glucose transporter availability and capillary density, although the specific mediator is not known.

In rats, it has been shown that chronic neuronal activation over days to a week can increase transporter density, while neuronal deactivation over the same period decreases transporter density, but to a lesser extent (Duelli & Kuschinsky, 2001). Since glucose is oxidized by oxygen in a fixed stoichiometric ratio (6 oxygen:1 glucose), the oxygen demand of any specific brain area is directly correlated to local glucose consumption, glucose transporter density, capillary density, and hence blood flow.

Mediation of the hemodynamic response: diffusion. In a systematic review of 79 animal research experiments exploring the mediating mechanism of the neurovascular coupling response, Hosford and Gourine (2019) found that two-thirds of neurovascular coupling appeared to be mediated by nitric oxide signaling, while the remaining third was of unknown mediation. Mediation is thought to be through a feed-forward design. Early pioneers like Sherrington and Kety hypothesized that waste products produced by cells triggered a feedback response of increased blood flow to replace the depleted supplies; however, according to Hosford and Gourine, experimental evidence does not support this conclusion.

Nitric oxide, a potent vasodilator generated prolifically in the brain, diffuses through cell membranes readily, and travels the equivalent of several cell diameters, has been shown to act by activating smooth muscle cells in the arterioles to cause the constriction. It causes a chain reaction that activates protein kinases that later produce

vasorelaxation to return the region to normal perfusion (Lourenço, Ledo, Barbosa, & Laranjinha, 2017).

Nitric oxide is the primary mediator evidenced in animal research; it is powerful and widely available from neurons, glia, vascular cells, and endothelial cells (Venkat, Chopp, and Chen, 2016). Regulation by nitric oxide is also referred to as the volume method, as the nitric oxide acts through diffusion in three dimensions. Research in vivo in humans supports the Hosford-Gourine conceptualization of neurovascular coupling. It has been shown that nitric oxide diffusion regulates rCBF in the hippocampus, with the nitric oxide being generated by glutamatergic neurons, then diffusing to proximate arterioles to act as a vasodilator (Lourenço et al., 2014).

Furthermore, neurovascular coupling functions symbiotically with neuroenergetic/neurometabolic coupling (the mechanism for metabolizing glucose and other energy sources to keep up with localized neuronal demand), forming an essential functional axis in the brain. The generation of nitric oxide immediately follows the activation of glutamate receptors, and the nitric oxide serves as a signal and modulator not only for vasodilation but simultaneously for regulation of the metabolism of glucose and oxygen (Lourenço et al., 2017).

Mediation of the hemodynamic response: astrocytic transmission. Another hypothesis is that increased neural activity causes glutamate release in the synaptic cleft, some of which activates metabotropic glutamate receptors on neighboring astrocytes. Calcium ion concentration in the astrocytes increases as a result, which causes potassium channels to open, and causes a vasodilation effect when potassium contacts arterioles (Attwell et al., 2010; Longden et al., 2017). This mediation relies on the vast

interconnected network of astrocytes, and transmission distance is limited to the width of synaptic gaps; it is not feasible in all vascular brain tissue and is not a complete explanation for control of vasodilation (Lourenço et al., 2017).

Mediation by both diffusion and transmission. A widely accepted hypothesis is that several sequential *and* parallel pathways mediate the signaling for neurovascular control. Strong evidence for the mediating role of diffusive nitric oxide on arterioles exists for the hippocampal and cerebellar areas, while there is evidence for astrocytic transmission to arterioles and capillaries in the cerebral cortex, but with nitric oxide acting as a modulator to the vasodilation (Lourenço et al., 2017; Lindauer, Megow, Matsuda, & Dirnagl, 1999; Attwell et al., 2010).

Signaling by prostanoids (part of the brain's immune and inflammatory response) and purines (adenosines and ATP) are possible transmission pathways. For instance, astrocytes release ATP into the gaps between cells, and the ATP and its byproduct adenosine (hydrolyzed ATP) activate purinergic receptors in smooth muscle and endothelial cells to cause vasodilation (Toth et al., 2015; Lourenço et al., 2017). Furthermore, while nitric acid activates smooth muscle cells in arterioles to cause vasodilation, capillaries are also subject to constriction by wrap-around cells (pericytes) activated by astrocytes, another example of a sequential pathway (Lourenço et al., 2017).

The standard configuration of neurovascular signaling has yet to be determined. However, it is likely that as opposed to monitoring output of byproducts at some hypothesized central or regional neurovascular comparator in a typical feedback design, instead a feed-forward design is indicated: Signaling transmitters are analyzed constantly in real-time, while blood flow is predictively regulated rather than retroactively adjusted.

Neurons signal blood vessels directly or activate astrocytes to signal blood vessels to dilate (Hosford & Gourine, 2019; Attwell et al., 2010).

Neuronal metabolic activity. Metabolic demand drives cerebral blood flow, but the underlying process has been (and still is) vigorously debated. Since cerebral oxygen consumption is correlated to overall neuron energy consumption, and neurons consume energy in proportion to neural activity, then, as a fundamental principle underlying neural imaging, the oxygen content in the neural vasculature can be used to determine an approximate regional blood flow (rCBF) and blood volume (rCBV; Van Audenhaege et al., 2015). Instead of direct measurement of oxygen concentration in the bloodstream, neural energy consumption can be measured as a concentration of radioactively tagged glucose, water, oxygen, or antioxidants.

However, the actual metabolic relationships are complicated. There are three different methods of fueling neuronal activity without burning oxygen (or, at least using smaller quantities of oxygen). First, there is glycolysis, which is an anaerobic, enzymatic, energy-releasing process that turns glucose into energy used to form adenosine triphosphate (ATP), reduced nicotinamide adenine dinucleotide (NADH), and pyruvates (Raichle, 1998). Second, pyruvate may be transformed by mitochondria within the cell to generate more ATP and NADH, in an aerobic process that uses less oxygen than direct oxidation. Third, glucose can be processed by pentose phosphate into NADH phosphate, which is light on oxygen consumption while providing energy for metabolism (Magistretti & Allaman, 2015). In addition, there is evidence that lactate, produced in the cell as part of the ATP cycle, is used as an energy substrate in place of glucose, but the frequency of this occurrence is not yet known (Lourenço et al., 2017).

Metabolic pathway effects on imaging. The critical point of the above descriptions is that up to 15 times more ATP is generated by anaerobic methods than aerobic methods (Magistretti & Allaman, 2015). As a result, functional imaging dependent on oxygen (fMRI) may show only a 5% change in oxygen consumption during a task, while PET or SPECT may show a 50% increase in blood flow for the same task, given a 50% increase in the consumption of glucose (Lourenço et al., 2017). Therefore, imaging that relies on oxygen depletion (i.e., fMRI) as a measure of blood flow or neural activity must take this distortion into account, and, in some ways, is less sensitive to neural activity than PET or SPECT.

Another confound to quantifying neural activity based on the imaging of a single compound is that the energy-to-excitation ratio for glucose is not a constant. One cannot state that a given quantity of glucose molecules in the bloodstream will fuel a given number of neurons for a set period during excitation because the efficiency of processing of glucose is variable and appears to be governed by the diffusion concentration of nitric oxide present (Lourenço, 2017). This also holds for the percentage of glucose converted to energy by way of oxidation or glycolysis. Since this difference in metabolic pathway directly affects the measurable blood deoxygenation, it, in turn, adds error to the measurement of activation as a function of oxygen use by fMRI.

To state this more simply, a fixed number of neurons activated to perform a perceptual function requires increased blood flow to supply glucose for the neurons' excitation and oxygen to oxidate the required glucose. The regional blood flow is increased due to signaling, primarily by diffusion of nitric oxide. However, the nitric oxide may also signal changes in the proportion of glucose molecules that are oxidized,

thus producing deoxidized hemoglobin for fMRI measurement and the proportion processed into energy by anaerobic processes. So, the fMRI output may attenuate somewhat, even though activation has not changed. The fMRI may underestimate neural activation after the initial activation as glucose metabolism changes from aerobic to anaerobic processes. The magnitude of this error has not yet been quantified through research and is still at the culture and animal research stage (Lourenço et al., 2017).

To summarize, as local neural activity increases, then blood flow increases, as does glucose consumption. Oxygen use, however, is not proportional to and lags, the quantity expected if glucose was only oxidized; one chief mechanism of glucose metabolism, then, is glycolysis, which is not measured in the BOLD signal from fMRI. fMRI BOLD also does not distinguish between dynamic changes during the processing in aerobic versus anaerobic glucose metabolism. PET and SPECT are likely unaffected by this confound because they trace the quantity of glucose or related compound before metabolism, while fMRI traces deoxygenation resulting from metabolism. However, the quantification of lactate as an energy source for neural activity would potentially affect all three imaging forms, but the effect's magnitude has not been defined in vivo studies with humans.

Hemodynamic dysfunction. The above paragraphs describe the hemodynamic function and vascular response in the healthy brain. One of the premises of the current study is that pathological brains have an altered hemodynamic response. Since relative cerebral blood flow is subject to intra- and inter-individual variability, this is addressed through experimental manipulations such as normalization techniques and a baseline state for comparison with an activation state. However, even after these compensations,

variance in blood flow due to anatomical, metabolic, and vascular malfunction has been documented in hypertension, diabetes mellitus, glioma, dementia, traumatic brain injury, and stroke, as well as in natural aging processes (Chen, Venkat, Zacharek, & Chopp, 2014; Agarwal, Sair, Yahyavi-Firouz-Abadi, Airan, & Pillai, 2016; Østergaard et al., 2014). Attribution to a single cause such as defective neurovascular coupling is tentative and the subject of ongoing research (Venkat, Chopp, & Chen, 2016).

A neuropsychological model for perfusion. In addition to the biological model of perfusion offered here, a brain-behavior description may also be of use in understanding default at-rest blood flow and introducing later models of pathological perfusion. In *The Working Brain* (1997), Aleksandr Luria described three functional units of the brain necessary for any mental activity: the unit for regulating tone or waking; the unit for obtaining, processing, and storing information; and the unit for programming, regulation, and verification of activity.

The first unit is composed of the ascending and descending reticular activating systems (RAS). The ascending system is associated with the reticular formation and its nuclei around the posterior hypothalamus and subthalamic regions of the mesencephalon and parts of the brain stem. In addition to cortical activation, the first unit regulates inhibition through the ascending-descending feedback from the subcortex to the cortex.

Activations are of three forms: the tonic and generalized activation arise from the lower brainstem, including the hippocampus and caudate nucleus, while the phasic and localized activation originates in the upper brain stem, thalamic region, and limbic system. These first two activations ascend to the cortices to maintain cortical tone. The third activation is the descending RAS, from the prefrontal cortex (PFC) to the RAS and

brainstem/thalamic/limbic areas. This is the pathway by which intention and goal-directed activity of the PFC directs the RAS to send efferent signals to other cortical areas to arouse goal-directed action.

The second unit, tasked with obtaining, processing, and storing information, is generally located in the occipital, parietal, and temporal cortices, particularly in the visual, sensory, and auditory association areas. The second unit is the home to gnostic neuropsychological processes, with information gathered in a modally specific format by dedicated neurons located in the primary association areas. This information is analyzed and stored by overlapping tertiary area neurons, where unimodal inputs are combined to make complex associations. The tertiary areas include the inferior and superior parietal cortex, part of the temporal cortex, and a portion of the temporal-parietal region. The second unit exhibits the property of lateralization of function, with unique functions ascribed to each hemisphere in some cases.

The third functional unit of the brain is the unit for programming, regulation, and verification of activity, responsible for conscious activity. These activities are essentially the function of the PFC: People form intentions, plan activities and responses, issue executive programs for the actions, then accept feedback from sensory systems and unit two, and subsequently compare the feedback to the plan and issue corrective adjustment programming; the third unit does this mainly in a conscious fashion, as compared to the largely unconscious functioning of the first unit. The third unit's extent includes the anterior cerebrum forward of the precentral gyrus, including the motor cortex and the descending corticomotor tracts. The basal motor ganglia and extrapyramidal tracts provide support.

Luria noted that the third functional unit is highly interconnected with subcortical and cortical areas; most of the connections are bidirectional (both efferent and afferent). Connection with unit one, the RAS, allows for the reception of tonal and activation signals and the issuance of efferent control signals, both excitatory and inhibitory, to regulate the RAS and associated limbic system. Connections with unit two allow for the exchange of sensory and perceptual data and motor supervision. Although the basal ganglia, cerebellum, and associated fiber tracts handle primary motor control, unit three creates the programs and provides higher-level motor task management. For example, gross and fine motor manipulation is needed for toolmaking, but only higher-level animals such as humans are successful toolmakers because of the executive management of motor movements according to a supervised plan by the PFC (Luria, 1997).

Experimental Paradigms Used In At-Rest Studies

Having reviewed the SPECT imaging modality used to obtain the measurements of rCBF, the neuroanatomical structures to be analyzed as ROI variables, and the source and characteristics of the biological underpinnings of rCBF, it remains to review the experimental paradigm used to study brain resting states and cerebral blood flow.

Connectivity designs. Connectivity is of three general types: anatomical, functional, and effective (Friston, 1994). Physical connections between ROI constitute anatomical connectivity and can be imaged through diffusion tensor imaging (DTI) that shows myelinated pathways. Effective connectivity refers to the apparent control of one ROI over another correlated ROI. It is approached with a prior hypothesis and specific regions with proposed connections and directionality and tested with the general linear model (GLM) or structural equation modeling (SEM). Functional connectivity is the

association or correlation of metabolic or blood flow properties between ROI. It is approached through non-hypothesis-driven statistical methods such as dimensional reduction; this third method is used in the current study.

Functional connectivity can be determined by using direct pairwise correlations between ROI, correlation with a selected reference seed ROI, factor analysis, PCA, or independent components analysis (ICA). PCA determines components in order of the most significant variance accounted for. ICA determines components without a hierarchical order, and components must be independent (rather than simply orthogonal) and primarily non-Gaussian. ICA and PCA vary from factor analysis in that noise and systemic error are not computed: The explicit assumption of component analysis is that all variance is ascribed to the components. On the other hand, factor analysis assumes error as part of the total variance (Lindquist, 2008). Factor analysis is, therefore, the method selected for this study.

When connectivity is discussed in this paper, it refers to functional connectivity and non-hypothesis-driven statistical relationships that do not infer causation or directionality.

Resting-state connectivity. fMRI first demonstrated that spontaneous activation could be seen in motor, visual, and other networks under no task load conditions in the awake state with reduced sensory input. This has been labeled *default mode network* (DMN) activity; in effect, when left to do nothing, the brain uses as much or more energy as when engaged in a single simple task. Buckner, Andrews-Hanna, and Schacter (2008) noted that the DMN is a "specific, anatomically defined brain system preferentially active when individuals are not focused on the external environment" (p. 1).

This focus on internal mental activity may include self-speech, evaluation of others' perceptions, assessment of the future, and retrieval and rehearsal of memory. Similarly, fMRI studies of participants asked to daydream showed the same default neural activity. The precuneus, posterior cingulate, retrosplenial cortex, and medial parietal region show activation under these conditions (Blumenfeld, 2010).

In the at-rest state, stored memories and learned associations are retrieved and used to create mental simulations, activating the medial temporal lobe. The internal mental activity also requires the frontal lobes to organize and plan the simulation. These two activity areas converge at the posterior cingulate gyrus, where PFC and hippocampal activity are believed to overlap to form cognitions (Buckner, Andrews-Hanna, & Schacter, 2008).

Resting-state studies in fMRI are well-replicated but have some inconsistent results due to methodology and variance between datasets. One consistent finding is that persons at rest metabolize almost as much energy in the brain as those at task (about 80-90%; Raichle, 2011). Raichle (2015) reviewed past research supporting the existence of a resting-state DMN with activity occurring in the absence of external stimuli in the ventral and dorsal medial prefrontal cortices, the posterior cingulate cortex and precuneus, the lateral parietal cortex, and the entorhinal cortex, as well as the parahippocampal gyrus and hippocampal formation.

In addition, Zhang and Raichle (2010) summarized other resting-state networks that are detected differently dependent upon experimental paradigms. These networks are typically anticorrelated with the DMN: The body is at rest in the DMN state, but any movement or activity may activate one of the other defined default states. This may be

intentional, or may be experimental artifact; for example, finger tapping may be part of the protocol, or may be unintentional due to fidgeting.

In addition to the DMN, these other default networks include attention, executive control, sensorimotor, visual, auditory, and salience, and are shown in Table 9 (Yeo et al., 2011). Other sources identify up to 14 resting-state networks (10 in Robinson et al., 2009; 14 in Shirer, Ryali, Rykhlevskaia, Menon, & Greicius, 2012). However, based on replication studies using major brain atlases, Doucet, Lee, and Frangou (2019) identified the five most replicable resting-state networks as the DMN, salience, central executive, sensorimotor, and visual networks.

In the case of an at-rest design like the current experiment, attention, visual, and auditory networks will likely activate, as this is a 20 min eyes-open state in a quiet (but not noise-proof or darkened) room. It is less likely that the sensorimotor, executive control, and salience networks were activated, but it is possible due to thought processes (planning, decision making), fidgeting, and competing stimuli. The only actual resting-state experiment is in a controlled isolation room.

At-rest protocol. In SPECT at-rest imaging, the participant is told to keep eyes open, relax, and not focus on one thought or idea, for about 20-30 min. A cannula is inserted in the wrist. They then lie or recline in a quiet room without disturbance. At some point towards the end of the period, a radiotracer is injected through the cannula, taking a few seconds to cross the blood-brain barrier into the neuronal tissue in proportion to neuronal activity and related glucose consumption. The SPECT camera scan occurs up to 45 min later, capturing rCBF at time of injection.

Table 9

Default Networks (from fMRI studies compiled by Yeo et al., 2011 and Doucet et al., 2019)

Network	Components	Citation
Default mode network: activated regions during at-rest state, eyes closed or open and fixated, quiet room, no task assigned	Inferior & superior frontal gyri, rectus gyrus, cingulate, middle temporal gyrus, angular gyrus, inferior parietal lobule, hippocampus/parahippocampal gyrus	Raichle (2001)
	Posterior cingulate cortex/precuneus, ventral anterior cingulate/medial prefrontal cortex, angular gyrus	Doucet (2019)
Attention (dorsal attention network): top-down modulation of attention, overtly or covertly oriented in space	Superior & inferior parietal lobules, middle & inferior frontal gyrus	Fox (2006)
Executive control: working memory and control processes activated during task demand	Superior, middle, & inferior frontal gyri; supramarginal gyrus, angular gyrus, inferior parietal lobule, frontal insula, caudate, thalamus	Seeley (2007)
	Middle frontal, inferior parietal, & posterior middle temporal cortices	Doucet (2019)
Sensorimotor: Activated in motor tasks, such as finger tapping	Postcentral gyrus, precentral gyrus, supplementary motor area	Chenji (2016)
	Postcentral, precentral, & superior temporal gyri	Doucet (2019)
Visual: Any visual task or fixation	Precuneus, cuneus, calcarine cortex	Cordes (2000)
	Medial (calcarine, lingual gyri) and lateral (inferior/middle) occipital lobe	Doucet (2019)
Auditory: Any auditory task, active, or passive listening	Inferior frontal gyrus, superior temporal gyrus	Cordes (2000)
Salience: responds when behaviorally relevant stimuli occur spontaneously; for the detection and selection of competing stimuli and interaction with multiple cognitive systems	Supramarginal gyrus, angular gyrus, superior temporal lobe, anterior cingulate, anterior insula, superior, middle, inferior frontal gyri, gyrus rectus, amygdala, nucleus accumbens, olfactory cortex, substantia nigra, ventral tegmental area	Menon (2015)
	Anterior insula, the dorsal ACC, and in the middle frontal cortex and supramarginal gyri	Doucet (2019)

Research and Clinical Studies

There are few published SPECT factor or component analyses in clinical or non-clinical samples, and most published studies are three decades old. This review focuses on four areas. First, we topically overview the seminal studies to establish perfusion research progression, although no longer directly relevant due to equipment, methodological, analytic, and software advances. Second, we review the sparse and outdated dimension reduction studies from 1992 through 2001 for methodology. Third, we review perfusion, metabolic, and functional activation findings in neurological and psychiatric clinical samples. Fourth, we review studies most closely resembling or supporting our hypotheses in depth.

Seminal perfusion studies. According to Devous, Stokely, Chehabi, and Bonte (1986) in an early Xenon-133-gas-SPECT study, at-rest cortical flow rates in the gray matter of medically normal individuals were found to average 71 ml/min/100g (with *SD* = 12), with equal flow rates in the frontal and temporal lobes in each hemisphere, but higher right-hemisphere flow in other cerebral areas. Women had higher flow rates, and flow decreased with age at a slope of -.33 ml/min/100g per year. The variance between subjects was high, while the SPECT imaging replication within 1-10 days after the first administration in 15 individuals showed no significant interindividual variation. The white matter flow rate average was 59 ml/min/100g, but this was determined to be an artificially inflated result due to mechanical artifacts unique to the scanner equipment used in the study.

Devous et al. (1986) summarized blood flow findings in 10 previous studies of cerebral blood flow from 1969 to 1982. The average frontal region flows ranged from 55

to 92 ml/min/100g; the parietal flow was in the range of 66 to 90 ml/min/100g; temporal flow average varied from 61 to 89 ml/min/100g; occipital flow rates ran from 63 to 87 ml/min/100g. Standard deviations ranged from 3 to 17.

In Devous et al.'s (1986) review of the 21 studies from 1969 to 1981 that published whole-brain-averaged flow rates for gray and white matter, average gray matter flow ranged from 57 to 89 ml/min/100g (*SD* from 3 to 21), with average white matter flow from 18 to 59 ml/min/100g (*SD* from 3 to 12). There was no obvious regional rCBF pattern; the frontal, parietal, central, and occipital areas were the highest flow areas in two or three studies, and the temporal area never had the highest flow. SPECT interindividual variability is high, and measurement differences due to method (these studies used Xenon-133), imaging orientation, and slice width, complicate interpretation.

Use of Dimension Reduction Methods in Prior Studies. Following are studies that analyze CBF from a dimensional-reduction approach.

Pagani et al. (2001). Regional CBF obtained at-rest using T-99 HMPAO SPECT imaging in 25 healthy men and 25 healthy women aged 35 to 78 years (*M* age = 53, *SD* = 13) was examined in a principal components analysis (PCA) and varimax rotation of 27 ROI in each hemisphere. Participants spent 30 min in a tranquil, dimly lit room with no task assignment. Twelve components explained 81% of the cerebral perfusion variance; the number of components was selected based on an eigenvalue greater than 1.2 and ROI component loading greater than .5.

Results indicated that CBF (average value of 27 hemisphere ROI) was higher in the right (44.52) than the left (44.20, normalized values) hemisphere ($p < .001$), and CBF (average value of 54 ROI) decreased with age in females, but not males. Decreases in

rCBF were noted in the left-hemisphere cortical areas, especially the left frontotemporal and temporal-cingulate cortices, while rCBF increased in the medial areas with age.

The primary component was the bilateral superior somatosensory parietal cortex, left premotor, motor, and posterior cingulate cortices, accounting for about 17% of the variance. This result indicates a bilateral and left hemisphere frontal-parietal-limbic network. The second component was the left anterior frontal cortex, accounting for 14% of the variance and describing the left frontal lobes. The third component was the right temporoparietal cortex, accounting for 9% of the variance and broadly describing the right temporal and parietal lobes. The fourth component represented the left frontotemporal cortex and hippocampus, accounting for 8% of the variance and describing the left frontal and temporal lobes. The fifth component was the occipital lobe, accounting for 7% of the variance. The sixth component was the right frontal lobe, accounting for 6% of the variance. The rest of the six components together described 21% of the variance and are not listed here.

Strengths and weaknesses. This older study is one of the few to explore SPECT data using a factor analytic technique. Unique to this study compared to modern functional imaging work is the laterality of the factors (or networks) in the at-rest state; most fMRI studies show mainly bilaterally loaded factors. The study's apparent weakness is the smaller sample size of 50 subjects, and the average age of subjects was much older at 53 years than in other studies. Participants were volunteers visiting stroke patients in the hospital, so there is the opportunity for some skewing towards pathology due to hereditary factors.

Translation to the present study. Pagani et al. (2001) offer the only SPECT factor-

analytic study less than 20 years old; therefore, results are of interest compared to the present study. However, because of the small sample size and the lack of replications in the literature, the results do not stand as highly reliable for comparison purposes.

Szabo et al. (1992). Factor analysis (FA) was the selected statistical method for quantifying cerebral glucose utilization by PET by Szabo and colleagues (1992). This early study aimed to seek covariance patterns in metabolism (as measured by glucose consumption) in brain regions and measure global metabolism (glucose metabolism is an analog of cerebral blood flow). More specifically, the authors sought to clarify where the most significant variance was to be found neuroanatomically, given the well-known inter- and intra-subject variability of PET imaging.

The study recruited 12 healthy young male volunteers (M_{age} = 26.7) for fluorine-18-fluoro-2-deoxy-D-glucose-based PET scans at rest on three (n = 6) or four (n = 6) occasions spaced over 11 days. The FA results indicated that 70% of the variance was attributable to a single factor, while the second factor increased variance accounted for 80%. The first factor was loaded by the frontal and temporal cortices, cingulate gyrus, caudate nucleus, thalamus, and putamen; this neuroanatomical pattern represents the limbic, frontal, and temporal systems and their interconnections. The second factor was loaded by the parietal and occipital cortices and the cerebellum, describing the motor-sensory and visual areas and their interconnections.

Moreover, the same factor structure was obtained using different factor extraction methods and rotation: First, analysis was by principal components extraction and varimax orthogonal rotation. Then, parallel extractions using principal axis factoring, imaging analysis, unweighted least squares, maximum likelihood, and alpha analysis, followed by

quartimax, equamax, and oblimin rotations, were employed (Szabo et al., 1992; Camargo et al., 1992).

Weaknesses. An apparent weakness in Szabo et al. (1992) is the limited sample size of $n = 12$; this is certainly not uncommon in early PET work restricted by expense, extended scan times, and access to radiopharmaceuticals with very short half-lives. SPECT imaging later circumvented these problems to an extent, allowing for more extensive studies. Because of the small *n* compared to the 24 ROI variables measured, rules-of-thumb for the ideal participant to variable ratios are violated. Although such rules are without empirical support, recommended methods to determine the robustness of the results, such as bootstrapping and parallel analysis, were not used either.

Furthermore, the selected sample was homogenous in gender and age, by design, to reduce the variability of metabolism dependent on age and gender. Unfortunately, this also limits the generalizability of the result. Thus, the replicability and generalizability of the experimentally derived factorization cannot be assumed.

Strengths. The Szabo et al. (1992) study is helpful because its approach to variability in PET imaging as a strength rather than a weakness. While other PET paradigms attempted to use brain metabolism to discriminate and diagnose psychiatric and neurological diseases and hence ran into variability as a confound to sensitivity and specificity, this study examined the latent variable structure. As described by regions of interest, the most variable metabolic activity would be grouped on the same factor; if this grouping of regions represented a logical pattern of connectivity in the brain, then that latent variable was interpretable even if not directly measurable in the experiment.

Interpretation. Indeed, the primary latent variable from Szabo et al. (1992) is

predicted by Aleksandr Luria's early theories of brain-behavior relationships resulting from observation and neuropsychological assessment of the brain-injured, as elaborated elsewhere in this discussion. The first factor, consisting of the frontal and temporal cortices, cingulate gyrus, caudate nucleus, thalamus, and putamen, represented Luria's first and third units of cerebral function: The first unit being responsible for regulating tone or waking, and the third unit for programming, regulation, and verification of activity (Luria, 1997).

Szabo and colleague's (1992) results are interpretable from a Lurian neuropsychological perspective combined with the current neuroscientific perspective. In a person at rest, the first unit is always active, acting as the biological clock (analogous to the clocking chip in a computer) that sets the pace and tone for neurological activity, and keeps default maintenance tasks running in the absence of specific environmental demands. The third unit, primarily represented by the PFC, is also active in the continuous supervision of *default programming*, i.e., monitoring and adjusting maintenance operations conducted during at-rest periods. The third unit acts as a comparator, comparing efferent and afferent signals, producing a feedback loop that adjusts efferent control signals based on the afferent feedback.

The first and third units conduct ongoing background activity; principles of economy and finite neural capacity offer support for assuming that this activity is relegated to the background during at-rest periods when neural capacity is not otherwise in demand. This is also commensurate with the description given by the DMN hypothesis described elsewhere in this review.

To recapitulate, Szabo et al. (1992) derived the results from individual at-rest PET

scans made over approximately an hour, in 12 participants, on three or four separate days, providing a temporally broad sample of at-rest brain behavior. The at-rest condition consisted of reclining with plugged ears and blindfold for 15 min before radiopharmaceutical injection, followed by 45 min after the injection, before the imaging. The highest covariance in brain regions was in the first and third units. These behave as a default mode network, showing high or low metabolic rates while engaged in default tone regulation and general activation.

The second factor found in Szabo et al. (1992) was loaded by the parietal and occipital cortices and the cerebellum. The second factor represents the posterior portions of Luria's second unit-- the unit for obtaining, processing, and storing information—as well as the cerebellum. Variance in these regions' grouping is highest (excluding the variance accounted for by the first factor), but increases variance accounted for by the first factor by just 10% (the first factor accounted for 70%). Thus, this network activity represents much less variance than the first factor but is still substantial compared to all other brain regions, where metabolic activity variance did not reach the level to produce a third factor.

Regarding the DMN, the second-factor regions appear to represent default (at-rest) activities of maintenance and consolidation of sensory and perceptual activity and memory in the cortex, both ongoing (even with eyes closed and at rest) and recent. Cerebellar activity variance represents the motor movement monitoring (balance and coordination), which is ongoing even at rest during shifting, fidgeting, or small voluntary movements.

The second factor may also be interpreted as a product of the occipital cortex's

activity in processing visual data to produce imagery in the eyes-closed condition, which requires some of the same processing as in eyes-open visual operations. Visual memories stored in the occipital cortex are activated, further processed, and encoded for deeper storage. Similarly, in the parietal lobe, sensory and perceptual information from the motor activity and the visual cortex is accessed, additionally processed, and encoded for further storage in the at-rest state.

Clinical Perfusion Findings

As previously discussed, the present study's focus was on resting-state rCBF in a clinical sample of mixed neuro- and psychopathology. The literature shows what might be expected in a healthy sample's resting-state blood flow, but little work has examined resting-state pathological samples. We compile those studies or reviews here as related background material and summarize pathological findings in the accompanying Tables 10 and 11. This summary of information provides the basis for later comparison and interpretation of results.

Nonpathological aging. Goals of neuroimaging research include understanding cerebral blood flow and basic neuroanatomical behavior and function; application of imaging to the diagnosis of pathology; the monitoring and follow-up of treatment effects; and exploring nonpathological changes in the brain due to aging. Although considered nonpathological in the sense that they are expected, these are the natural alterations that may lead to memory dysfunction, decreased attention and concentration, motor problems, and similar difficulties. Because some individuals exhibit natural decline more slowly and some more quickly, and no one wants to experience even a naturalistic decline, these nonpathological changes in cerebral function are of intense interest.

Table 10

Neuropathological Perfusion

Neuropathology	Regions Hypoperfused	Study
Nonpathological aging	Superior & middle frontal gyri; cingulate; middle temporal gyrus; superior parietal lobule	Damoiseaux (2008)
Cerebrovascular disease	Varies- specific to location of diseased vasculature	Camargo (2001); Shi (2016); Warwick (2004)
Alzheimer's disease	Parietal lobe; temporal lobe; cingulate; frontal lobe; temporal-parietal junction	Dickerson (2005); Warwick (2004)
Vascular dementia	Diffuse foci, multiple foci, cortical and subcortical	Camargo (2001); Catafau (2001); Warwick (2004)
Frontal-temporal dementia	Frontal lobes (right in behavioral disturbance, left in aphasia); temporal lobes	Camargo (2001); Catafau (2001)
Parkinson's disease	Temporal and parietal (posterior) in 10%; modified radioligand to detect dopamine	Camargo (2001); Eckert (2005); Catafau (2001)
Huntington's disease	Basal ganglia; parietal lobe; temporal lobe	Camargo (2001)
Dementia-hypothyroidism	Global cortical	Camargo (2001)
Pseudodementia	Frontal lobes; temporal lobes	Catafau (2001)
Dementia- HIV	Multifocal	Catafau (2001)
Creutzfeldt-Jakob	Multifocal	Catafau (2001)
Epilepsy	Localized interictal hypoperfusion in 50%; ictal focal hyperperfusion in 90%	Kuzniecky (2005); Camargo (2001)
Traumatic brain injury	Location/size dependent; may appear without loss of consciousness or structural findings	Camargo (2001); Warwick (2004); Lee (2005)
Neoplasms	Increased uptake in tumor with T99 HMPAO; specialized radioligands give different results	Devous (2005); Lee (1998)
Autism	Cerebellum; cingulate; amygdala; thalamus; frontotemporal lobes; basal ganglia	Amen (2017); Ota (2018); Wen-han (2011)

Neurodegeneration due to aging is evidenced by structural changes such as atrophy, primarily in the hippocampus, lateral prefrontal cortex, cerebellum, amygdala, and entorhinal cortex (at older ages); and in white matter, where localized progressive deterioration, including ischemic lesions, gliosis, axonal degeneration, demyelination, microinfarcts, or perivascular spaces, has been noted. Changes at the cellular level include deposition of A-beta-amyloid plaques and iron accumulations. Potential risk factors for neurodegeneration within normal aging include vascular health, inflammation, and stress (Kennedy & Raz, 2015).

Table 11

Psychopathological Perfusion

Psychopathology	Regions Perfused	Study
Obsessive-compulsive disorder	Hyperperfused: cingulate, orbitofrontal, basal ganglia; hypoperfused: superior temporal gyrus (l), superior/middle frontal gyri, caudate (r), thalamus (r); decreased serotonin binding	Wen (2013); Pian (2005); Lindauer (2008); Camargo (2001); Muller-Vahl (2019)
Tourette's syndrome	Hyperperfused: frontal lobes, cingulate, basal ganglia, thalamus	Camargo (2001)
Posttraumatic stress disorder	Hypoperfused: superior temporal gyrus (l), superior/middle frontal gyri	Lindauer (2008)
Schizophrenia	Hyperperfused: visual or auditory cortex during hallucination; basal ganglia (r); hypoperfused: frontal lobes, temporal lobes	Camargo (2001); Molina (2003)
Depression	Hyperperfused: occipital lobes; hypoperfused: prefrontal lobes, temporal lobes, limbic system, cingulate, caudate (l)	Camargo (2001); Li (2018)
Panic disorder	Hyperperfusion: Superior and middle frontal gyrus, occipital lobe (l); hypoperfusion: frontal lobes, hippocampal regions	Camargo (2001); Eren (2003); De Cristofaro (1993)
Anxiety	Hyperperfused: amygdala(l), insula, fusiform gyrus(l)	Kaczkurkin (2018)

Also observed in aging is neurocognitive decline, most consistently in memory and learning domains (long-term declarative memory), processing speed, and executive function (working memory; Kennedy & Raz, 2015). Neurocognitive deterioration, however, typically starts later than the structural changes: Before age 75, the decline is significant in some portion of the population in episodic (fact) and semantic (word) memory; after age 75, most people have some decline over all domains, although the magnitude varies greatly (Small, Dixon, & McArdle, 2011).

CBF decline and metabolic dyscontrol have been proposed as possible causal agents in brain aging. Neurodegeneration resulting from deleterious changes to the neurovascular and neuroenergic coupling axis is hypothesized. One theory is that this occurs by reducing available nitric oxide through ongoing competing reactions with superoxide radicals (superoxide radicals are dioxide ions with a double negative charge that are very reactive; Lourenço et al., 2017).

Imaging findings have led to several theories of aging and aging processes. Cabeza (2002) proposed the Hemispheric Asymmetry Reduction in Older Adults (HAROLD) model to explain fMRI activation findings that younger adults show lateralized prefrontal activation in episodic and semantic memory, working memory, perception, and inhibitory control, while older adults show bilateral activation. This effect has been attributed to inefficient cognitive strategies; dysfunctional communication between the left and right hemispheres; dedifferentiation, a biological tendency to reduce specificity and selectivity of regions in performing localized functions; and compensatory functioning to make up for aging-related changes (Reuter-Lorenz and Cappell, 2008).

Reuter-Lorenz and Cappell (2008) noted another oft-observed feature in

functional imaging. Compared to a younger cohort, older adults performing activation tasks demonstrated activations in unique regions; displayed increased activation over the lower activations of younger persons performing the same task; and had nonlinear activation during complex tasks in functional imaging (Grady & Craik, 2000; Reuter-Lorenz, 2002).

In older persons, the increased activation leveled or dropped off, as did performance relative to younger subjects; this was attributed to reaching the cognitive resource ceiling and labeled the compensation-related utilization of neural circuits hypothesis (CRUNCH). This model assumes that older persons recruit more regions and neural groups to match younger cohort performance, but at some point, this compensation fails due to limited resources. This ceiling is seen in experiments using progressively more complicated tasks (Reuter-Lorenz and Cappell, 2008).

If there is compensation taking place in the form of increased brain activation in older adults, it is not clear whether it is necessary due to a deficiency in the activated region or if it is due to reduced or inefficient connectivity for other reasons. Information transmitted from other regions can be disrupted by demyelinated pathways or received in a garbled condition. Thus, multiple areas may hyperactivate to supplement a hypoactivated area or support a hyperactivated area to compensate for subsequent decreased efficiency (Reuter-Lorenz & Cappell, 2008).

For example, younger adults processed incidental memory for complex scenes with accompanying medial temporal lobe activation; in older persons, under the same task requirements and equivalent performance, the prefrontal cortex activated while the medial temporal lobe did not. Those who used the prefrontal regions more during recall

also used the hippocampal regions less and vice-versa (Gutchess et al., 2005).

The interpretation of this apparent compensation is speculative; it could be interpreted as prefrontal mediation of memory recall, possibly related to verbal mediation, cognitive strategies used in encoding, or cue retrieval. It has been postulated that the frontal lobe may mediate memory encoding and retrieval in determining familiarity, localization in time and space, and relational processing. Prefrontal activation might also be due to perseveration and problem-solving activity, as the older cohort may have had more need of self-management to continue to complete the task successfully using a lower-efficiency hippocampal system. Other executive functions such as attentional selection, inhibition, rule switching, and context processing may play a similar role in the task difficulty (Gutchess et al., 2005).

Normal aging has also been implicated in decreased efficiencies within the DMN that constitutes a regularized regional pattern that show activation while the person is at rest. The DMN may have reduced long-range connectivity between regions in older adults, a decreased dorsal attention network performance (Tomasi & Volkow, 2012), and longer latency to shift from DMN to activation (Kennedy & Raz, 2015). Damoiseaux et al. (2008) found decreased activity in older versus younger persons at rest in the superior and middle frontal gyrus, posterior cingulate, middle temporal gyrus, and the superior parietal lobule; all regions that are associated with the DMN.

Cerebrovascular disease. In the medically pathological brain, disorders may cause detectable hypo- or hyperperfusion in specific ROI. Cerebrovascular disease shows focal or diffuse hypoperfusion in the affected region immediately after an ischemic event; diaschisis (hypoperfusion at a region remote to the event origin) is sometimes evident in

the opposite hemisphere (crossed-cerebellar diaschisis; Warwick, 2004). Luxury perfusion (hyperperfusion) may appear in regions before a stroke. Transient ischemic attacks (TIA) may be detectable on imaging at the time of the event (sensitivity of 60% within 24 hours, declining to 40% in the first week), but might not show on post-event SPECT (Camargo, 2001; Devous, 2005). However, if there are indicators post-TIA, this can be taken as an increased risk of early stroke. In post-TIA SPECT, sometimes acetazolamide is injected, which causes vasodilation and a 30-50% increase in rCBF for a few hours; abnormally perfused regions do not typically show this increase. A stroke will show focal hypoperfusion immediately after the event, with a sensitivity of 85% and specificity of 97% (Camargo, 2001). Luxury perfusion of the focus or region may occur from 1-5 days after the stroke, lasting up to 20 days.

Although cerebrovascular disease is a pathology unto itself, it is also the contributor to vascular neurocognitive disorder or vascular dementia. Small vessel disease, the disruption of vascular activity within the white matter that often shows as small hyperintensities on imaging, is thought to contribute to 40% of all dementias (Kisler, Nelson, Montagne, & Zlokovic, 2017). A meta-analysis of rCBF results in small vessel disease by Shi et al. (2016) noted that rCBF was reduced in relation to quantities of white matter hyperintensities in cross-sectional studies, but there is no available longitudinal evidence for this effect.

Dementia. Alzheimer's disease (AD) can appear on SPECT imaging as symmetrically hypoperfused parietal and posterior temporal lobes, especially the posterior association cortex, but typically with spared motor and sensory cortex. The most common finding is reducing perfusion in posterior temporoparietal, posterior

cingulate, and frontal regions. Temporoparietal junction hypoperfusion is seen in late-onset AD more so than early-onset (Warwick, 2004). These SPECT findings may occur in the presence of normal MRI and CT imaging. Progressed AD shows temporal and frontal hypoperfusion (Dickerson & Sperling, 2005). SPECT is used both in the early detection of AD and in following the longitudinal course through autopsy. In addition, SPECT images can detect medication effects in the resting state, and therefore have a role in therapeutic applications (Dickerson & Sperling, 2005).

The two-hit vascular hypothesis of Alzheimer's postulates that neurovascular damage may cause neuronal and synaptic damage, while amyloid-β proteins independently and synergistically cause further damage in conjunction with the neurovascular pathology. For example, CBF is decreased due to degeneration of vascular smooth muscle cells in the arterioles independent of amyloid-β, while damage to the arterioles also occurs due to amyloid-β angiopathy, causing micro-hemorrhaging. Several other mechanisms act in parallel and degenerative effects, including pericyte degeneration, reduced capillary circulation, endothelial damage, and increased astrocytic and microglia-initiated inflammatory effects. The reduction of CBF in Alzheimer's is complex and multifactorial, but every vessel and cell type that controls regional perfusion is implicated in the process (Kisler et al., 2017).

The sensitivity of SPECT in AD diagnosis is 86%, with 96% specificity (Camargo, 2001). In the case of vascular dementia (VD), hypoperfusion shows in multiple foci, seemingly at random locations, including possibly the motor and sensory cortices, and hypoperfusion can be cortical or subcortical (Warwick, 2004). Frontal lobe dementia (FTD) is indicated by bilateral frontal hypoperfusion, often with no CT or MRI

indicators of atrophy in the early stages. Right-hemisphere hypoperfusion may correspond to behavioral disturbance and left-hemisphere involvement with aphasia. Approximately 10% of SPECT imaging in PD patients shows posterior hypoperfusion like that of dementia patients and is likely an indicator of comorbidity of the disorders. Huntington's disease patients may demonstrate posterior hypoperfusion like dementia and hypoperfusion in the basal ganglia. Dementia due to hypothyroidism may show as global cortical hypoperfusion (Camargo, 2001).

Frontal and frontotemporal hypoperfusion may be seen in pseudodementia and frontotemporal dementia. Multiple focal defects are more likely to indicate AIDS-related dementia, multi-infarct dementia, or Creutzfeldt-Jakob disease (Catafau, 2001).

Epilepsy. SPECT findings in epilepsy patients are used to localize seizure foci for presurgical purposes rather than to diagnose the disease, and usually, a comparison is made between ictal SPECT and interictal SPECT. SPECT captures the expected rCBF increases during ictal states, as well as decreases in rCBF during interictal states; hypoperfusion is shown in up to 50% of patients, although it may be in the analogous ROI in the opposite hemisphere in 5-10% of patients (Kuzniecky, 2005).

Postictal imaging may also reveal abnormalities not evident interictally. Interictal hypoperfusion may be seen in the anteromedial temporal and frontal lobe in temporal epilepsy. However, 10% of studies indicate diffuse hyperperfusion, and half indicate no findings. In the ictal image, findings are dependent on the proximity of injection of the bolus of the radiopharmaceutical to the seizure event; if the latency of injection is too long, the generalization of a focal seizure may be captured, and focal location may be impossible to locate (Kuzniecky, 2005). If latency is less than 10 sec after onset,

hyperperfusion in the temporal lobe, basal ganglia, and possibly the motor cortex and contralateral cerebellar cortex may be captured.

Postictally (1-10 min after seizure), hypoperfusion in the focal hemisphere and possibly the contralateral temporal lobe may be indicated. Hyperperfusion in the anteromedial temporal lobe may persist up to 5 min after the onset. The sensitivity of SPECT in temporal lobe epilepsy is 44%, with 43% specificity, interictally; 97% and 100% respectively for ictal imaging; and 75% and 77% respectively for postictal images (Camargo, 2001).

Interictal hypoperfusion combined with ictal hyperperfusion is indicative of a focus. In cases of extra-temporal epilepsy, interictal findings may be uninterpretable, but ictal results show a sensitivity of 60%-90% (Kuzniecky, 2005). On the other hand, frontal lobe seizures may show less hyperperfusion for very short durations and may be indistinguishable on ictal imaging (Camargo, 2001). Up to 90% of epilepsy patients show ictal hyperperfusion in the epileptogenic focus (Kuzniecky, 2005).

Traumatic brain injury (TBI). SPECT is generally more sensitive to TBI lesions than is CT or MRI, especially in the acute phase of less than 24 hours from injury; the lesion on a SPECT image may appear larger than that on CT or MRI. Imaging can reveal focal, multifocal, and regional hypoperfusion due to subdural hematoma, cerebral contusion, or subarachnoid hemorrhage. SPECT may show hypoperfusion even in cases where consciousness is not lost (Camargo, 2001).

CBF hypoperfusion may be seen in SPECT images even in the absence of structural damage in mild TBI cases with chronic symptoms. SPECT offers better prognosis indicators than MRI or CT. The absence of SPECT findings after trauma is a

better indicator of complete recovery than the absence of images in CT or MRI, and prognosis worsens in connection with lesion size, number, and location in the brainstem, temporal lobes, parietal lobes, or basal ganglia (Warwick, 2004; Lee & Newberg, 2005).

The location of the hypoperfusion may indicate particular behavioral sequelae of TBI: frontal lobe hypoperfusion is associated with disinhibition, frontal lobe and thalamic hypoperfusion with poor executive functioning, left hemisphere with social isolation, and the right hemisphere with aggression (Camargo, 2001; Devous, 2005; Lee & Newberg, 2005).

Cerebral neoplasms. SPECT has been used to localize, differentiate, and therapeutically follow brain tumors (Devous, 2005). Various tracers (such as T-99m Methionine) are used depending on suspected tumor type. SPECT has been used to follow recurrent glioma with 76% sensitivity and 90% specificity (Arora et al., 2018). SPECT using thallium-201 has been shown to be more effective than PET and MRI in differentiating brain tumors by grade (Yamanaka et al., 2018).

Movement disorders. The nigrostriatal dopaminergic system has been implicated in Parkinson's Disease, and disease progression can be determined from SPECT scans (modified to detect dopamine rather than blood flow) of the presynaptic region, showing from 4-13% per annum reduction against the baseline putamen uptake of dopamine (Eckert & Eidelberg, 2005). Temporal-parietal hypoperfusion is seen in Parkinson's-related dementia like other dementias (Catafau, 2001).

Autism. Regional perfusion differences between individuals with autism and typical controls have been demonstrated in the cerebellum and vermis, anterior cingulate gyrus, amygdala, thalamus, frontal lobes, and temporal lobes (Amen et al., 2017). Ota et

al. (2018) found a significant correlation between social responsiveness scores and blood flow in the posterior cingulate gyral cortex of healthy males, suggesting the cingulate gyrus's implication in the presence of a common autistic trait. Wen-Han et al. (2011) found regional flow reductions in autistic children versus healthy controls in the bilateral frontal and temporal lobes and the limbic system and basal ganglia, as well as asymmetric CBF in the hemispheres in a subgroup diagnosed with Asperger's syndrome.

Obsessive-compulsive disorder (OCD). Research has indicated hyperperfusion in the anterior cingulate gyrus, bilateral orbitofrontal region, and sometimes the basal ganglia, which returned to normal in OCD patients treated with fluoxetine (Wen, Cheng, Cheng, Yue, & Wang, 2013), and showed decreased thalamic blood flow in response to fluvoxamine (Pian et al., 2005). Lindauer et al. (2008) showed that response to psychotherapy correlated positively with increased perfusion in the left superior temporal and superior/middle frontal gyri. Hypoperfusion has also been noted in the right caudate nucleus, right thalamus, and frontal lobes in some studies. It has been postulated that the degree and polarity of perfusion in the frontal lobe are related to the degree of insight into condition (Camargo, 2001).

In Tourette's syndrome, hyperperfusion has been noted in the frontal lobes, cingulate gyrus, basal ganglia, and thalamus (Camargo, 2001). The serotonergic system's role in Tourette's syndrome in conjunction with OCD was investigated using SPECT, and decreased serotonin binding was implicated in OCD but not in Tourette's (Muller-Vahl et al., 2019).

Posttraumatic stress disorder. In PTSD treatment studies. SPECT demonstrated that citalopram resulted in significant hypoperfusion in the left medial temporal cortex,

regardless of the clinical response (Seedat et al., 2004). Response to psychotherapy positively correlates with activation in the left superior temporal and superior/middle frontal gyri (Lindauer et al., 2008).

Schizophrenia. The common finding in schizophrenia is hypofrontality and left temporal hypoperfusion, with changes to the basal ganglia flow that may be iatrogenic. Findings vary based on the presence of positive and negative symptoms. Injection of radioligand during a hallucination showed hyperperfusion in the primary visual or auditory cortex, corresponding to whether the hallucination was visual or auditory (Camargo, 2001).

In treatment-resistant schizophrenia, SPECT imaging indicated decreased perfusion, particularly in the right posterior temporal lobe and left ventral prefrontal and left dorsolateral frontal cortices, and increased perfusion in the right basal ganglia (Molina et al., 2003). Under treatment with Risperidone, there was decreased activity in the medial prefrontal cortex, middle cingulate gyrus, and insula, with hypoperfusion in the brainstem, hippocampus, and a small part of the left posterior occipital and temporal region (Molina et al., 2008). Liu, Zhuo, and Yu (2016) noted that treatment-resistant patients had decreased blood flow at rest, with a smaller increase in blood flow than healthy controls while performing the Wisconsin Card Sorting Task (WCST).

Depression. Unmedicated depressed patients have demonstrated hypoperfusion in the prefrontal, temporal, paralimbic, limbic, cingulate gyrus, and left caudate nucleus, with lateral frontal hypoperfusion in older adults with acute depression. Hypofrontality corresponded to the severity of negative symptoms (Camargo, 2001). There were findings of increased blood flow in the bilateral occipital lobe. Depression severity was

negatively correlated with hypoperfusion in the left ventral anterior cingulate cortex and positively correlated with hypoperfusion in the left inferior prefrontal gyrus and increased flow in the right associative visual cortex (Li et al., 2018).

Panic disorder. SPECT imaging has indicated hypoperfusion in the bilateral frontal lobes in patients with panic disorder, accompanied by a relative increase in perfusion in the right medial and superior frontal regions (Camargo, 2001; Eren, Tükel, Polat, Karaman, & Ünal, 2003). In patients subject to lactate-induced panic attacks, where CT imaging did not reveal the brain's structural abnormalities, there was a significant asymmetry between right and left inferior frontal cortices in panic disordered patients. Also observed were flow increases in the left occipital cortex and hypoperfusion in the bilateral hippocampal regions (De Cristofaro, Sessarego, Pupi, Biondi, & Faravelli, 1993).

Anxiety disorders. Meta-analyses of case-controlled studies of anxiety and depression show higher anterior cingulate cortex perfusion during activation tasks than baseline at-rest flow as a consistent result. This perfusion is consistent under activation conditions across a wide variety of psychopathology, as well as increased rCBF in the postcentral gyrus, parahippocampal cortex, and midbrain (Kaczkurkin et al., 2018).

However, Andreescu et al. (2011) found increased blood flow in the right insula, bilateral amygdala, and temporal-occipital association areas in healthy older adults during worry induction paradigms (repeated rehearsal of individualized statements of an anxiety-provoking nature) compared to at-rest states. Older adults with generalized anxiety disorder showed similar increased blood flow over the rest state in the temporal-occipital association areas when given the worry induction protocol, but no significant increases

were noted in the insula or amygdala. In a worry suppression protocol (individuals instructed to engage in a pre-determined individualized replacement behavior), blood flow increased in the prefrontal cortex and dorsal anterior cingulate cortex in healthy older adults. However, no significant changes were noted in anxious older adults.

Therefore, blood flow differences in anxiety are subject to nuance, and the experimental paradigm must be carefully designed and interpreted for meaning, as shown by Andreescu's results. The evidence, however, persists that in anxiety, anterior cingulate abnormalities begin early in development (Kaczkurkin et al., 2018). Kaczkurkin at al. (2016) found increased rCBF in the left amygdala, bilateral insula, and left fusiform gyrus in adolescents scoring higher in state and trait anxiety. Compared to Andreescu et al.'s (2011) finding of no increase in blood flow in the insula and amygdala in older adults with GAD, this finding may indicate a developmental change or habituation; it is not apparent that blood flow patterns in anxiety are pervasive and stable throughout development.

SPECT imaging was used to evaluate select serotonin reuptake inhibitor (SSRI) treatment for social anxiety disorder. SSRIs in medicated patients led to significant hypoperfusion in the left temporal and left mid-frontal cortices and the left cingulum (Van der Linden et al., 2000).

Related Studies

Kaczkurkin et al. (2018). This Philadelphia Neurodevelopmental Cohort study used MRI-CASL (3 Tesla) imaging to compute resting-state CBF in 1042 youths aged 11 to 23 (mean age = 16.1 years; 468 males; 45% Caucasian; 12% on psychiatric medication; 27% typically developing). A common phenotype measured by rCBF

variation across psychiatric disorders was sought as measured by a modified version of the Kiddie Schedule for Affective Disorders and Schizophrenia.

Statistical analysis was by confirmatory bifactor analysis (CbFA), which yielded four orthogonal dimensions of psychopathology (anxious-misery, psychosis, externalizing behavioral, and fear) and a fifth common factor (overall psychopathology). CbFA is similar to a standard confirmatory factor analysis with the restriction that each test item (the pathology symptom endorsements) loads on the single common dimension (overall psychopathology) and at most one orthogonal secondary dimension (anxiety-misery, psychosis, behavior, or fear). The CbFA model included covariates for demographics (age, sex, and interactions) and data quality (motion in the scanner) at $p <$ .001. An additional analysis was made for functional connectivity based on the anterior cingulate cortex as seed (a seed is a reference ROI subtracted from all other ROI before statistical analysis) for 833 subjects who also underwent fMRI resting-state imaging in addition to CASL (Kaczkurkin et al., 2018).

Results indicated that elevated CBF in the anterior cingulate cortex (dorsal and rostral portions), right postcentral gyrus, parahippocampal cortex, and midbrain are associated with overall psychopathology in youths, with significant negative associations between (rising) age and (declining) perfusion in many regions. In addition, age by gender interactions was significant, with perfusion decreasing in males with age but holding steady or decreasing in females. A sensitivity analysis removing those persons on psychopharmaceutical drugs showed equivalent results.

Specific findings related to psychopathological symptoms found psychotic symptoms correlated with the reduced flow in the left frontal operculum and insula and

fear associated with reduced perfusion in the right occipital lobe, fusiform gyrus, and the left subgenual portion of the anterior cingulate cortex. In the seed-based connectivity analysis, higher psychopathology levels were associated with reduced connectivity bilaterally between the dorsal anterior cingulate cortex and the caudate and supramarginal gyrus unilaterally with the right thalamus and putamen; increased connectivity was found with the dorsomedial PFC.

Strengths. Kaczkurkin et al. (2018) have many features that make the results robust and generalizable to the young adult population, including the large cohort size, the examination of age and gender as covariates, and the psychopathology measure's dimensional nature. The use of a clinical sample makes the result immediately generalizable, and CbFA methodology estimated shared variance across perfusion differences common to general psychopathology and differences related to specific pathologies. Thus, participants with comorbidities were still analyzable. Rather than just controlling for the shared variance, the CbFA allowed quantification on a dimensional scale.

Weaknesses. Kaczkurkin et al. (2018) was a cross-sectional design, reducing the opportunity to note within-subject perfusion changes and psychopathological progression. The young age of the mixed clinical/non-clinical sample limits generalization to adults. The use of fMRI and MRI CASL imaging was expensive and possible due to generous funding and a medical university training environment; the cost for over a thousand participants may be around USD 250,000 per hour of scanner time, and that limits practical health applications. Effect sizes were small (.11 to .18); replication may be unlikely. The small effect sizes may also be related to the MRI

methodology, which typically has smaller effect sizes due to large signal-to-noise ratios and low sensitivity. Also, regions of significant difference are very isolated and specific, which makes generalizability less likely.

Translation to the present study. In Kaczkurkin et al. (2018), the implication of increased anterior cingulate cortex perfusion in general psychopathology indicates the limbic system may emerge as one of the primary factors in our current analysis. Moreover, the anterior cingulate has been implicated in cognitive control, reward-based decisions, and affect regulation and is a linchpin between unit three (programming, regulation, and verification of activity) and unit one (activation and tone regulation) in the Lurian model. The anterior cingulate embodies affect modulation.

The increased perfusion in the right postcentral gyrus, parahippocampal cortex, and midbrain indicated that the perfusion variance within psychopathology spreads across the limbic system, parietal, and medial temporal lobe, which aligns with the hypothesis of our present study. Findings of decreased perfusion in males with increasing age versus level or decreasing perfusion in females indicate a possible confound to be examined in our present study.

Summary

In this preamble to the experiment, we laid out the state of the science in neuroimaging of regional cerebral blood flow, examined statistical approaches to the large amounts of data generated in a study of resting-state blood flow, and examined the clinical utility of knowledge to be gained from resting-state studies in pathological samples. We reviewed the published literature in detail in these areas, particularly in neuroimaging and SPECT, neuroanatomy of the regions to be studied, biological

mechanisms that cause changes in cerebral blood flow, and experimental paradigms in resting-state blood flow studies. We will now address the purpose and hypotheses of the current study.

Purpose of the Study

The purpose of this study is to derive the latent constructs underlying resting-state rCBF in a large clinical outpatient sample with mixed neuropathology and psychopathology. Corollaries to this purpose are: First, we wish to demonstrate that SPECT neuroimaging is an economically feasible alternative to other neuroimaging modalities, which is vital to realizing the widespread clinical use of neuroimaging in neuropsychological and neuropsychiatric settings to diagnose and monitor treatment efficacy in these disorders.

Second, the results will provide a generalizable pattern of resting-state regional blood flow associated with neuropathology and psychopathology, useful in direct clinical comparisons to assess and diagnose, and in research to compare against subjects with specific pathologies, comorbid pathologies, and healthy normal subjects.

Third, the results will provide a summary of resting-state cerebral perfusion connectivity relationships that will supplement metabolic and functional neuroimaging in PET and fMRI research, adding multimodal replication to substantiate the validity of resting-state brain behavior.

Hypothesis

It is hypothesized that factor analysis of at-rest SPECT rCBF in a clinical sample will reduce the 67 measured ROI variables into a latent three-factor structure. Together, these three factors are predicted to describe 80% of the variance in rCBF blood flow at

rest, with the remaining 20% of variance attributable to noise or error. In general terms, the three factors will represent higher integrative functions, emotional and salience functions, and input-output functions.

The first factor, higher integrative functions, including attention and executive control, was loaded by ROI variables from the prefrontal cortex (inferior, middle, and superior frontal gyri), the cingulate gyrus (anterior, mid, and posterior), the medial temporal lobe (parahippocampal/hippocampal formation), the parietal areas (superior gyrus, inferior parietal lobule, and precuneus), and occipital lobe areas (cuneus, calcarine cortex, and superior, mid, and inferior occipital gyri). Each ROI variable will load at greater than .50.

The second factor, emotional and salience functions, was loaded by ROI variables from the subcortical and insular regions (amygdala, cingulate gyrus, insula, parahippocampal/hippocampal formation, pallidum, thalamus, and caudate). Each ROI variable will load at greater than .50.

The third factor, input-output functions, was loaded by ROI variables from the occipital areas (cuneus; calcarine cortex; lingual gyrus; and superior, middle, and inferior occipital gyri), auditory cortex (superior temporal gyrus), and sensorimotor areas (Rolandic operculum, supplementary motor area, postcentral gyrus, and precentral gyrus). Each ROI variable will load at greater than .50.

Justification for the Hypothesis

Empirical support. Given the lack of research using resting-state rCBF data from a clinical sample to analyze common patterns of blood flow, empirical support for the hypothesis was partially derived from the results of Szabo et al. (1992), which found, in a

factor analysis of a tiny sample of healthy PET scans, that two factors emerged: a limbic factor, characterized by frontal, temporal, limbic, and basal ganglia ROI loadings, and a sensorimotor factor, loaded by ROI of parietal and occipital lobes and the cerebellum.

The hypothesis's three-factor structure stems from the two factors determined by Szabo, combined with the findings of fMRI research in at-rest research participants. Resting-state studies in fMRI are well replicated and have very consistent results, showing that persons at rest metabolize almost as much energy in the brain as those at a task (about 80-90%; Raichle, 2011). Raichle (2015) reviewed past research supporting the existence of a resting-state DMN with activity occurring in the absence of external stimuli in the ventral and dorsal medial prefrontal cortices, the posterior cingulate cortex and precuneus, the lateral parietal cortex, and the entorhinal cortex, as well as the parahippocampal gyrus and hippocampal formation.

In addition, Zhang and Raichle (2010) found that other resting-state networks exist dependent upon experimental paradigms, as at-rest states vary greatly in designs, and the internal activities of participants vary. In addition to the DMN, other networks include attention, executive control, sensorimotor, visual, auditory, and salience. This work was replicated by Yeo et al. (2011). Given the experimental conditions of at-rest in the current study, in a quiet, dimly lit room without sensory blocking measures, the participant was expected to use all these networks at some point. Noises may be heard, activating the auditory, salience, and attention networks; in the absence of an assigned task, the participant may engage in self-speech, planning, fine motor movements, visualization, and autobiographical recall.

Thus, the hypothesis reflects three factors that include the areas activated by not

just one but seven at-rest networks. In fMRI imaging, the repetitive acquisition of data over short time intervals allows these networks to be separated with signal analysis, but in the case of SPECT imaging, all the influences of the seven may be seen, combined, within the affected ROIs, as measured by rCBF.

Clinical and scientific significance. This study is useful to clinicians and researchers for several reasons. First, there are presently no empirically supported or standardized templates for rCBF in clinical patients. Measuring the resting state of blood flow in the brain allows the clinician to view the patient's physiological and mental functioning because blood flow represents neuronal activity; it is analogous to the general practitioner assessing health with blood pressure and pulse rate. Standards and norms are necessary to establish the range of healthy behavior and function, but patterns for unhealthy states are also needed. Comparing resting-state neuropathological or psychopathological rCBF will allow assessment of degree and type of pathology. Through the factor analysis of rCBF, this study provides a normative template for clinical outpatient rCBF to allow for these comparisons.

A second feature that makes the present study important to clinicians and researchers is that the sample size is large and diverse enough to generalize to U. S. clinical outpatient populations. Although exploratory, and confirmatory analysis is necessary for generalizability, the wide range of outpatients provides a foundation for the later confirmatory steps. The size of the current sample is unparalleled by past research with either healthy or pathological samples.

A third significant aspect is that this study is a step towards advancing the science beyond the at-rest healthy brain to the pathological brain's at-rest blood flow patterns.

Without a process of model-building and testing, there is no way to study rCBF and diagnosis of pathology methodically.

If the exploratory factor analysis (EFA) does not provide an adequate model (or if it lacks parsimonious interpretation), it may signify that a pattern does not exist, but more likely, it suggests underlying assumptions procedures may not be appropriate. Several robust analysis techniques are included to maximize replicability. Choice of the number of factors to be used post-extraction was checked by Velicer's test and parallel analysis, using large numbers of bootstrap-type sample-with-replacement analyses to establish the reliability of the quantity selected.

Another obstacle in the interpretation of results is potential confirmation bias given previous research results. Although other researchers' work necessarily informs the hypothesis, these studies' weaknesses and differences are thoroughly reviewed. There is no study equivalent to the present study, and results may vary from the literature based on differences in imaging method, pathology of the sample, and analysis techniques.

CHAPTER III: METHOD

Sample

A deidentified archival neuroimaging database of 15,777 clinical adult patients who underwent SPECT imaging in six U.S. clinics between 1992 and 2013 and consented to research was studied. Of the 15,777, a subset of 3,498 cases did not undergo at-rest SPECT imaging for unknown reasons (i.e., they were imaged during activation tasks only) and were excluded from the study, leaving 12,279 cases for analysis (Table 12).

Table 12

Database Description: Demographics

Descriptor	Proportion (%) or *M*(*SD*)
Total participants	12,217
Race (Caucasian)	65.2
Gender (Male)	58.3
Geographic Location (Pacific U.S.)	62.2
Age (years)	40.58 (16.12)

An additional 62 cases had missing values for 26 of the 67 measured ROI. These cases were deleted listwise (rather than imputed) because the underlying reason for data omission was not known and imputation of such a large proportion of data left incomplete for unknown reasons appeared to offer more risk than reward. Only .5% of total cases were affected, and pattern analysis indicated missing cases were randomly distributed across other variables such as clinic location, date of assessment, gender, age, and race.

In addition, Little's missing-completely-at-random (MCAR; Enders, 2010)

maximum likelihood test was employed to evaluate mean, variance, and covariance differences between the observed (n = 12,217) and complete data (n = 12,279, representing the observed plus expectation maximation [EM] algorithm imputed missing data). If Little's test is significant, the null hypothesis that missing data are MCAR is rejected. Little's test was not significant, $\chi^2(995) = .000$, $p = 1.00$, failing to reject the null that removed data are MCAR. Thus, listwise deletion of these presumed MCAR cases appeared to have minimal possibility of biasing the remaining data. Listwise deletion left 12,217 cases with complete ROI variables for analysis.

Clinic psychiatrists made diagnoses for each participant (Table 13) by integrating clinical interview and history, the Structured Clinical Interview for DSM-IV (SCID-I; or else the current version at the time of assessment; First, Spitzer, Gibbon, & Williams, 1996), Brief Symptom Inventory from the Symptom Checklist (SCL-90; Derogatis, 1994), Beck Depression Inventory (BDI-II or current version; Beck, Steer, & Brown, 1996), and WebNeuro assessment software (Silverstein et al., 2007). Diagnoses indicated frequent comorbidities.

Table 13

Database Description: Diagnoses

Diagnostic Group	Proportion (%)
Mood Disorders	65.4
Anxiety Disorders	57.4
Disorder Diagnosed in Childhood	54.5
Brain Trauma	38.5
Substance Disorder	17.6
Dementia	5.9
Schizophrenia or Psychotic Disorder	4.5

Variables

SPECT imaging data were grouped into 67 ROI including 33 bilateral ROI pairs and the cerebellar vermis per the Automated Anatomical Labeling (AAL) Merged Brain Atlas, and then additionally sub-grouped into eight generalized brain structures (Table 14). Since these eight larger structures are not canonically defined (for instance, the amygdala and the hippocampus may be considered part of the temporal lobe or, alternately, of the limbic system), the analysis focuses on the full 67 ROI variables and the eight regions are used only to supplement interpretation.

Table 14

Variables

Major Brain Structure	Constituent Regions (67 variables)
Limbic System	Amygdala, parahippocampal/hippocampal formation; cingulate gyrus (anterior, mid, posterior)
Basal Ganglia	Caudate nucleus, pallidum, putamen, thalamus
Frontal Lobe	Olfactory cortex; superior, middle, & inferior frontal gyrus; gyrus rectus; paracentral lobule
Temporal Lobe	Superior, middle, & inferior gyri; superior and mid pole; amygdala; parahippocampal/hippocampal formation; fusiform gyrus; Heschl's gyrus
Motor-Sensory Area	Precentral gyrus; Rolandic operculum; supplementary motor area; postcentral gyrus
Parietal Lobe	Supramarginal gyrus; angular gyrus; precuneus; superior & inferior parietal gyri
Occipital Lobe	Calcarine cortex; cuneus; lingual gyrus; superior, middle, & inferior gyri
Cerebellum	Cerebellum, cerebellar crus, cerebellar vermis

Procedure

Data acquisition. The following information is generalized, as the 20-year scope of data collection encompassed multiple hardware and software configurations. Each participant underwent SPECT imaging in an at-rest state: the participant sat upright in a quiet, dimly lit room with eyes open for at least 10 min, then was injected with age- and weight-adjusted dosage of Tc99m-HMPAO. Image scanning took place 30 min later using a high-resolution Picker Prism 3000 triple-headed gamma camera with fan beam collimators. Acquisition parameters were set to voxel size 2.16 mm x 2.16 mm x 6.48 mm, in 128 x 128 x 29 matrices, yielding 120 axially sliced images per scan, with each image separated by 3 degrees, spanning a total circumference of 360 degrees.

Preprocessing- attenuation. Images were corrected for gamma-ray attenuation in brain tissue using general linear methods during filtered back projection (Chang, 1978). The Chang method is a multiplication of each pixel by a correction coefficient computed as the average attenuation of all projections passing through that pixel, the distance the projection passes through tissue, and the constant of attenuation for tissue type.

Preprocessing- reslicing/reconstruction. All images were reconstructed and resliced to match the fixed MNI-305 standard adult brain template and to smooth abrupt transitions, resulting in a 79 x 95 x 68 matrix with voxel sizes of 2 mm x 2 mm x 2 mm with 8 mm full-width, half-maximum (FWHM) isotropic Gaussian kernel smoothing. Smoothing compensates for anatomical variability and improves the signal-to-noise ratio in exchange for a loss in precision; an 8 mm kernel used on a 2 mm square pixel implies the averaging of up to four neighboring pixels in any direction. The axial slices were compiled into a three-dimensional structure with coronal and sagittal slices (i.e.,

computerized tomography) using imaging camera proprietary software.

Preprocessing- warping and registration. SPM software (Wellcome Centre for Human Neuroimaging, https://www.fil.ion.ucl.ac.uk/spm/; versions SPM-96, SPM-99, SPM-2, SPM-5, SPM-8, and SPM-12; Friston, Frith, Liddle, & Frackowiak, 1991) was used to warp (or nonlinearly spatially normalize) data to the MNI-305 template, using the Automated Anatomical Labeling merged atlas for the MNI-305 (AAL; http://www.pmod.com/files/download/v35/doc/pneuro/6750.htm#o6752). Registration (a linear transformation) then optimized goodness-of-fit with a 12-parameter affine transformation (adjusting for translation, rotation, scaling, and shear.) Goodness-of-fit was determined by minimizing the residual sum-of-squares between scan and MNI template (Ashburner & Friston, 1999).

These processed images created a graphical picture of individual brains; however, the current study relied on the associated numerical T-99m tissue deposit values (representing rCBF) for analysis. These numerical values are unitless quantities with meaning only relative to one another.

Statistical analysis. Factor analysis for data reduction was selected for three reasons: First, it is the appropriate statistical method to discover latent variables hypothesized to underlie cerebral blood perfusion patterns (with blood perfusion representing neural activity through coupling). Second, reducing data to fewer factors reduces family-wise error (FWE) in statistical manipulation of massive data points. Third, ROI tissue and vasculature are continuous throughout the brain, so blood flow is inherently highly correlated between neighboring regions. Factor analytic techniques combine highly correlated variables into factors, and rotational transformations allow

these factors to be expressed as uncorrelated (orthogonal) or correlated (oblique) factors.

EFA, confirmatory factor analysis (CFA), and principal components analysis (PCA) are the most frequently encountered among analysis techniques. CFA is not an appropriate method because there are no previous studies of the factorial nature of rCBF in the human brain, and CFA is reserved for hypothesis testing when good evidence already exists for a particular result.

EFA employs numerical computation to extract the latent dimensions (underlying constructs of the common variance that are not directly measurable) that account for the variance in a data set not otherwise attributable to error. Variance in a variable is classifiable as common (shared with at least some other variables), unique (specific to only one variable), and error (random, unreliable, and attributable to a specific variable) variance. Unlike PCA, EFA focuses on calculating common variance while allowing unique and error variance to remain in the model (Osborne, 2014).

Given larger error due to background (or white) noise present in neuroimaging, PCA runs the risk of overinflating variance accounted for (VAF) in determining components because all VAF is attributed to those components, and error is ignored. Furthermore, PCA does not seek out latent structure underlying variables but instead (similar to regression) combines observed variables into linear weighted components to establish the data's best representation. EFA computes underlying latent constructs (factors) first, then determines variable loadings on these constructs. Therefore, EFA is the appropriate method for this study.

Extraction. Within EFA, there are several statistically descriptive methods for factor extraction, including PCA, principal axis factoring (PAF), generalized least

squares (GLS), unweighted least squares (ULS), maximum likelihood (ML), and image factoring. PAF in a robust EFA package was selected for this experiment for the following reasons.

First, PCA extraction, as discussed above, is not appropriate for the goals of this study. Second, GLS and ML have underlying assumptions of multivariate normality and outlier sensitivity that are not met in this study. Alpha imaging does not allow for rotation, making interpretation difficult. Third, PAF and ULS (roughly equivalent with minimum residuals or MINRES; Jöreskog, 2003) are appropriate for use with data violating assumptions of multivariate normality (Kaplan, 2009; Osborne, 2014). ULS (minimizes the sum of the squared differences between the observed and reproduced correlation matrices, ignoring the diagonals) is also robust to collinearity and non-normal distributions.

However, only PAF (extracts factors from the original correlation matrix with squared multiple correlation coefficients placed in the diagonal as initial estimates of the communalities) is currently implemented in a robust EFA implementation. PAF was found to be most stable extraction in robust simulations including multivariate outliers (Pison, Rousseeuw, Filzmoser, & Croux, 2003) and PAF gives more reliable results with non-normal data than ML or GLS (Osborne, 2014).

Extraction will therefore be made via PAF, and then the robust and classic EFA results will be compared for differences. In addition, comparisons will be made to a ULS model, since it is generally robust to multicollinearity (Jöreskog, 2003), an inevitable occurrence in the analysis of brain regions that are adjacent and share blood flow, or are similar in functionality and activate simultaneously (Schmitt, 2011; Zygmont & Smith,

2014; Osborne, 2014).

Reliability. To increase reliability of the results, the factor analysis will be bootstrapped, selecting new samples from the 12,217 participants at random (with replacement) over 1000 iterations, then computing confidence intervals (CI) for comparison to key statistics such as loadings. Bootstrapping with replacement exceeds cross-validation in simulations and functions as a smoothing mechanism for replication analysis (Efron & Tibshirani, 1997).

Rotation. The extracted factor analysis results will be first obliquely rotated to capture the expected ROI flow intercorrelations, as expected in actual rCBF (Tinsley & Tinsley, 1987; Zygmont & Smith, 2014; Osborne, 2014). Tinsley and Tinsley (1987) recommend Promax over Oblimin for factor rotation. Promax fits a target matrix to the extracted data using a simple structure, while Oblimin minimizes the sum of the squared variable loadings' cross-products. Because most methods of oblique rotation yield similar results (Tinsley & Tinsley, 1987; Zygmont & Smith, 2014; Osborne, 2014), the Promax will be used and compared to an orthogonal Varimax rotation to verify assumptions.

Selection and interpretation of variables loading on factors will be based on a cutoff of loadings above .50 with consideration of confidence intervals of each loading. The factor analytic literature does not support a clear cutoff for interpretive meaning since this is largely dependent on subjective considerations of the researcher.

As noted by Peterson (2000), factor loadings greater than .30 are typically considered to meet minimal requirements for interpretation (approaching the 10% of variance threshold), and .50 is a general rule-of-thumb for non-empirical significance (representing 25% variance), but these thresholds are not based on empirical research.

Metanalysis of psychological and behavioral research EFAs indicated a third of all studies used the .40 cutoff, while one-fifth used .50 as cutoff for loadings.

Practical significance loading thresholds of |.30| for minimal, |.40| for more important, and |.50| for practically significant loading (Hair, Black, Babin, Anderson, & Tatham, 2006) were recommended based on small sample sizes (for instance, |.50| requires a sample size of 120, while |.30| may be practically significant for a sample size of greater than 350).

Stevens (2002) advised the following criteria for factor reliability based on simulations: Reliable factors should have more than three variables with loadings exceeding .80, four exceeding .6, or 10 exceeding .4 (and n >150); or factors with fewer loadings should have n > 300.

O'Toole and coauthors (2007) remarked that neural research on brain activity attempts to "quantify free-floating variance in neural activation patterns without regard to their source, experimental or otherwise (p. 4)" in post-hoc subjective interpretations of meaning using preconceived ideas of regional brain function. By setting an a priori cutoff value, we hope to limit this phenomenon.

Because this EFA computes bootstrapped confidence intervals for all loadings, each loading selected for a factor will be statistically significant if the CI does not cross zero. Each loading will be of practical significance if it equals or exceeds |.50|. This threshold corresponds to 25% variance in the factor that is accounted by that variable.

Factor selection. This study will compare several methods for selecting the optimal number of extraction factors, including Kaiser's criterion/ Guttman's rule (greater-than-unity eigenvalues), Cattell's scree test, parallel analysis, Velicer's minimum

average partial (MAP) test, Bayesian Information Criterion (BIC), and Next Eigenvalue Sufficiency Tests (NESTs).

In parallel analysis, random data sets are generated using the same sample size and number of variables as in the study to produce eigenvalues. The randomly generated eigenvalues are compared to the PAF-generated eigenvalues, and factors with eigenvalues not exceeding the random values are discarded as random-error factors. Parallel analysis is insensitive to distributional assumptions (Dinno, 2009) but may overestimate number of factors in large samples because the eigenvalues of the random data approach unity (Revelle, 2019).

The R subroutine *fa.parallel* uses minimal residual computed first factor communalities rather than the squared multiple correlations (SMC) for the diagonal of the reduced correlation matrix (as is done in the classic Horn procedure; Horn, 1965), thereby minimizing bias attributable to minor factors in comparisons with random calculated eigenvalues (Revelle, 2019). Factors are extracted (using ULS) until the eigenvalues of the observed data are less than the corresponding random dataset of the same size.

Velicer's MAP (Velicer, Eaton, & Fava, 2000) partials out common variance on a factor-by-factor basis, leaving just unique variance. The minimum point in the derivation represents the number of roots best suited to capture unique variance. MAP consists of running a PCA followed by a comparison of systematic versus nonsystematic variance in the correlation matrix after each iteration of PCA to find best fit.

BIC fits a maximum likelihood function of a statistical model to observed data with a “complexity” penalty for the number of estimated parameters used (in order to

favor simple structure; Schwarz, 1978).

Achim (2017) proposed NESTs as an alternative better-suited method to compute number of factors to be extracted. Achim demonstrated in simulations using 144 parameter sets (including correlated factors that NESTs outperform comparison data (CD), parallel analysis (PA), Mean Average Partial method, and maximum likelihood methods. NESTs use features of CD and PA in 4 different tests that rank $k + 1$ eigenvalues of the observed data against estimated data (1000 iterations). The k factor model is rejected if the $k + 1$ model ranks higher because common variance is still indicated beyond the k model.

According to Pearson, Mundfrom, and Piccone (2013), parallel analysis is the preferred method of determining number of extracted factors given large sample size, large number of variables, and high collinearity of variables, with secondary choice of an information criteria model fit analysis.

Higher order extraction. High factor intercorrelations in the initial rotation may indicate the presence of higher order factors. Extraction of these factors is recommended as standard practice by some **(**Gorsuch, 2015; Thompson, 2010), while it is seen by others as less useful or reliable than the use of extensive replications of EFA and then CFA modeling (Osborne, 2014). Gorsuch posited that higher order factors are implicit in oblique rotations, and should be examined to aid in the understanding of results in most cases. Osborne argued that extraction of higher order factors may capitalize on spurious EFA results.

In the present study, theory may allow for the possibility of higher order factors of blood flow patterns in ROI; if interpretation is made of first-order factors as default

resting states, then higher factors could be indicative of more generalized states of blood flow at rest. Moreover, the inclusion of bootstrapped replications in factor analysis serves as evidence of replicability of the result by randomly resampling from the very large sample. Similarly, use of several empirically supported methods in determining optimal number of factors will lend reliability to the determined factor structure. Spurious results are therefore not expected, and the eight-factor solution is not likely to be unreliable, given these measures. If higher order factors are found, they should be examined for possible meaning.

CHAPTER IV: RESULTS

Preprocessing

All analyses were run using RStudio Version 1.4.1106. Pattern analysis of missing data in the 12,217 cases indicated 14.8% of ROI values in the cerebellar vermis were missing, constituting just 0.19% of all ROI values. Multiple imputation using a fully conditional specification linear regression with Markov chain Monte Carlo method (MCMC; Van Buuren, Brand, Groothuis-Oudshoorn, & Rubin, 2006) was used to replace these missing values via 25 imputations of 99 iterations each of MCMC (Enders, 2010). Evaluation of pooled means to original data with missing values revealed that M_{diff} = .37 (*SD* = 3.29, *SE* = .37) was not significantly different (failed to reject the null of no difference), $t(79) = 1.00$, $p = .32$, 95% CI [-.36, 1.10].

Each of the cells represents rCBF for a particular ROI (columns) and participant case (row or vector). Outliers were determined using the minimum covariance determinant (MCD), a robust version of the Mahalanobis distance criteria (Rousseeuw & van Driessen, 1999). In a sample of size *n,* MCD selects all possible subsamples of size 3/4*n* to *n* (to improve the positive breakdown estimator). MCD then computes mean and covariance determinants as affine-equivariant estimators (i.e., not subject to variance under rotation), and then determines outliers using a low breakdown point (thus avoiding the effects of extreme observations on mean and covariance, as when Mahalanobis's distance is used). The minimum determinant from this least-varying subset is then selected, and values above a chi-square cutoff at $p = .001$ are determined to be outliers (FAST-MCD; Leys, Klein, Dominicy, & Ley, 2018).

In other words, in the multidimensional space represented by the 67 ROI

variables, calculating distance from the theoretical center (using Mahalanobis-MCD formulas) reveals a distribution that can be characterized by a chi-square, and a cutoff is preset at a conservative alpha of .001 to identify these outliers. In this case, the numerical cutoff value was 108.53, and 2,425 cases were above MCD cutoff (20% of active cases). Setting the subsample size range from 3/4*n* to *n,* and alpha at .001, are best-practice recommendations based on Monte Carlo simulations (Leys, Klein, Dominicy, & Ley, 2018).

These outliers were the kept in the analysis due to the large proportion of the data (about 20%) that they represented (removal of outliers would reduce the dataset to 9,792 from 12,217 cases). Instead, a robust-to-outliers EFA method using the MCD covariance matrix was selected to detect and minimize the influence of outliers without deletion (Pison, Rousseeuw, Filzmoser, & Croux, 2003; Todorov & Filzmoser, 2009).

The *robustfa* function in R (Zhang, 2013) was selected because it uses the robust MCD covariance matrix and the central half of the multivariate data (repeatedly resampled) to estimate location and scatter as the basis of EFA extraction, rather than the standard EFA parameters based on mean and standard deviation (Table 15).

Each vector (rows representing rCBF pattern per participant) of the 67 columns (each column representing an ROI) were normalized by barycentering. Barycentering is used to scale each vector by the centroid of mass of the data set. This barycenter-scaled vector then represents the minimized weighted sum of the generalized squared Euclidean distances from each vector to any point in data space (Abdi, 2007; Abdi & Williams, 2010). Each vector was then centered; each vector value was divided by the vector summation, and then converted to a unitless T-score format for ease of interpretation.

Table 15

Regions of Interest (ROI = 67; L = Left, R = Right)

Precentral Gyrus L	Fusiform Gyrus L	Supramarginal Gyrus L
Precentral Gyrus R	Fusiform Gyrus R	Supramarginal Gyrus R
Rolandic Operculum L	Heschl's Gyrus L	Angular Gyrus L
Rolandic Operculum R	Heschl's Gyrus R	Angular Gyrus R
Supplementary Motor Area L	Insula L	Precuneus L
Supplementary Motor Area R	Insula R	Precuneus R
Olfactory Cortex L	Cingulate Gyrus Anterior L	Parietal Superior/Inferior Gyri L
Olfactory Cortex R	Cingulate Gyrus Anterior R	Parietal Superior/Inferior Gyri R
Frontal Superior Gyrus L	Cingulate Gyrus Mid L	Occipital Gyri L
Frontal Superior Gyrus R	Cingulate Gyrus Mid R	Occipital Gyri R
Frontal Middle Gyrus L	Cingulate Gyrus Posterior L	Calcarine Cortex L
Frontal Middle Gyrus R	Cingulate Gyrus Posterior R	Calcarine Cortex R
Frontal Inferior Gyrus L	Caudate Nucleus L	Cuneus L
Frontal Inferior Gyrus R	Caudate Nucleus R	Cuneus R
Gyrus Rectus L	Pallidum L	Lingual Gyrus L
Gyrus Rectus R	Pallidum R	Lingual Gyrus R
Paracentral Lobule L	Putamen L	Cerebellar Vermis
Paracentral Lobule R	Putamen R	Cerebellar Crus L
Temporal Gyri L	Thalamus L	Cerebellar Crus R
Temporal Gyri R	Thalamus R	Cerebellum L
Amygdala L	Postcentral Gyrus L	Cerebellum R
Amygdala R	Postcentral Gyrus R	
Parahippocampal/Hippocampal Formation L		Parahippocampal/Hippocampal Formation R

A check for multicollinearity found only 1 of 4,489 Pearson intervariable correlations (.02%) was greater than or equal to .90. Given the use of robust EFA parameters and collinear-robust ULS extraction, this small proportion of highly correlated values was not expected to be problematic, and the statistical analysis routines did not flag any singularity, not-positive-definite, or collinearity conditions during parametric and matrix analysis.

Multivariate normality of distribution was investigated through Mardia's multivariate chi square distribution tests of skewness and kurtosis (Mardia, 1970). Skew was less than |1.5| for 65 variables. Of the remaining two variables, multivariate skew for the cerebellum left was 2.53 (the univariate skew was .61) while the cerebellum right was 5.90 (univariate skew was 1.25). Kurtosis was less than 4.50 for 65 variables. For the cerebellum left, multivariate skew was 98.91 (univariate kurtosis was 7.00) while the cerebellum right was 272.01 (univariate was 26.28). Multivariate standard error was *SE* = .09, while univariate *SE* = .04 for kurtosis, and .02 for skew. The Mardia multivariate skew value was significant, $b_{1,p} = 618$ with A = 1,258,710 at $p < .001$, supporting a skewed condition. Similarly, kurtosis was significant, $b_{2,p} = 7{,}730$ with a value of B = 1,785 at $p < .001$, indicating a kurtotic condition. Mardia's statistics indicated multivariate non-normality of the data. The multivariate quantile plot indicates a positively skewed distribution (Figure 1).

Univariate statistics were significant, indicating non-normality. The Lilliefors (Kolmogorov-Smirnov) composite test of normality (computing the maximal absolute difference between the empirical and hypothetical cumulative distribution functions for normality) found D = 0.03 at $p < .001$, rejecting the null of a normal distribution.

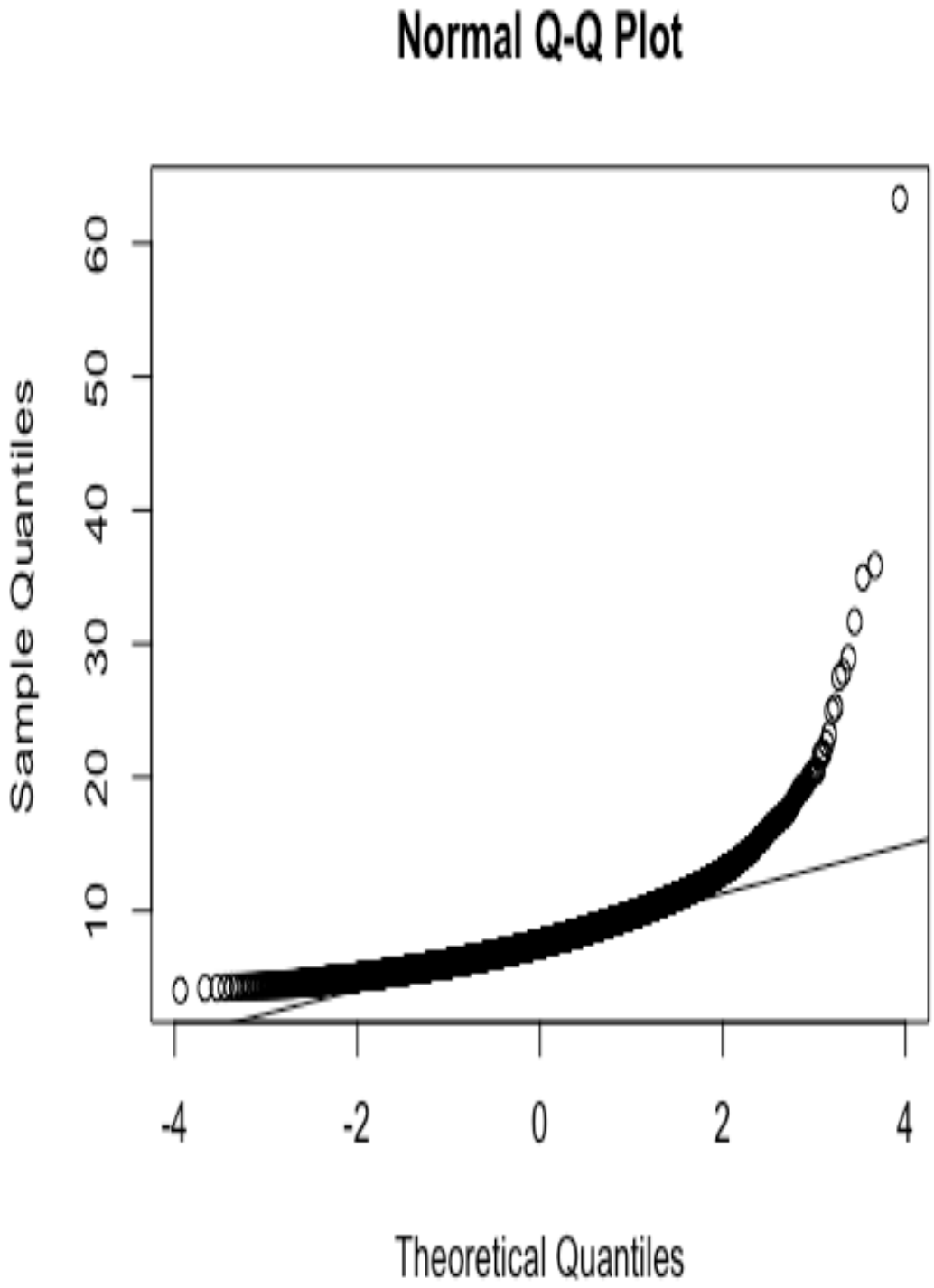

Figure 1. Chi-square Quantile vs. Squared Mahalanobis Distance Quantile Plot

As a second exploration, the Cramer-von Mises normality test found W = 247.38 at $p < .001$, again rejecting the null of normality.

As a third confirmatory investigation, the Anderson-Darling normality test for the composite hypothesis of normality (a comparison of individual means and deviations to the cumulative distribution function of the standard normal distribution) returned a result of A = 1,423.40, $p < .001$, also rejecting the null.

Variable histograms revealed gross univariate normality (as would be expected per the central limit theorem). Figure 2 shows worst-case examples of univariate skew and kurtosis in the cerebellum, demonstrating the positive skewness found in the Mardia statistics, but also indicating that the right tail of the histogram is extended, representing very few cases in frequency, and is not likely to be of significant influence. However, the use of robust factor analysis tolerates multivariate and univariate non-normality. Similarly, use of ULS or PAF extraction is appropriate because ULS is not reliant on assumptions of normal distribution, and PAF is relatively immune to non-normality at large samples in a well-defined model (Osborne, 2014; Zygmont & Smith, 2014).

The central limit theorem states that, from a population of mean μ and standard deviation σ, large random samples drawn from the population (with replacement) will be approximately normally distributed, regardless of whether the population is normal or skewed, provided the sample size is sufficiently large (greater than $n = 30$). This theorem suggests that non-normality would be of little consequence in the case of the current sample size. Moreover, some univariate tests, such as the Shapiro-Wilk test, have little meaning with large sample sizes due to extreme sensitivity, and typically return a result of significance for even minor normality deviation in large samples (Field, 2009).

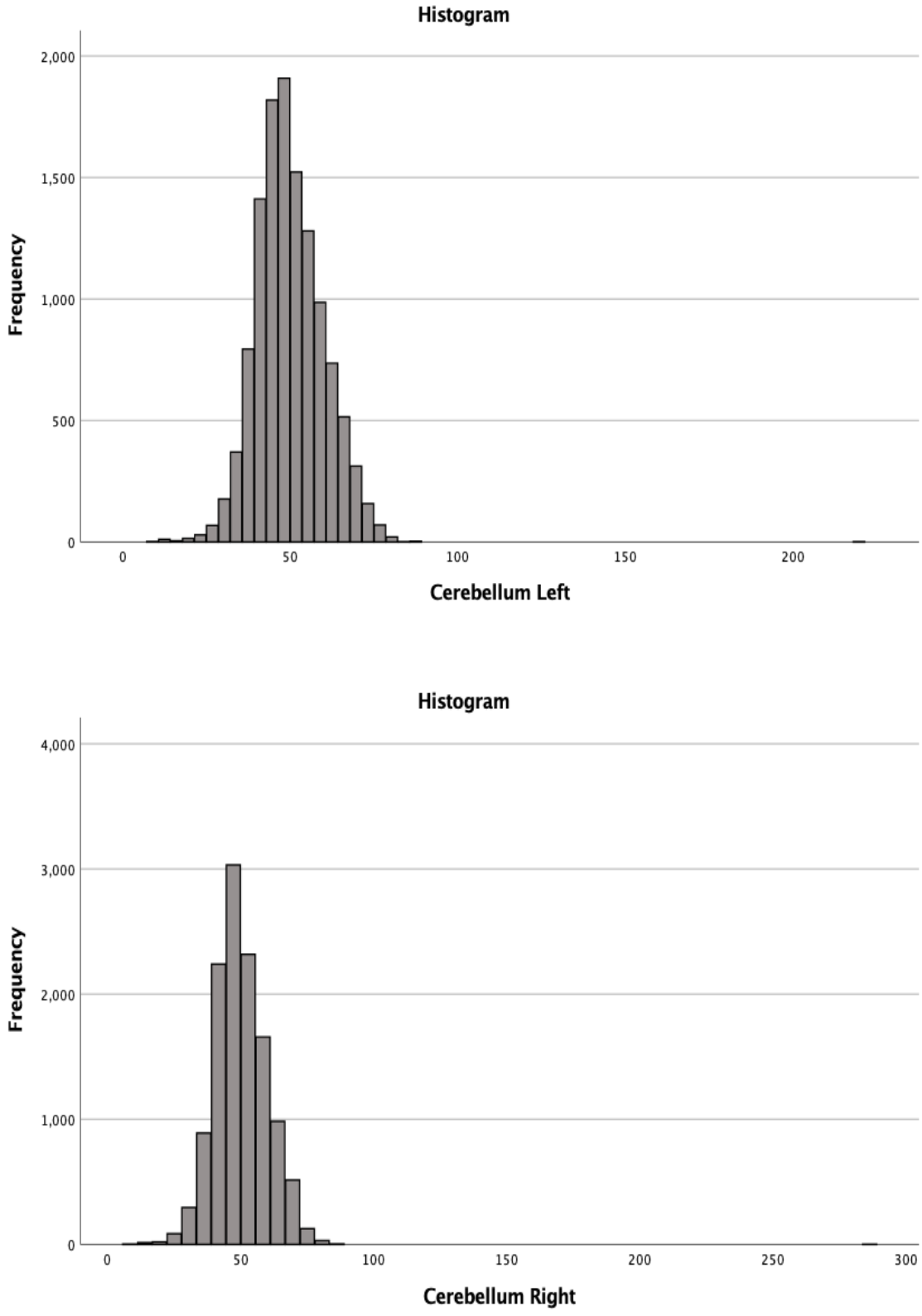

Figure 2. Histograms: Cerebellum- Left and Right

Participant Characteristics

The 12,217 participants ranged from 18 to 94 years in age (M = 40.58, SD = 16.12; Figure 3) and were more male (58.3%) than female (41.6%).

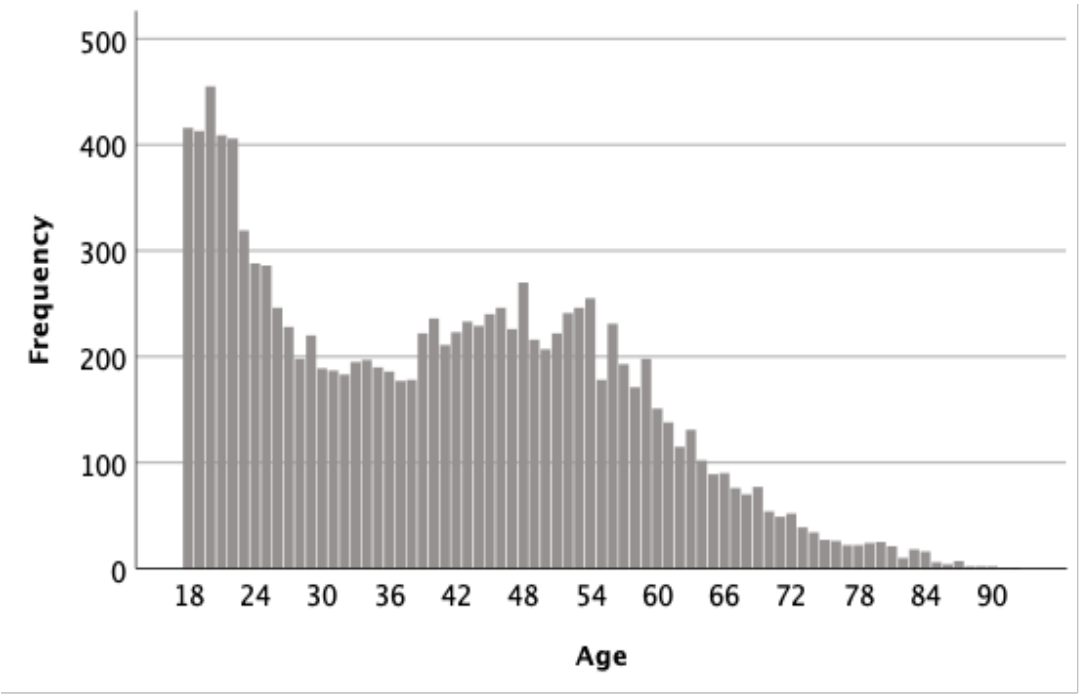

Figure 3. Age distribution (n = 12,217)

Age and gender. To further investigate the influence of age and gender on rCBF, a general linear model (MANOVA) was constructed (gender: male or female, by age: oldest, older, middle age, younger, youngest) with planned comparisons of rCBF differences by age level. Significance of Box's Test of Covariance [Box's M = 45236; F(18720, 8.7E7) = 2.36; p < .001] and Levene's Test of Equality of Errors ($p \leq .001$) indicated conservative interpretation was in order due to possible unequal covariance and variance. The multivariate omnibus was significant for age [Pillai's Trace = .04; F(268, 12217) = 1.84; p < .001], gender [Pillai's Trace = .44; F(134, 24436) = 52.1; p < .001], and interaction [Pillai's Trace = .10; F(536, 97736) = 2.24; p < .001].

Contrasts (ANOVA) showed age significance in the gyrus rectus-L (youngest to oldest levels), amygdala-R (middle, older, and oldest to youngest levels), parietal superior-inferior gyri-R (between all age levels), calcarine cortex-R (older and oldest to youngest levels), and bilateral putamen (older and oldest to youngest levels; $p < .001$). In gender, significant differences occurred in most ROI (except for the gyrus rectus-R, bilateral paracentral lobule, bilateral fusiform gyrus, and calcarine cortex-R; $p < .001$). Notably, there was no clear pattern as to which gender had higher values of rCBF: 28 of the ROIs had higher values in males, and 30 were higher in females.

In the interaction of both age and gender, significant differences were found in the frontal superior/middle gyrus bilaterally (younger and male had higher values than older and female individuals), insula-L (rCBF peaked in middle-aged women more than in men), putamen-R (rCBF increased with age in each sex, but started much lower in men than in women), postcentral gyrus-R (rCBF declined with age in both men and women, but values overall were higher in men and declines in both sexes leveled off after middle age), and the parietal superior/inferior gyri-R (younger and male had higher values than older and female individuals).

Race. Most participants self-reported their race as Caucasian (65.2%). For almost a quarter of the sample that declined to specify, no data was supplied on race for unknown reasons, so additional analysis of race-based differences was deemed to be not meaningful. Exploratory analysis (ANOVA) indicated if the Caucasian sample is compared to the Unknown classification, there is no significant difference across all ROIs. Conversely, if the Caucasian (n = 7,961) and African American (n = 124) samples are compared, 28 of 64 ROI are significantly different, with note to the large sample size

discrepancy that points to this finding as unreliable. However, if the Unknown group is assigned to any other racial category, the significant differences disappear (Table 16).

Table 16

Race Breakdown (n = 12,217)

Race	Frequency	Percent
Caucasian	7961	65.2
Unknown	2915	23.9
Hispanic	332	2.7
Other	251	2.1
Asian	195	1.6
Caucasian/Hispanic	135	1.1
African American	124	1.0
Arab/Middle Eastern	85	0.7
Asian/Caucasian	75	0.6
Caucasian/Native American	52	0.4
Indian	51	0.4
Caucasian/African American	18	0.1
Native American/Eskimo	15	0.1
Hispanic/African American	5	<.1
Hispanic/Native American	2	<.1
Declined to specify	1	<.1

Location. Geographical distribution indicated 36.8% of participants were imaged at clinics on the East Coast, with the remainder on the West Coast. Although locations of imaging assessments are known, the origins of patients were not collected, and many outpatients may have traveled long distances or internationally for imaging services.

Diagnostic groups. Typical participants were referred for SPECT imaging by self or medical providers for diagnostic clarification and treatment recommendations related to a suspected psychiatric or a neurological disorder. Diagnoses were made based upon intake assessments, clinical interview, and imaging data by licensed medical professionals and are categorized in Table 17.

Table 17

Diagnostic Classifications

Diagnostic Category	Quantity	Percent
Mood Disorder	7726	65.7
Anxiety Disorder	6757	57.4
Childhood Disorder	6434	54.7
Traumatic Brain Injury	4555	38.7
Substance Abuse Disorder	2096	17.8
Dementia	679	5.8
Psychotic Disorders	531	4.5

Comorbidity of diagnoses is indicated in Table 18. The largest proportion of participants (almost a third) have three comorbidities, with approximately another third having two comorbidities.

Table 18

Comorbidities

Number of Diagnoses	Quantity	Percent
0	930	7.9
1	1581	13.4
2	3292	28.0
3	3646	31.0
4	1905	16.2
5	399	3.4
6	10	0.1

The number of comorbid diagnoses was examined for effect on ROI blood flow. For seven levels of the number of diagnoses (0 to 6) as independent variable, the omnibus was significant [Pillai's Trace = .07; $F(384, 70188) = 2.20$; $p < .001$]. Table 19 lists the ROI with significant rCBF mean difference using univariate planned contrasts. The mean rCBF for each ROI differed significantly for the stated number of comorbidities versus individuals with no diagnosis.

Variance between diagnostic categories was examined a priori using discriminant analysis using seven diagnostic categories. The 64 ROI (dependent variables) in linear combination successfully discriminated each of the diagnostic categories (independent variables) as a single variate. This a priori investigation showed some effect of specific neurological and psychiatric disorders on rCBF and is to be considered in the interpretation of the factor analysis.

Table 19

Number of Diagnoses for Significance (p < .0008) in rCBF as Compared to No Diagnosis

Region of Interest	# Diagnoses	Region of Interest	# Diagnoses
Rolandic Operculum L	2	Pallidum L	5,6
Olfactory Cortex R	2	Pallidum R	5,6
Frontal Sup/Middle Gyrus L	4,5	Putamen L	5,6
Frontal Sup/Middle Gyrus R	4,5	Postcentral Gyrus R	4
Amygdala L	4,5	Angular Gyrus L	5
Amygdala R	4,5	Angular Gyrus R	5,6
Para-/Hippocampal Formation L	4,5	Precuneus R	5
Para-/Hippocampal Formation R	4,5	Parietal/Sup/Inf Gyri L	4,5
Heschl's Gyrus L	1,2	Parietal/Sup/Inf Gyri R	4,5
Insula R	2	Occipital Gyri Sup/Mid/Inf L	5,6
Cingulate Gyrus Anterior R	4,5	Occipital Gyri Sup/Mid/Inf R	5,6
Cingulate Gyrus Mid L	5	Calcarine Cortex R	5
Cingulate Gyrus Mid R	5	Lingual Gyrus L	4
Cingulate Gyrus Posterior L	4,5	Lingual Gyrus R	4,5
Cingulate Gyrus Posterior R	4,5	Cerebellar Crus L	5
		Cerebellar Crus R	5

Table 20 shows effect size as the squared canonical correlation for the variate; the full structure matrix is not displayed due to space limitations.

Table 20

Discriminant Analysis Variates

Diagnostic Category	Effect Size	Wilk's λ	χ^2 (p<.0001)
Mood Disorder	.02	.98	254.6
Anxiety Disorder	.03	.97	355.6
Childhood Disorder	.05	.95	610.6
Traumatic Brain Injury	.03	.98	299.4
Substance Abuse Disorder	.04	.96	448.0
Dementia	.09	.91	1150.6
Psychotic Disorders	.01	.99	170.7

Variable Correlations/ Goodness of Fit

The ROI rCBF correlation matrix (too large for tabular presentation) indicated strong Pearson correlations of $|r| \geq .80$ between the left and right hemispheres in 10 bilateral ROI: supplementary motor area, frontal superior and middle gyrus, gyrus rectus, paracentral lobule, anterior cingulate gyrus, middle cingulate gyrus, thalamus, superior/inferior parietal gyri, superior/middle/inferior occipital gyri, cuneus, and cerebellar crus. Other strong ROI rCBF intercorrelations (r >.80) included the putamen-L to pallidum-L, postcentral gyrus-L to precentral gyrus-L, and postcentral gyrus-R to precentral gyrus-R; these ROI are noted to be contiguous in location and function. As discussed elsewhere, only one intervariable correlation exceeded .90.

On the other hand, weak correlations ($|r| \leq .20$) were found in about a third of the 2,048 ROI rCBF correlations; in particular, the bilateral ROI of the gyrus rectus, fusiform gyrus, precuneus, cuneus, and cerebellum showed little relationship to other ROI blood flows. Bartlett's Test of Sphericity, a measure of differentiation of the correlation matrix from the identity matrix, was significant and quite large [$\chi^2(2211) = 2{,}436{,}599$, $p < .001$], indicating that correlations were large enough to provide sufficient contrast for dimensional reduction.

The reproduction matrix (correlations resulting from reproduced model-based data rather than the observed data) and the resulting residual matrix (differences between observed correlation and reproduction matrix) showed 5% of residuals with values above .05. Low residuals signify a good fit of model versus observed data. The anti-image correlation matrix approached the identity matrix, with a Kaiser-Meyer-Olkin statistic of .97 for the data before normalization. Thus, the data appeared to be well qualified for factor analysis due to sufficient contrast between squared correlations and partial correlations in the data, indicating high signal (matrix diagonal values) to low noise (off-diagonal values) ratios that are ideal for dimension reduction.

Extraction

Ideal number of extracted factors. The initial eigenvalues of the Pearson correlation matrix prior to extraction appear in Table 21. Pearson correlation is subject to assumptions of normality, and heteroscedasticity may cause distortion in conventional EFA computations, so Table 21 is used here only for the application of Kaiser's rule. The actual MCD bootstrapped covariance values are used in extraction of factors from the robust EFA.

Table 21

Initial Eigenvalues

Factor	EV	VAF	Factor	EV	VAF	Factor	EV	VAF	Factor	EV	VAF
1	22.60	33.74	18	0.65	0.97	35	0.25	0.37	52	0.11	0.17
2	6.61	9.87	19	0.62	0.93	36	0.23	0.35	53	0.11	0.17
3	5.04	7.51	20	0.58	0.86	37	0.22	0.33	54	0.10	0.15
4	3.78	5.64	21	0.53	0.79	38	0.21	0.32	55	0.10	0.15
5	3.03	4.52	22	0.48	0.72	39	0.19	0.29	56	0.10	0.14
6	2.58	3.85	23	0.46	0.69	40	0.19	0.28	57	0.08	0.13
7	1.74	2.59	24	0.44	0.66	41	0.18	0.28	58	0.08	0.11
8	1.73	2.57	25	0.41	0.61	42	0.17	0.26	59	0.07	0.11
9	1.43	2.13	26	0.39	0.58	43	0.17	0.25	60	0.07	0.10
10	1.26	1.89	27	0.37	0.55	44	0.16	0.24	61	0.06	0.08
11	1.19	1.77	28	0.34	0.51	45	0.15	0.23	62	0.05	0.08
12	0.98	1.46	29	0.32	0.47	46	0.14	0.21	63	0.05	0.08
13	0.91	1.36	30	0.31	0.46	47	0.14	0.20	64	0.03	0.04
14	0.89	1.32	31	0.29	0.43	48	0.13	0.20	65	0.02	0.03
15	0.81	1.22	32	0.28	0.42	49	0.13	0.19	66	0.01	0.01
16	0.76	1.13	33	0.28	0.42	50	0.12	0.18	67	0.00	0.00
17	0.73	1.09	34	0.27	0.40	51	0.12	0.18			

Note: Abbreviations: EV = eigenvalue; VAF = variance accounted for

Based on the Kaiser rule-of-thumb, 11 eigenvalues exceeded one and could be considered factors, accounting for 76.08% of total variance (VAF). The first factor accounts for just over a third of total variance.

The scree plot curve of factor versus eigenvalue is shown in Figure 4 with an inflection breakpoint through factors 7 and 8, indicating 6 factors as a solution.

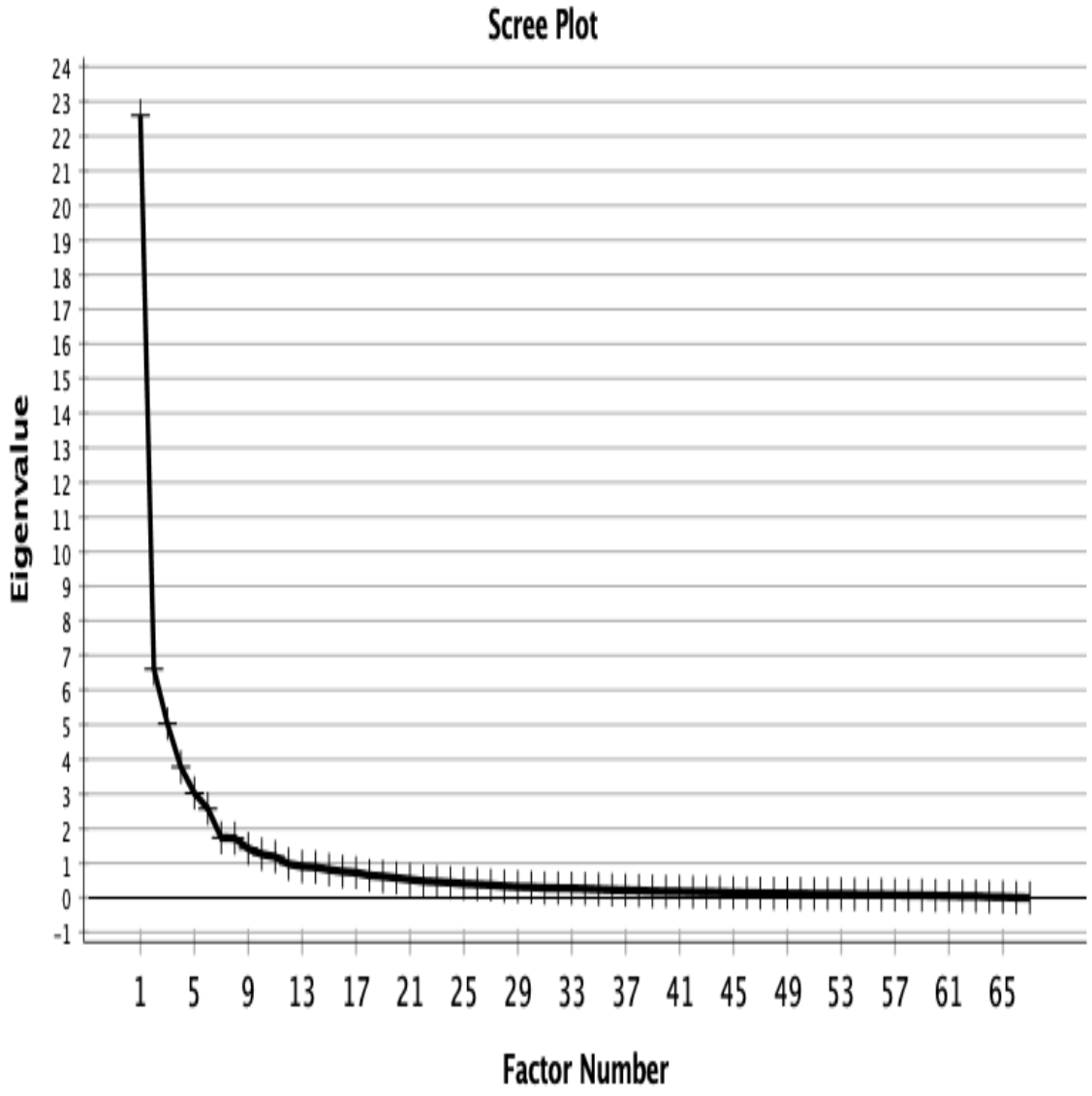

Figure 4. Scree Plot

Velicer's MAP minima occur at $r^2_{partial}$ = .01 at the eighth root and $r^4_{partial}$ = .001 beginning at the sixth root (Table 22), indicating from six to eight viable factors.

Table 22

Average Partial Correlations

Root	Partial Correlation- squared	Partial Correlation- 4th Power
0	0.12	0.032
1	0.04	0.008
2	0.03	0.005
3	0.03	0.004
4	0.02	0.003
5	0.02	0.002
6	0.02	0.001
7	0.02	0.001
8	0.01	0.001
9	0.01	0.001
10	0.01	0.001
11	0.01	0.001
12	0.01	0.001
13	0.01	0.001
14	0.01	0.001
15	0.01	0.001
16	0.01	0.001

Results of parallel analysis indicated eight factors are optimal for extraction. BIC indicated a result of best fit with eight factors at a minimum of -14,375.21 (smaller/ more negative scores represent better fit in BIC). The result of the NESTs was eight factors, consistent with modified (non-SMC) parallel analysis and BIC. Considering the parallel analysis, BIC, and NESTs tests as most reliable and given that they agree, eight factors will be considered for extraction, although the solutions for seven and nine factors will also be examined for interpretive meaning (Pearson, Mundfrom, & Piccone, 2013).

Extraction. Planned factor extractions were conducted of the eigenvalues to determine the eight principal roots using robust PAF (with MCD estimation of center location and scatter), which was then compared to classic PAF (tolerant of non-normality but possibly reactive to outlier dispersion and collinearity) and ULS (with tolerance for multicollinearity). In addition, planned comparisons of the seven and nine factor solutions were made.

Table 23 displays the orthogonally rotated 8-factor solution for both a classic PAF and a ULS against a robust PAF; the three results are very similar. The classic EFAs were bootstrapped with over 1000 iterations to assure reliability, and averaged results are reported. The inference may be made that the classic ULS and PAF are essentially similar procedures when the assumption of data normality is sustained. Although they each begin with different diagonals in the correlational matrix, successive iterations continuously compute closer approximations to bring the margin of difference to a very small number. Osborne (2014) noted similar results in a comparison of ULS to PAF extractions; the results were not significantly different when data were normal, large in sample size, and variables were not excessively collinear.

Table 23

8-factor Solution: Extraction Sums of Squared Loadings (Varimax Rotated)

	Robust PAF		Classic PAF		Classic ULS	
Factor	EV	VAF	EV	VAF	EV	VAF
1	9.72	15	9.75	15	9.65	14
2	7.40	11	7.40	11	7.40	11
3	6.80	10	6.79	10	6.81	10
4	5.30	8	5.28	8	5.34	8
5	5.27	8	5.26	8	5.30	8
6	3.74	6	3.75	6	3.73	6
7	3.34	5	3.35	5	3.34	5
8	2.91	4	2.91	4	2.91	4
Total		66		66		66

Note: VAF = Variance accounted for; EV = eigenvalue

The robust procedure uses a PAF design with the substitution of an MCD-computed correlational matrix in the extraction; again, the similarities in results indicate that outliers have little effect (most likely due to the very large sample size) over averaging of successive iterations of extraction. Additional result presentations will be of the robust PAF extraction only, unless classic ULS or classic PAF show a difference.

Communalities (Table 24) represent the values on the diagonal of the reproduced correlations matrix; the reproduction matrix is computed using data from the model instead of data from the observed cases. The communalities represent the shared common variance attributable to each of the 67 ROI.

Table 24

Communalities- Robust PAF

ROI	Left	Right
Precentral g.	0.73	0.79
Rolandic Operculum	0.52	0.55
Supplementary Motor	0.72	0.78
Olfactory c.	0.55	0.53
Frontal Superior g.	0.81	0.86
Frontal Mid g.	0.82	0.83
Frontal Inferior g.	0.49	0.65
G. Rectus	0.75	0.70
Paracentral l.	0.83	0.77
Temporal g.	0.72	0.78
Amygdala	0.49	0.51
Para-/Hippocampal Form.	0.66	0.70
Fusiform g.	0.48	0.46
Heschl's g.	0.42	0.47
Insula	0.66	0.64
Cingulate g. Anterior	0.69	0.68
Cingulate g. Mid	0.64	0.71
Cingulate g. Posterior	0.64	0.59
Caudate Nucleus	0.61	0.62
Pallidum	0.66	0.67
Putamen	0.64	0.61
Thalamus	0.65	0.65
Postcentral g.	0.77	0.80
Supramarginal g.	0.62	0.73
Angular g.	0.60	0.74
Precuneus	0.74	0.69
Parietal g.	0.83	0.85
Occipital g.	0.83	0.81
Calcarine c.	0.70	0.58
Cuneus	0.73	0.76
Lingual g.	0.56	0.62
Cerebellar Crus	0.78	0.79
Cerebellum	0.55	0.55
Cerebellar Vermis	0.11	

Communalities ranged from a high of 86% of shared variance from the frontal superior gyrus (right hemisphere), leaving just 14% to be accounted for by unique blood flow, associated function, and noise, to a low of 11% in the cerebellar vermis.

In general, communalities were high, with most values higher than .60, and only one value (cerebellar vermis) was under the .32 threshold that equates with 10% overlapping variance (a cutoff attributed to Tabachnick and Fidell in Costello & Osborne, 2005). This indicated good prospects for determining individual ROI networks that are performing semi-synchronously as predicted in the Hypotheses. Lower communalities would be indicative of independently acting ROI and a lack of brain blood flow networks.

Rotation. In the unrotated factor matrix (showing the loadings of the 67 ROI onto respective factors 1-8), the first factor showed loadings of SS = 22.30, which was reduced to 9.75 with rotation, and 65% of the variables loaded above .50 in the unrotated extraction compared to 22% in the orthogonal rotation. offering subjective confirmation that the rotated solution is a better representation of the data; the unrotated factor structure lacked simple structure and interpretability. This is also supported by guidelines from Gorsuch (2015) to maximize recognition of variable clusters during factor extraction. Next, oblique and orthogonal rotations were compared. Table 25 shows sums of squared loadings and proportion of variance for the Promax-rotated PAF analysis of the eight factors. The oblique rotation consisted of a Kaiser-normalized Promax, performed as first an orthogonal Varimax rotation, followed by a Procrustean oblique rotation with exponential power of k=4. The pattern matrix consisted of the loadings on the eight factors.

Table 25

PAF-Extracted Promax-Rotated 8-factor Analysis

Factor	Sum of Squared Loadings	% of Variance	Cumulative %
1	8.67	13	
2	6.94	10	
3	6.91	10	
4	6.24	9	
5	5.52	8	
6	3.88	6	
7	3.18	5	
8	3.13	5	66

Table 26 shows select loadings (due to space limitations) that had a portion of the confidence interval exceeding |.50|, as well as the contralateral analog variable, regardless of loading, for comparison.

Factor 1 represents the parietal lobe regions, showing the loadings and confidence intervals (CI) above |.50|. Factor 1 is reliable by Stevens (2002) criterion of 4 or more variable loadings greater than |.60|. Factor 1 will be labeled as the Parietal factor to reflect its primary loadings.

Factor 2 was loaded by motor-sensory components, again with CI above cutoff of |.50| apart from the postcentral gyrus (particularly in the right hemisphere). Factor 2 is reliable by Stevens' (2002) criterion of 4 or more variable loadings greater than |.60|. Factor 2 is labeled Motor/Sensory factor to reflect its primary loadings.

Table 26

Oblique and Orthogonal Rotations Comparison (Loadings ≥ |.50|)

Factor[a]	ROI	Varimax		Promax				
					99.5% CI			99.5% CI
		Left	Right	Left	Lower	Upper	Right	Lower Upper
1	Supramarginal g.	0.75	0.82	1.09	**0.98**	**1.17**	1.11	**1.00** **1.20**
	Angular g.	0.63	0.66	0.83	**0.74**	**0.90**	0.84	**0.75** **0.90**
	Parietal g.	0.59	0.59	0.67	**0.60**	**0.73**	0.69	**0.61** **0.74**
	Postcentral g.	0.63	0.67	0.63	**0.59**	**0.72**	0.65	**0.58** **0.71**
2	Precentral g.	-0.74	-0.67	0.79	**0.71**	**0.86**	0.64	**0.58** **0.70**
	Supplementary motor	-0.83	-0.87	1.03	**0.93**	**1.13**	1.10	**0.99** **1.19**
	Paracentral lobule	-0.87	-0.81	1.02	**0.94**	**1.09**	0.93	**0.86** **0.99**
	Postcentral g.	-0.60	-0.56	0.50	0.45	0.55	0.42[b]	0.38 0.46
3	Cingulate (anterior)	0.68	0.68	0.70	**0.63**	**0.78**	0.68	**0.61** **0.76**
	Cingulate (middle)	0.68	0.68	0.78	**0.70**	**0.88**	0.77	**0.70** **0.85**
	Cingulate (posterior)	0.68	0.68	0.88	**0.80**	**0.98**	0.88	**0.80** **0.97**
	Occipital g.	-0.73	-0.72	-0.67	**-0.75**	**-0.60**	-0.64	**-0.73** **-0.58**
	Cuneus	-0.65	-0.67	-0.76	**-0.86**	**-0.69**	-0.78	**-0.70** **-0.88**
	Frontal superior g.	-0.56	-0.61	-0.40[b]	-0.48	-0.33	-0.47[b]	-0.55 -0.41
	Frontal middle g.	-0.51	-0.54	-0.30[b]	-0.25	-0.35	-0.35	-0.29 -0.41
	Calcarine cortex	-0.52	-0.05[b]	-0.41[b]	-0.47	-0.37	-0.06[b]	-0.10 -0.02
4	Gyrus rectus	-0.69	-0.68	0.96	**0.80**	**1.08**	0.98	**0.84** **1.09**
	Frontal g. (sup)	-0.52	-0.50	0.53	0.37	0.66	0.48[b]	0.36 0.59
	Frontal g. (mid)	-0.62	-0.59	0.70	**0.51**	**0.73**	0.65	**0.55** **0.82**
	Frontal g. (inf)	-0.47[b]	-0.43[b]	0.63	**0.51**	**0.73**	0.47[b]	0.39 0.52
	Caudate	0.46[b]	0.50	-0.61	**-0.66**	**-0.52**	-0.65	**-0.70** **-0.56**
	Thalamus	0.56	0.56	-0.64	**-0.71**	**-0.54**	-0.62	**-0.71** **-0.50**
5	Cerebellum	-0.67	-0.66	-0.87	**-1.03**	**-0.68**	-0.83	**-0.77** **-0.59**
	Cerebellar crus	-0.60	-0.59	-0.69	**-0.77**	**-0.59**	-0.67	**-0.74** **-0.58**
	Rolandic operculum	0.49[b]	0.52	0.47[b]	0.33	0.58	0.61	0.47 0.74
	Insula	0.45[b]	0.55	0.36[b]	0.23	0.47	0.52	0.42 0.61
	Heschl's g.	0.30[b]	0.46[b]	0.22[b]	0.12	0.32	0.46[b]	0.35 0.56
	Putamen	0.35[b]	0.46[b]	0.26[b]	0.18	0.33	0.44[b]	0.32 0.54
	Temporal gyri	0.16[b]	0.42[b]	0.04[b]	-0.12	0.17	0.44[b]	0.33 0.54
6	Caudate	-0.37[b]	-0.34[b]	-0.56	-0.44	-0.68	-0.51	-0.61 -0.42
	(Para)Hippocampus	0.56	0.51	0.55	0.48	0.62	0.49[b]	0.43 0.55
	Temporal gyri	0.58	0.57	0.61	**0.50**	**0.71**	0.65	**0.54** **0.76**
	Fusiform g.	0.62	0.63	0.73	**0.65**	**0.82**	0.78	**0.70** **0.86**
7	Lingual g.	-0.64	-0.67	-0.69	**-0.76**	**-0.62**	-0.72	**-0.80** **-0.66**
	Calcarine cortex	-0.53	-0.65	-0.56	**-0.61**	**-0.52**	-0.71	**-0.76** **-0.68**
	Olfactory cortex	0.48[b]	0.46[b]	0.48	0.45	0.52	0.46[b]	0.42 0.49
8	Precuneus	0.67	0.70	0.77	**0.69**	**0.77**	0.73	**0.73** **0.81**
	Cuneus	0.49[b]	0.45[b]	0.51	0.48	0.54	0.47[b]	0.45 0.50
	Cerebellar crus	-0.46[b]	-0.46[b]	-0.52	-0.55	-0.49	-0.51	-0.54 -0.49

Note. Bold faced entries represent CIs completely above the |.50| threshold.

[b]Subthreshold (less than |.50|) loading. [a]Factor number based on oblique Promax.

Factor 3 was primarily loaded by the cingulate gyrus with opposite loadings from occipital components. The frontal gyri and calcarine cortex, although loading to this factor in the orthogonal rotation, were largely subthreshold in the oblique rotation and therefore not included in Factor 3. Factor 3 is reliable by Stevens' (2002) criterion of 4 or more variable loadings greater than |.60|. Factor 3 is labeled Cingulate-Occipital factor to reflect its primary loadings.

Factor 4 consisted of subcortical regions from the basal ganglia and some frontal and medial cortex areas. The frontal superior and inferior right hemisphere loadings were noted to have loading CIs crossing below the |.50| threshold, but were included in this factor due to interpretability. Factor 4 is reliable by Stevens (2002) criterion of 4 or more variable loadings greater than |.60|. Factor 4 is labeled Frontal-Basal factor to reflect its primary loadings.

Factor 5 was loaded by cerebellar areas and oppositely loaded by right hemisphere temporal gyri components. The temporal components, however, demonstrated CIs largely below the threshold, particularly in the left hemisphere, and therefore are of relatively low influence compared to cerebellar components. It was decided to include the cerebellum, cerebellar crus, right Rolandic operculum, and right insula in this factor, discarding the subthreshold right temporal components of Heschl's gyrus, the temporal gyri, and the putamen, for the sake of simple structure. Factor 5 is reliable by Stevens (2002) criterion of 4 or more variable loadings greater than |.60|. Factor 5 is labeled Cerebellar-Insular factor to reflect its primary loadings.

Factor 6 was loaded by temporal components and reverse loaded by the caudate, with the parahippocampal/hippocampal area and the caudate loading CIs extending into

the subthreshold zone. However, all four components (caudate, parahippocampal/hippocampal area, temporal gyri, fusiform gyrus) were selected for inclusion in the factor due to interpretability. Factor 6 is reliable by Stevens (2002) criterion of 4 or more variable loadings greater than |.60|. Factor 6 is labeled Temporal-Caudal factor to reflect its primary loadings.

Factor 7 was loaded by occipital components with a weaker loading by the olfactory cortex (with subthreshold CI). The olfactory cortex was not selected for inclusion on the factor due to simple structure concerns. Factor 7 is reliable by Stevens (2002) criterion of 4 or more variable loadings greater than |.60|. Factor 7 is labeled Occipital factor to reflect its primary loadings.

Factor 8 was loaded by the parietooccipital components (cuneus and precuneus) and oppositely loaded by cerebellar components (crus), with subthreshold portions of the CI for the cuneus making this a weaker loading. All three components were included in the factor. Factor 8 is reliable by Stevens (2002) criterion of 4 or more variable loadings greater than |.60|. Factor 8 is labeled Parietooccipital-Cerebellar factor to reflect its primary loadings.

Pattern versus structure matrix. The most common procedure in obliquely rotated EFA appears to be interpreting only the pattern matrix, since the pattern matrix represents the effects of allowing factors to correlate in the solution (Graham, Guthrie, & Thompson, 2003). The caveat is that both pattern (the regression coefficient, or correlation of variable to factor with all other variables held constant) and structure (the correlation coefficients of variable to factor) matrices should be examined for useful information (Gorsuch, 2015). Table 27 shows a comparison of structure and pattern

matrices for the first factor only, for reasons of space.

Table 27

Comparison of Pattern and Structure Loadings- Factor 1 Only (loadings ≥ .50)

	Pattern Loadings		Structure Loadings	
Region	Left	Right	Left	Right
Supramarginal g.	1.09	1.11	0.58	0.77
Angular g.	0.83	0.84	0.69	0.76
Parietal g.	0.67	0.69	0.77	0.78
Postcentral g.	0.63	0.65	0.74	0.80
Precentral g.			0.60	0.74
Insula			-0.60	-0.48
Para/hippocampal g.			-0.59	-0.65
Temporal g.			-0.59	-0.49
Amygdala			-0.57	-0.56
Cingulate (ant) g.			-0.46	-0.51
Frontal (inf) g.			0.37	0.57
Pallidum			-0.69	-0.70
Putamen			-0.68	-0.61
Thalamus			-0.58	-0.58

Notable in the structural loadings of the first factor is the increase from 4 to 14 bilateral loadings above the |.50| threshold. This increase was typical throughout the eight factors, increasing the number of loaded variables for each factor (thereby making interpretation more difficult with complex factor structure), and increasing the number of cross-loaded variables. The structure matrix was therefore not used in interpretation of factors in order to favor simple structure; Table 28 shows pattern loadings above |.30|.

Table 28

Pattern Matrix (loadings ≥ |.30| shown; loadings ≥ |.50| in bold)

	F1		F2		F3		F4		F5		F6		F7		F8	
	L	R	L	R	L	R	L	R	L	R	L	R	L	R	L	R
1		0.39	**0.79**	**0.64**												
2		0.41							0.47	**0.61**						
3	-.43	-.44	**1.00**	**1.10**												
4							0.32						0.48	0.46		
5	-.30				-.40	-.47	**0.53**	0.48								
6					-.30	-.35	**0.70**	**0.65**								
7							**0.63**	0.47	0.31							-.36
8							**0.96**	**0.98**					0.37	0.34		
9	-.30		**1.00**	**0.93**												0.34
10			-.30							0.44	**0.61**	**0.65**				
11											0.39	0.37				
12											**0.55**	0.49				
13									-.30		**0.73**	**0.78**				
14										0.46						
15									0.36	**0.52**						
16					**0.70**	**0.68**										
17					**0.78**	**0.77**										
18					**0.88**	**0.88**							-.32			
19			-.31				**-.61**	**-.65**			**-.56**	**-.51**				
20	-.30	-.32														
21	-.35	-.35								0.44						
22							**-.64**	**-.62**								
23	**0.67**	**0.65**	**0.50**	0.42												
24	**1.10**	**1.10**	-.32													
25	**0.83**	**0.84**	-.36	-.35	-.30	-.30										
26			**0.51**	0.34											**0.73**	**0.77**
27	**0.67**	**0.69**												0.36	0.36	
28					**-.67**	**-.64**							-.31			
29					-.41								**-.56**	**-.71**		
30					**-.76**	**-.78**									**0.51**	0.47
31													**-.69**	**-.72**		
32									-.33							
33									**-.69**	**-.67**					**-.52**	**-.51**
34									**-.87**	**-.83**						

Note. L = left; R = right; 1 = precentral gyrus; 2 = Rolandic operculum; 3 = supplemental motor area; 4 = olfactory cortex; 5 = frontal superior gyrus; 6 = frontal middle gyrus; 7 = frontal inferior gyrus; 8 = gyrus rectus; 9 = paracentral lobule; 10 = temporal gyri; 11 = amygdala; 12 = parahippocampal/hippocampal gyri; 13 = fusiform gyrus; 14 = Heschl's gyrus; 15 = insula; 16 = cingulate gyrus anterior; 17 = cingulate gyrus middle; 18 = cingulate gyrus posterior; 19 = caudate; 20 = pallidum; 21 = putamen; 22 = thalamus; 23 = postcentral gyrus; 24 = supramarginal gyrus; 25 = angular gyrus; 26 = precuneus; 27 = parietal gyrus; 28 = occipital gyrus; 29 = calcarine cortex; 30 = cuneus; 31 = lingual gyrus; 32 = cerebellar vermis; 33 = cerebellar crus; 34 = cerebellum.

Orthogonal rotation. In the orthogonal rotation (Kaiser-normalized Varimax), Factor 1 was like that of the oblique rotation, and loaded by the cingulate gyrus (anterior, middle, and posterior) with opposed loadings from occipital components (cuneus and occipital gyri) plus loadings from the frontal superior and middle gyri and calcarine cortex that were subthreshold in the oblique loadings.

Factor 2 was loaded by motor-sensory components, unchanged from the oblique rotation.

Factor 3 was represented by parietal regions (similar to Factor 3 of the oblique model).

Factor 4 was loaded by right hemisphere temporal components (insula and Rolandic operculum) and oppositely loaded by cerebellar areas (similar to Factor 5 in the oblique model).

Factor 5 (similar to oblique Factor 4) consisted of subcortical regions from the basal ganglia (caudate and thalamus) and some frontal and medial cortex (frontal gyri and gyrus rectus).

Factor 6 was loaded by temporal components, similar to Factor 6 in the oblique loadings, but without the caudate loadings of significance in the oblique case.

Factor 7 was loaded by a single parietal variable (the precuneus).

Factor 8 was loaded by occipital components (lingual gyrus and calcarine cortex), similar to the oblique case.

The choice between oblique and orthogonal rotation methods is both subjective and objective, based on which rotation better demonstrates simple structure and has ease of meaningful interpretation. Subjectively, the factor structure did not vary greatly

between rotations, and either result is interpretable.

Consistent with theory, the oblique rotation allows for correlation of factors, which is sensible given that brain behavioral functions are correlated, and neuronal activation would also be likely to be related rather than independent between neural networks (e.g., coactivation of networks). Furthermore, use of oblique rotation is inconsequential if orthogonal rotation would have sufficed, but use of orthogonal rotation preempts the consideration of higher-order relationships and factors.

Objectively, simple structure may be measured by the number of hyperplanes (represented by near-zero variable loadings on factors, with more zero loadings considered simpler structure) and number and magnitude of variables loading on multiple factors (Gorsuch, 2015; Costello & Osborne, 2005). There were more hyperplanes in the oblique method (127) versus the orthogonal method (103) at a cutoff of |.05|.

The orthogonal rotation had one-third more variables (41) that cross loaded at |.32| or more to multiple factors than the oblique rotation (28), and more of the orthogonal cross loadings were on three or more factors. The Promax oblique rotation was selected based on the above evidence and reasoning.

Table 26 shows a comparison of rotation results with confidence intervals (bootstrap $i = 1000$, $p \leq .01$) of the Promax loadings. Table 29 shows the selected factor loadings of the PAF-extracted Promax-rotated factor analysis.

The 8-factor structure as shown in Table 29 can be more simply described. Factor 1 is representative of the parietal lobe. Factor 2 is motor/sensory. Factor 3 represents the cingulate gyrus and occipital lobe. Factor 4 depicts the frontal lobe and basal ganglia. Factor 5 is cerebellar areas with the insula. Factor 6 is the temporal gyri with some basal

ganglia. Factor 7 is occipital components. Factor 8 is parietooccipital components with cerebellar components.

Table 29

Summary of Selected Factor Structure and Loadings (greater than or equal to .70 in bold)

		Loadings			Loadings	
Factor	Region	Left	Right	Region	Left	Right
1	Supramarginal g.	**1.09**	**1.11**	Parietal g.	0.67	0.69
	Angular g.	**0.83**	**0.84**	Postcentral g.	0.63	0.65
2	Supplementary motor	**1.03**	**1.10**	Precentral g.	**0.79**	0.64
	Paracentral l.	**1.02**	**0.93**	Postcentral g.	0.50	0.42
3	Cingulate (ant, mid, post) g.	**0.70-0.88**	**0.68-0.88**	Cuneus	**-0.76**	**-0.78**
				Occipital g.	-0.67	-0.64
4	Gyrus rectus	**0.96**	**0.98**	Caudate	-0.61	-0.65
	Frontal g. (sup, mid, inf)	0.53-0.70	0.47-0.65	Thalamus	-0.64	-0.62
5	Cerebellum	**-0.87**	**-0.83**	Rolandic oper.	0.47	0.61
	Cerebellar crus	-0.69	-0.67	Insula	0.55	0.52
6	Fusiform g.	**0.73**	**0.78**	Temporal g.	0.61	0.65
	(Para)Hippocampus	0.55	0.49	Caudate	-0.56	-0.51
7	Lingual g.	-0.69	**-0.72**	Calcarine c.	-0.56	**-0.71**
8	Precuneus	**0.77**	**0.73**	Cerebellar crus	-0.52	-0.51
	Cuneus	0.51	0.47			

Note. g. = gyrus; c. = cortex; l. = lobe

An analysis of oblique rotation factor intercorrelations (Table 30) indicated moderate to high positive intercorrelations (≥ .50) between Factors 1 and 2, 1 and 4, 3 and 5, and 3 and 6. Moderate to high negative correlations were noted between 1 and 3, 1 and 6, 3 and 4, and 4 and 5. High intercorrelations may imply the existence of higher-order factors (Gorsuch, 2015).

Table 30

Factor Intercorrelations- Oblique (moderate and high correlations in bold)

	1	2	3	4	5	6	7	8
1	1.00							
2	**0.63**	1.00						
3	**-0.54**	-0.40	1.00					
4	**0.59**	0.45	**-0.68**	1.00				
5	-0.43	-0.47	**0.63**	**-0.58**	1.00			
6	**-0.53**	-0.39	**0.52**	-0.47	0.29	1.00		
7	-0.27	-0.17	0.35	-0.16	0.41	0.14	1.00	
8	-0.05	0.06	-0.05	0.02	-0.17	0.04	0.01	1.00

Secondary rotation. A secondary dimensional reduction was examined for the factor correlation matrix of the eight-factor oblique solution. Promax-rotated PAF extractions for 1, 2, 3, and 4 factors yielded results shown in Table 31.

The eight-factor solution of the first-order EFA was previously described as accounting for 66% of the variance. Deriving a single second-order factor accounts for 40% of the variance as described by Factors 1 through 6 inclusive (representing parietal, motor-sensory, limbic-occipital, frontal-basal ganglia, cerebellar-insular, and temporal-basal ganglia components), indicating that Factors 7 and 8 (occipital, parietooccipital, and cerebellar components) are less explanatory in this higher-order model.

In comparison, allowing two second-order factors to explain a cumulative 50% of the variance splits the previous solution into one secondary factor representing Factors 1-

4 and 6 , and a second representing Factor 5 alone. This second-order model describes 10% additional variance using the same components as the first second-order model, simply by describing the cerebellar-insular areas as a separate factor.

Table 31

Second-Order Factors

Factor Solution	Cumulative Variance %	Sum of Squared Loadings				% of Variance				First-Order Factor Clusters			
1	40				3.2				40				1-6
2	50			2.92	1.09			37	14			1-4, 6	5
3	62		2.95	1.36	0.62		37	17	8		1-4, 6	7	5
4	63	2.13	1.44	1.01	0.43	27	18	13	5	3, 4, 6	1-2	7	5, 8

The second-order model positing three higher-order factors is a re-expression of the two-factor model with added variance from Factor 7 (occipital lobe), and accounts for 62% of variance. A four-factor higher-order model accounts accounting for 63% of variance uses all eight factors.

Representing the 8-factor solution by higher-order derivative factors is useful if the higher-order factors offer additional explanatory meaning. For instance, the single higher-order factor model with Factors 1-6 explaining 40% of the variance may be useful in a diagnostic context, in which higher-order factor scores on this single factor could be considered a surrogate expression for generalized blood flow, with additional empirical research supporting interpretations of this single score. Likewise, the two- or three-higher-order solutions may be found to be explanatory based on future empirically derived associations.

Similarly, higher-order derived factors may have utility if they represent hierarchical constructs with interpretable meaning and significance. However, for the current exploration, these higher-order factor structures do not add variance explained (the original 8-factor solution explains 66%, better than the higher-order solutions). Therefore, utility of the second-order factors is deferred to the Discussion, where final interpretations of the lower-order factors can be considered.

Other factor solutions. Examination of 6-, 7-, and 9-factor obliquely rotated solutions was made for comparison purposes (Table 32).

Table 32

Alternative Factor Extraction Comparisons

Number of Factors	Cumulative Variance %	Proportion of Variance Explained (%)								
		F1	F2	F3	F4	F5	F6	F7	F8	F9
6	62	27	11	8	6	5	4			
7	64	26	11	5	5	5	5	4		
8	66	15	11	10	8	8	6	5	4	
9	68	17	11	10	6	6	5	5	4	4

Cumulative variance was highest in the 9-factor solution, albeit the other solutions were within a 6% range. More importantly, the 7-factor solution distributed 26% of the variance to the first factor, thereby decreasing interpretability and working counter to the logic of using factor rotation.

The 6-factor solution also tended to overload the first factor with higher proportions of variance (27%). The 9- factor solution maintained a similar factor

structure to the 8-factor solution. The ninth factor was loaded by right-hemisphere amygdala, putamen, and temporal gyri, in ascending order of magnitude, resembling Factor 6 (but unilateral components only).

Since the 6-, 7- and 9-factor interpretations add little or nothing to interpretability, the selection of an 8-factor model was retained due to it having the simplest structure with high explanatory variance (Table 33).

Table 33

Named Factor Summary (Loadings ≥ .30)

Parietal	Motor/Sensory	Cingulate-Occipital	Frontal-Basal
Supramarginal g.	**Supp motor**	**Cingulate g. ant**	**Gyrus rectus**
Angular g.	**Paracentral l.**	**Cingulate g. mid**	**Frontal sup g.**
Parietal g.	**Precentral g.**	**Cingulate g. post**	**Frontal mid g.**
Postcentral g.	**Precuneus**	***Cuneus***	**Frontal inf g.**
Precentral g.	**Postcentral g.**	***Occipital g.***	***Caudate***
Rolandic oper.	*Angular g.*	*Frontal sup g.*	***Thalamus***
Supp motor	*Supramarginal g.*	*Frontal mid g.*	Olfactory c.
Frontal sup g.	*Caudate*	*Angular g.*	
Paracentral l.	*Temporal g.*	*Calcarine c.*	
Pallidum			
Putamen			

Cerebellar-Insular	Temporal-Caudal	Occipital	Parietooccipital-Cerebellar
Cerebellar crus	**Fusiform g.**	***Calcarine c.***	**Precuneus**
Cerebellum	**Temporal g.**	***Lingual g.***	**Cuneus**
Rolandic oper.	***Caudate***	Olfactory c.	***Cerebellar crus***
Insula	Para/Hipp g.	Gyrus rectus	Parietal g.
Heschl's g.	Amygdala	Parietal g.	Paracentral l.
Temporal g.		*Occipital g.*	*Frontal inf g.*
Frontal inf g.		*Cingulate g. post*	
Fusiform g.			
Cerebellar vermis			

Note. Bold indicates loadings ≥ |.50|; italics indicates anticorrelated loading.

Summary. Table 33 shows a summary of all loadings greater than |.30|. Although the threshold for consideration of variable loadings on the factors was set at |.50| for analysis, to facilitate comparisons of simple structure among extraction and rotation method alternatives, the lower threshold of |.30| was reasoned to be more appropriate for application to final factor interpretation.

Using a very large dataset (n = 12,217), robust methods to minimize effects of outliers and assumptions of multivariate normality, best practices to determine the nominal number of factors to be extracted, and comparisons with results obtained using other factor extraction quantities and methods, 8 latent variables were found for the SPECT-derived participant blood flows across 67 brain areas of interest (Table 33). The replicability of this result is supported by the use bootstrapping to select 1000 random samples from the data in various permutations for factor extraction, and the resulting loading confidence intervals were employed to select variables of interest loading to factors.

In the next chapter, we will offer an interpretation of the eight factors based on the variable loadings.

CHAPTER V: INTERPRETATION

The present experimental results show ROI loadings of practical significance for each latent variable. The underlying premise of this study is that resting-state functional connectivity (a temporal correlation across neural regions when a person is not engaged in deliberate activity) is detectable in SPECT blood flow patterns through factor analysis. Further, these factors are comparable to resting-state networks as demonstrated in fMRI studies through correlated hemodynamic ROI activations. In SPECT image data, these patterns appear as latent variables; a fundamental difference between SPECT and fMRI imaging data is the lack of a temporal component in SPECT, thus different analysis and interpretation methods must be applied in SPECT than in fMRI.

The premise of interpreting SPECT blood flow data to indicate functional connectivity of brain regions is based on the hypothesized relationship of blood flow to metabolic requirements due to neuronal energy needs tied to activation. Regions that increase in blood flow simultaneously are assumed to be activated in the same task or function; conversely, regions that decrease in blood flow are assumed to deactivate related to that same function. Regions that are anticorrelated (reversals of algebraic sign of the correlation) are assumed to be simultaneously activating and deactivating in a function, and based on extended time frames in fMRI research, these anticorrelated regions often appear to switch as a couple at a set frequency.

The observation that regional blood flows correlate is useful for exploration, but and interpretations of functional purpose and connectivity are hypothetical and speculative until replication shows consistent reliable findings. We know little about actual functions of topographical regions of the brain. The science is still new: The first

published study on the resting state was in 1995, and the subject did not generate serious publication interest until 2005 (Bandettini, 2020). Therefore, we can infer functional purpose in our interpretation of clustered regions correlating in perfusion, but these are merely inferences until empirical evidence is obtained to directly support these assumptions.

Imaging modality effects on the interpretation of results. Because fMRI research has reliably determined the existence of an at-rest connectivity pattern in brain regions (see Zhang & Raichle, 2010, for a concise summary), we will rely heavily on fMRI literature comparisons in our interpretation. It may be helpful if we quickly review some of the introductory material stated earlier as pertains to interpretation of present results.

Resting-state networks are usually determined in fMRI research by noting the temporal correlation of activation in adjacent or distal regions. Because fMRI rapidly acquires a complete volume of slices in as little as 2 s, capturing behavioral activations lasting around 3 s or more, multiple volumes are obtained during a typical 30 to 60 min session, and simultaneous activations over those many volumes can be statistically compared with an additional time-series parameter (Bandettini, 2020).

In the fMRI at-rest paradigm, comparison of slices from multiple contiguous fMRI volumes shows if there is correlated activity in neural regions. Several different resting-state networks, activated for varying durations, may be observed within the experimental time frame, and results are usually averaged over multiple participants and multiple trials. The at-rest state is influenced by breathing, blinking, heartbeat variation, thought processes, finger or toe tapping, head turning, visual focus, and many other

possibilities; the resulting data is not a homogenous result, but instead varies considerably over time.

On the other hand, SPECT shows the state of brain blood perfusion at a timepoint several seconds after bolus injection (usually made through a cannula placed prior to the experiment, and therefore unobtrusive to the participant). The radiotracer takes time to travel the bloodstream and blood-brain barrier to enter brain tissue, where imaging later detects the radioactive deposits.

The SPECT image is a snapshot of blood flow representative of several seconds that it took to deposit the radiotracers throughout brain tissue. Since the data is from a single point in time (and therefore lacks the temporal element in fMRI), any resting-state network activated during the several second window of tissue saturation is likely to be overlaid into the single image slice. The dimensional reduction through EFA then may yield several simultaneously correlated perfusion networks (as represented by factors).

To summarize, in comparing and interpreting the present SPECT findings considering previous fMRI research, the difference in acquisition modalities forces comparisons to be made between continuously gathered data (i.e., a movie), and time-limited data (a still frame). In SPECT, some default networks may not be observable if they fall outside of the temporal period of tissue saturation, and those that are observed will presumably appear as clusters or factors in statistical analysis, with a ranking of prominence based on accounted variance. In fMRI, more networks may be observable over time, without comparative rankings of prominence.

Neither method currently purports to show proportion of time that each resting-state network is active within the at-rest period, although fMRI allows more of an

understanding of frequency of activation during a set period. Furthermore, although both methods have the capability of designing experimental paradigms to isolate or parse out specific at-rest state behaviors during the resting state (e.g., breathing, thinking and planning, drowsiness), limited experiments of this type have been published.

Therefore, interpretations that follow are exploratory in nature (in the spirit of the present study) and subject to empirical confirmation through additional multimodal experimentation and confirmatory analysis. Table 34 shows a summary of the interpretations of the 8-factor result from the current study, followed by elaborations on the factor interpretations.

Table 34

Summary of First-order Factor Interpretations

Factor	Description
Parietal	Attentional & salience always-on network: Cognitive control and filtering of perceptual information while monitoring and adjusting motor movements.
Motor/Sensory	Monitoring and control of motor/sensory system and incorporation into somatic consciousness or self-conceptualization, synchronized to alternate with Parietal factor.
Cingulate- Occipital	Manages or generates spontaneous (stimulus-independent) higher-level conscious and unconscious cognition during rest, with complementary control of eye movement and visual processing.
Frontal- Basal	Manages working memory, executive control, memory, and emotional salience of inner cognition at rest.
Cerebellar- Insular	Somatic and emotional homeostasis maintenance with ongoing salience monitoring and self-speech generation activities.
Temporal- Caudal	Emotionally valenced memory processing (storage and consolidation, retrieval), especially for faces.
Occipital	Task-based gathering, processing, and management of visuoperceptual and possibly multimodal sensory information; salience determination.
Parietooccipital- Cerebellar	Housekeeping factor representing non-specific miscellaneous at-rest functions.

First-Order Factors

Parietal factor. Factor 1 in Table 33 expresses primarily parietal components (the supramarginal gyrus, angular gyrus, parietal gyri-inferior and superior, and postcentral gyrus), accounting for about 13% of variance in the overall data, and is labeled the Parietal factor. Also loading at moderate levels (|.30|-|.50|) on this factor are the precentral gyrus and Rolandic operculum, with anticorrelations from the supplementary motor gyrus, frontal superior gyrus, paracentral lobule, pallidum, and putamen.

Structural elements. The supramarginal and angular gyri (also known as the ventral parietal cortex or inferior parietal lobe) are associated with sensory processing and integration from afferent auditory, visual, and somatosensory sources, as well as visuospatial awareness, episodic memory processing, motor planning and control, and working memory. The ventral parietal region is implicated in bottom-up attention, or the ability to distinguish behaviorally salient stimuli (Cabeza, Ciaramelli, Olson, & Moscovitch, 2008). Lesions in this area are associated with hemispatial neglect, a condition in which spontaneous response to stimuli in the contralateral field is diminished or absent, while voluntary functions are preserved. Efferent outputs usually consist of phonological, semantic, or calculation-related information (Haines, 1995).

The superior and inferior parietal gyri are typically involved in visuomotor and visuoperceptual functions and spatial cognition. However, these areas appear to be critical in operations involving working memory, reasoning, attention, and recognizing and responding to salient environmental stimuli. These components of the parietal lobe together may act as an always-on sensory and perceptual processing area (Wang et al., 2015). While at rest, the senses are still at full function, gathering information. Even if

masked (eyes closed, for instance), visualization occurs that may activate sensory visual perception. This perception network forms the base for attention and salience recognition (Cabeza et al., 2008).

The postcentral (sensory strip) and precentral (motor strip) gyri, together with the Rolandic operculum (lateral end of motor/sensory strip) and paracentral lobule (the medial end), govern sensory afferents and voluntary motor efferents. These components can be envisioned in an always-on mode of monitoring and controlling micromotor movements while at rest. The Rolandic operculum has been studied for its role in somatic self-consciousness and integration of exteroceptive and interoceptive afferent information (Blefari et al., 2017; Haines, 1995).

The supplementary motor area is the association cortex of the frontal lobe associated with motor movement and planning, where cognition is transformed into motor action, and prediction, outcome planning, initiation, switching, and inhibition take place (Shepherd, 1994). The adjacent frontal superior gyrus also functions in motor planning, control, execution, working memory, impulse control, and spatial processing (Haines, 1994).

The pallidum (globus pallidus exterior and globus pallidus interior) and the putamen lie adjacent in the basal ganglia, forming the lenticular nucleus, and are associated with GABAergic inhibition of movement through the direct pathway: high density myelinated efferent connections from pallidum to the motor cortex via the thalamus, and afferent connections from the cortex to the striatum (the putamen and caudate). The basal ganglia are thought to function as an always-on damper or inhibitory system; signals from the cortex via the striatum temporarily release the inhibition,

allowing movement. Alternatively, an indirect pathway (through the subthalamic nucleus) increases inhibition (Purves et al., 2008).

The basal ganglia are also associated with habitual behavior, reinforcement and punishment of motor movements, emotion, and cognition, though these connections are not well understood. Dysfunction in the basal ganglia is implicated in Parkinson's disease (a failure to release inhibition of motor movement), Huntington's disease (failure to maintain inhibition resulting in choreic movement), Tourette's syndrome, schizophrenia, depression, autism, and obsessive-compulsive disorder (Purves et al., 2008).

Functional integration. Integrating the possible and likely functions of these component areas in the at-rest state (with respect to the algebraic sign on the supplementary motor area, frontal superior gyrus, paracentral lobule, pallidum, and putamen, which all correlate counter to the more strongly loaded variables), the Parietal factor appears to represent an attentional and salience network that is in the always-on state, continually monitoring for salient stimuli (even in a quiet room), with smaller at-rest functions as inhibiting excess motor activity (in response to the instruction to be still), and controlling micromovements that inevitably occur at rest. The anticorrelated areas listed above represent less variance, and possibly are engaged in the inhibitory or suppressive role.

The Parietal factor appears to most resemble fMRI-detected resting-state networks of attention and salience (Fox et al., 2006). Corbetta and Shulman (2002) described the *dorsal attention* network as a top-down information processing flow that conveys experiential knowledge (as opposed to perceptual information from the senses) with feedback control from high-order structures on lower structures. The dorsal network

includes the bilateral intraparietal and superior frontal cortices. The *ventral attention* network features bottom-up processing of information gained from senses and ending in motoric activation without feedback control, and may direct the dorsal network in directing attention to salient stimuli. The ventral network consists of the right-hemisphere temporoparietal and inferior frontal cortices.

It is noted that Corbetta, and later Fox, found the attentional salience network for spontaneous or unexpected stimuli to be ventrally directed, and stimuli selection and response to be dorsally directed, with an integrating function served by the PFC. More specifically, according to Fox, the dorsal attentional selection network consists of the bilateral inferior and superior parietal lobules on the dorsal parietal cortex and the frontal eye fields that overlap the precentral gyrus, supplementary motor area, and frontal gyri, corresponding to the Parietal factor areas. Fox's ventral attentional salience network includes primarily right-hemisphere angular and supramarginal gyri and the inferior frontal gyrus.

The present findings indicate bilateral function, and do not include a ventral frontal component. Thus, the present Parietal factor may represent more of the dorsal than frontal attentional salience networks noted in fMRI activation studies, or possibly a combination of active dorsal and ventral networks. In broad terms, the Parietal factor represents cognitive control and filtering of the senses to determine what is of significance and what is to be ignored, while also asserting a dampening effect on unwanted motor movements, while at the ready in case motor activation is suddenly required. This primary latent construct in blood flow patterns is representative of the default state of the awake brain.

One might expect the attentional salience network to be subject to interparticipant variance in persons with pathological conditions versus healthy individuals, particularly in disorders commonly associated with failures to correctly judge salience (PTSD, anxiety, depression) or to disproportionately engage in attention and motor activity (impulse control disorders, ADHD, bipolar disorders). Since the present dimensional reduction is derived from blood flow averages of pathological brains, these results speculatively may be skewed (hypothetically with less frontal lobe control), or they may be consistent with the network of a healthy brain but with faulty thresholds.

Thus the Parietal factor appears to represent an attentional & salience always-on network: Cognitive control and filtering of perceptual information while monitoring and adjusting motor movements.

Motor/Sensory factor. The second factor, accounting for 10% of the blood flow variance, had largest loadings from bilateral supplementary more area, paracentral lobule, precentral gyrus, postcentral gyrus, precuneus, with low- to moderate- anticorrelated loadings from the angular gyrus, supramarginal gyrus, caudate nucleus, and temporal gyri. This factor has many of the same variable loadings as the first factor, with subtle differences.

The Motor/Sensory factor loadings differ from the Parietal factor in that the Parietal loadings are strongest from ventral and dorsal components of the parietal lobe (associated with attention and salience), followed by motor/sensory components, with small contributions from the basal ganglia and PFC. The Motor/Sensory components are strongest from the motor-sensory strip, with the action of the precuneus area replacing the parietal gyri in the first factor, then anticorrelated and weaker loadings are seen from the

ventral parietal areas and basal ganglia, as well as some small contribution from the temporal lobe. Notably, there is no contribution from the frontal gyri.

Structural elements. The precuneus forms the medial surface of the parietal lobe, bordered by the occipital cortex at the parietooccipital junction to the posterior and the parietal gyri at the dorsal surface of the parietal lobe. Notably, it is not part of the dorsal or ventral pathways. Functionality is thought to be related to visuospatial imagery and mental visualization, episodic memory retrieval, and self-processing operations (perspective of the first-person, agency). Of note, the precuneus is one of the earliest and strongest findings in default networks, because it consistently appears as metabolically active when an individual is at rest in fMRI studies, and progressively deactivates as the individual engages in deliberate activity (Cavanna & Trimble, 2006).

Hypothesized functions of the precuneus during at-rest states include continuous information gathering to develop and maintain perception of self, processing of episodic memory stores, and manipulation of information in planning and problem-solving (Gusnard, Akbudak, Shulman, & Raichle, 2001; Raichle et al., 2001). The anterior portion of the dorsal precuneus has been shown to be related to motor execution and attention, while the posterior dorsal surface is associated with motor and visual imagery (Zhang & Chiang-shan, 2012).

It appears that the ventral portion of the precuneus is integral to developing representations of oneself and in referencing these conceptions during periods of internal dialog and perhaps metacognition; the precuneus may be considered a substrate of consciousness (Zhang & Chiang-shan, 2012). Of particular note, the precuneus is typically hypoactive during sleep, anesthesia, and coma (Cavanna & Trimble, 2006).

Activation of the precuneus appears to require conscious self-referential cognition.

The precuneus interconnects with higher-level association areas in the cortex and subcortex, with the absence of connection to primary sensory areas, indicating a role in higher-level processing versus routine surveillance of perceptual information as in the more lateral and ventral parietal surfaces such as the angular and supramarginal gyri, which show weaker, and anticorrelated, loadings on this factor. Thus, precuneal activity appears to increase as attentional and salience activity decreases; speculatively, increased self-referential thought diverts resources from ongoing attentional monitoring in the parietal lobe, however, the prominence of the Parietal factor's ongoing attentional operations indicates that overall, attentional monitoring is not decreased during cognitions of consciousness.

The absence of correlations with the occipital areas indicates the role of the precuneal activation in this factor is minimally associated with visualization and the dorsal posterior area of the precuneus. Instead, function appears to be related to motor and attention associated with the anterior dorsal area, and self-reference and conscious attention associated with the ventral precuneus (Zhang & Chiang-shan, 2012).

The presence of extensive cortical connections with the frontal regions, including the visual eye fields and supplementary motor area, and subcortical pathways to the striatum and caudal nucleus, provide support for the argument that the precuneus is a mid-level processor between eye motor sequences and secondarily processed sensory information from the supplementary motor area association cortex. Connections to the lateral parietal lobe and motor-sensory areas are presumed to play a role in hand-eye coordination and reaching (Cavanna & Trimble, 2006). Furthermore, sensory-motor

connections are thought to feed somatosensory information to the precuneus that is hypothesized to be used in the formation of a representation of the self (Damasio, 1999).

Where the first factor was loaded by basal ganglia components of the putamen and pallidum, the second factor is loaded by the caudate. The caudate, adjacent to the lenticular nucleus, and with the putamen and nucleus accumbens forming the body known as the striatum, serves as the input for the corticostriatal pathway bringing information on motor movements (particularly, in the present circumstance, eye movements) and transferring GABA-based inhibitory instructions to the pallidum and putamen, and from there to the thalamus. The caudate also serves roles in goal-directed behavior, attention, reinforcement, and habit learning. It is thought that the caudate contributes to the selection of correct or most appropriate action sequence based on evaluation outcomes (in connection with the PFC), while the neighboring putamen acts in stimulus-response, habit formation and learning. The caudate is the neural substrate for cognitive planning of behavior (Grahn, Parkinson, & Owen, 2008).

Lesions or degeneration to the caudate are associated with working memory and attentional deficits in disorders such as Huntington's disease, and may contribute to motor and cognitive concerns in Parkinson's disease. There are also associations with OCD and ADHD and the caudate nucleus (Grahn, Parkinson, & Owen, 2008).

The role of basal ganglia components in both the Parietal factor and the Motor/Sensory factor in the at-rest paradigm may be associated with motor or cognitive and behavioral learning functions. Since ongoing motor movements (eye movement, minor movement of the extremities such as shifting and fidgeting, purposeful but semiautomatic movements such as scratching or grooming) occur throughout the resting

state, some minor activation of the striatal area as seen in the first two factors is expected as a background condition. It appears less likely that basal ganglia activity as represented in these first two factors is employed in learning or cognition during the at-rest state; although the participants may experience some activation while ruminating or processing recent experiences involving reward and motivation, these would be assumed to be transitory thoughts not captured as a significant change in group average blood flow.

Robinson et al. (2009) documented a reproducible network in the at-rest state (with eyes closed), labeled the motor control network of the basal ganglia, with low frequency activity in the pallidum, putamen, subthalamic nucleus, substantia nigra, temporal gyrus, and supplementary motor area. This motor control network mimics the structure of the cortico-subcortical motor control circuit of the basal ganglia during motor task activation, at a substantially reduced frequency. In addition, an independent component was detected (when eyes were open and fixated) incorporating the caudate nucleus, thought to be implicated in saccadic movement inhibition.

Furthermore, Robinson reported that the basal ganglia network is anticorrelated with the default mode attentional network, similar to findings herein. The anticorrelated action between the networks has been hypothesized to indicate the basal ganglia network may act to control fluctuations in the default mode attention network, using motor control of eyes and body to reorient to the at-rest state when otherwise disrupted. Findings have been replicated (Damoiseaux et al., 2008; DiMartino et al., 2008).

Functional integration. Given the similarities to Robinson's motor control network, the Motor/Sensory factor name appears appropriate. The function of the network appears to partially involve the monitoring and correction of motor activity at

the micro level, such as eye movements, small adjustments to posture, and fidgeting. The sensorimotor information is also processed as part of bodily self-concept, in the precuneus' hypothesized role as monitor of consciousness and self-conceptualization. Although closely related with similar brain regions as the Parietal factor, the Motor/Sensory factor is anticorrelated, and is hypothesized to peak and ebb in activity complementary to the Parietal factor. As attentional monitoring and determination of salience (in the Parietal factor) is an ongoing background activity, the Motor/Sensory factor activity may be occurring during intervals where attentional demand is decreased, or there may be a switching function (possibly by the frontal cortex loading on the Parietal factor) that allots activation based on current needs.

Possible effects of pathology on the Motor/Sensory factor include those of the Parietal factor due to basal ganglia involvement: Parkinson's and Huntington's disease, depression, bipolar disorder, and ADHD may affect the caudate's role in this factor. Alzheimer's disease may have more prominent effects, given evidence of parietal tangles in the precuneus particularly. Moreover, the precuneus has been associated with theory of self and may play a role in schizophrenia spectrum and autism spectrum disorders (Cavanna & Trimble, 2006). Therefore, there may be some differences between factor loadings and ranking in a non-pathological population, as well as between pathologies within the present database.

Thus, the Motor-Sensory factor appears to represent monitoring and control of motor/sensory system and incorporation into somatic consciousness or self-conceptualization, synchronized to alternate with the Parietal factor.

Cingulate-Occipital factor. The third factor, accounting for 10% of the variance

in blood flow, is primarily loaded by the anterior, middle, and posterior cingulate, with anticorrelated loadings from the occipital lobe (the cuneus and occipital gyri). Weaker loadings from the frontal gyri (superior and middle), angular gyrus, and calcarine cortex are also present.

This factor appears to be most similar to reliably replicated fMRI resting-state findings of the DMN (the posterior and ventral anterior cingulate gyrus, angular gyrus, and medial cortex from the prefrontal and precuneus regions) and the visual network (the medial and lateral occipital lobe; Doucet, Lee, & Frangou, 2019). The DMN has been characterized as a higher-level conscious resting state of the brain representing stimulus-independent cognition (Greicius, Krasnow, Reiss, & Menon, 2003), and the visual network as a lower-level perceptual activation related to eye movement, default visual recognition and processing at rest, and possibly visualization associated with higher-level at-rest cognition (Raichle, 2015).

These two networks appear simultaneously in this factor in an alternating fashion as indicated by opposing algebraic loadings. This appears to be consistent with the definition of the DMN as being present in the absence of specific task activation (Raichle, 2015). When the visual network is working, the DMN is in low activation; when the visual network reduces activity, DMN functionality resumes.

Structural elements. The anterior cingulate cortex has functionality related to affect regulation, association of emotions with internal and external stimuli, autonomic regulation, and decision-making (Blumenfeld, 2010). The posterior cingulate cortex is associated with cognition and affect, recall of autobiographical and emotional memories, and previously learned information, is known to be active during the absence of external

stimuli, and may have a role in selective attention between internal and external events (Leech & Sharpe, 2014).

It is hypothesized that the role of the cingulate gyrus in the DMN is emotional processing, self-referential mental activity, and the recollection of prior experiences. These functions are likely supported and directed by the PFC (Raichle, 2015) and possibly the angular gyrus, as indicated by the smaller anticorrelated loadings.

The cuneus is in the medial posterior occipital lobe, and processes visual information from retinotopic mappings of the visual fields with additional modulating connections with efferent attention, working memory, and reward expectation information, and may be associated with inhibition (Haldane, Cunningham, Androutsos, & Frangou, 2008). There is evidence that lesions and dysfunction in the cuneus is associated with visual hallucinations in dementia with Lewy bodies (Delli Pizzi et al., 2017).

The calcarine cortex surrounds the primary visual cortex, involved in the summoning of visual mental images (Blumenfeld, 2010). The inferior, middle, and superior occipital gyri contain the visual association area, and receive afferent data from the calcarine cortex for processing (Shepherd, 1994). The occipital components likely support visual activity while at rest (with eyes open), and perhaps internally-mentated visualization as well.

Functional integration. Greicius and others (2003) noted the probable role of the cingulate gyrus in emotional processing during the default at-rest brain state, and differentiated this processing as higher-level conscious cognition and more basic unconscious cognition. The proper balance of the two during at-rest states may bear on

affective calibration in the autonomic state; in other words, emotional reactions that spontaneously erupt or appear to be nearly automatic reactions to stimuli may be attenuated by proper amounts of default network processing. This hypothesis directly bears on mental health pathologies associated with deactivation in the cingulate gyrus, such as mood disorders, anxiety disorders, and OCD.

Thus the Cingulate-Occipital factor appears to manage or generate spontaneous (stimulus-independent) higher-level conscious and unconscious cognition during rest, with complementary control of eye movement and visual processing.

Frontal-Basal factor. The fourth factor, accounting for 9% of blood flow variance, is loaded primarily by the frontal lobe components of the gyrus rectus and frontal superior, middle, and inferior gyri, along with basal ganglia anticorrelations from the caudate nucleus and thalamus. There is a further minor loading from the olfactory cortex in the medial ventral frontal lobe.

Structural elements. Gyrus rectus activation is one of the earliest and strongest findings in resting-state studies, and is associated with higher cognition, emotional experience, and inhibition (Shepherd, 1994).

The superior frontal gyrus functions in higher cognitive function, control and execution, working memory, and spatial processing (Haines, 1995). The middle frontal gyrus is engaged in executive functioning, working memory, prospective memory and memory retrieval, planning, reallocation of attention, multiple task coordination, motor planning and organization, inhibition, and abstract reasoning (Shepherd, 1994). The inferior frontal gyrus is associated with response inhibition and attention and autobiographical memory retrieval (Shepherd, 1994).

The olfactory cortex functions in odor discrimination, perception, and memory (Haines, 1995).

The caudate nucleus is associated with afferent reception of movement and learning information for the striatum. The thalamus, among many functions, is engaged in motor control and learning, executive functioning, inhibition, selection, and emotion, attention, and time estimation, through the cortex-basal ganglia-thalamus-cortex loops (Lanciego, Luquin, & Abeso, 2014).

Functional integration. Given its frontomedial component loadings, the Frontal-Basal factor may function during the resting state in managing working memory for the purposes of internal cognition, asserting executive control (inhibition, task management, attention selection and switching) over inner cognitive tasks, and retrieving and manipulating memories and emotional perspective.

Internal mentation includes spontaneous and largely involuntary activities such as daydreaming, mind wandering, or stimulus-independent thoughts, as well as cognition, problem-solving, and planning based on memory retrieval (Greicius et al., 2003; Raichle, 2015).

The anticorrelated basal ganglia loadings likely manage motor functions through the corticothalamic pathways when the resting brain is not engaged in mental rumination using the frontomedial circuits. The basal ganglia possibly also are called on at times for stimuli selection and switching functions in conjunction with the frontal gyri; since the two areas are anticorrelated, this is likely a hand-off and return scenario rather than simultaneous processing.

Notably, Raichle (2015) remarked that an individual's balance of default network

activity with at-rest attentional and executive control may be associated with impulsivity and impulsive disorders. The Frontal-Basal factor is an example of anticorrelated network functions that may be affected in ADHD, conduct and antisocial behaviors, and personality dysfunction.

A strong cortico-basal control pathway with manifestation in the at-rest state (as opposed to an overly strong frontomedial function) may hypothetically maintain the necessary balance required for proper behavior selection and inhibition. Speculatively, daydreaming and private rumination may also serve a restorative function much like sleep does for memory and cognition.

The ranking of the Frontal-Basal factor amongst other factors in accounting of blood flow variance may be indicative of impulsivity/inhibitory dysfunction or strength, and amount of time spent in the default at-rest state may represent a possible neuropsychological measure of mental health.

Thus the Frontal-Basal factor appears to manage working memory, executive control, memory, and emotional salience of inner cognition at rest. Given the involvement of a large portion of the PFC, there are likely unknown or poorly understood functions of this factor that are not addressed herein.

Cerebellar-Insular factor. Factor 5 accounts for 8% of the total blood flow variance throughout the brain, and is loaded primarily by the bilateral cerebellum and the anticorrelated right-hemisphere lateral temporal lobe (insula, Rolandic operculum, Heschl's gyrus, temporal gyri, and fusiform gyrus). There is a minor loading of the frontal inferior gyrus in the direction of the temporal components.

Structural elements. The cerebellum is a higher-level motor system involved in

regulation of balance and equilibrium, muscle tone, sensorimotor movement coordination and programming, vestibular-ocular control, and timing regulation for the rest of the brain. Cerebellar neurons have a learning function and a role in attention, processing speed, and visuospatial processing (Blumenfeld, 2010; Shepherd, 1994).

The cerebellum collects proprioceptive, sensory, and perceptual data in advance of action to calculate the best approximation of potential motoric responses and their possible results; it is predictive rather than reactive. The cerebellum appears to maintain a trove of afferent data that is overwritten if not used (Blumenfeld, 2010; Haines, 1995). The cerebellum signals gradual muscle tension and contraction changes to maintain posture, equilibrium, and skilled voluntary movements, and inhibits lower motor circuits (Carpenter, 1985).

The insula is associated with self-awareness and emotional and somatic awareness, and is believed to continuously collect somatic and emotional status information, while incorporating salient environmental information (Craig, 2009). The temporal gyri and Heschl's gyrus are involved in auditory, speech, and language processing, semantic association (including visual images), as well as visual perception and multimodal sensory integration, and the nondominant anterior pole serves as an association cortex for personal, episodic, social, and emotional multimodal processing.

The fusiform gyrus has facial and categorical recognition functions (Shepherd, 1994). The Rolandic operculum is associated with bodily self-consciousness and an integrator of exteroceptive–interoceptive signals (Blefari et al., 2017).

The likely function of the Cerebellar-Insular factor is maintenance of homeostasis, both somatic and emotional, through constant predictive feed-forward data

collection on bodily and emotional behavior from the cerebellum and the insula. It may also play a role in self-speech during private cognitive activity. Another potential role is salience monitoring, especially of potential threats to somatic and emotional equilibrium; in fMRI resting-state studies, the insula has been found to play a role in the salience and executive control networks (Yeo et al., 2000).

The inverse loading of the cerebellum indicates that processing of emotional status may alternate with that of bodily movement and functions, rather than simultaneous processing. If this is true, weaknesses in activity in the insular components may affect emotional well-being. Consequently, ties to mental health pathologies such as somatic and conversion disorders, bipolar disorders, and others may be possible.

Thus the Cerebellar-Insular factor appears to be involved in somatic and emotional homeostasis maintenance with ongoing salience monitoring and self-speech generation activities.

Temporal-Caudal factor. The sixth factor accounts for 6% of the overall variance in blood flow, and is loaded primarily by the bilateral temporal gyri and fusiform gyrus as well as the caudate nucleus. The bilateral temporomesial parahippocampal and hippocampal gyri and amygdala also load on the factor at lower loadings. The temporal components are anticorrelated with the caudate nucleus.

As in the previous factor, the temporal gyri may be involved in auditory, speech, and language processing, semantic association (including visual images), visual perception and multimodal sensory integration, and personal, episodic, social, and emotional multimodal processing. The fusiform gyrus has facial and categorical recognition functions. The parahippocampal and hippocampal gyri are associated with

learning and memory. The amygdala is associated with emotional experiences, fear, aggression, and affective valence. Taken together, these four components may be functioning in emotionally-valenced memory processing and storage, particularly memories of faces. Whether this is a default behavior of encoding and storing faces seen recently and attaching an emotional valence to them, or a recall process that takes place from memory during resting periods, is not known.

The caudate nucleus serves roles in goal-directed behavior, attention, reinforcement, habit learning, and evaluation of outcomes, and is associated with working memory. In this factor, the role of the anticorrelated caudate nucleus (adjacent to the amygdala and hippocampal area) may be related to valence judgment and assignment based on reinforcement and punishment history.

Thus the Temporal-Caudal factor appears to represent emotionally valenced memory processing (storage and consolidation, retrieval), especially for faces.

Occipital factor. The seventh factor accounts for 5% of overall variance, and is loaded most strongly by the calcarine cortex and lingual gyrus. It has lesser loadings from the occipital gyri and posterior cingulate gyrus, and anticorrelated lesser loadings from the parietal gyri, olfactory cortex, and gyrus rectus.

The calcarine cortex, also called the primary visual cortex, is involved in the summoning of visual mental images (Blumenfeld, 2010). The lingual gyrus engages in visual processing, especially letters, encoding visual memories, and logical ordering (Shepherd, 1994). The inferior, middle, and superior occipital gyri contain the visual association area (Shepherd, 1994). The olfactory cortex functions in odor discrimination, perception, memory, and habituation (Haines, 1995). The gyrus rectus functions in higher

cognition, emotional experience, expression, impulse control, and inhibition (Shepherd, 1994). The parietal gyri/lobules are engaged in action processes, visuomotor functions, visual perception, spatial cognition, reasoning, working memory, maintaining attention on current goals, selectively responding to salient novel information, and responding to environmental stimuli (Wang et al., 2015). The posterior cingulate cortex is associated with cognition and affect, recall of autobiographical and emotional memories, and selective attention between internal and external events (Leech & Sharpe, 2014).

The integration of the parietooccipital and frontomedial components loading on the Occipital factor leads to the interpretation that this factor is primarily a visual perception network (and possibly for multimodal sensory perception, including olfactory), tied to cognition through the gyrus rectus and posterior cingulate. The perceptual regions may be processing information already gathered for storage, or involved in current eyes-open visual perception during the resting state. The opposite sign on the loadings for the parietal gyri and gyrus rectus may indicate cognitive processing or active salience determination regarding visual stimuli is conducted serially and not in parallel with perceptual processing.

Because the third factor (Cingulate-Occipital factor) shared many of the same variable loadings, but had stronger loadings from the cingulate and cuneus, while this Occipital factor has stronger loadings from the occipital components than from the frontomedial components, the functions in visual perception likely are different. The Cingulate-Occipital factor appears to be related towards visualization as in daydreaming, while the Occipital factor appears to have a more task-based orientation towards visual image salience.

Thus, the Occipital factor appears to function in task-based gathering, processing, and management of visuoperceptual and possibly multimodal sensory information, and salience determination.

Parietooccipital-Cerebellar factor. The final and eighth factor accounts for a total of 5% of variance in blood flow, and is primarily loaded by the bilateral precuneus and cuneus, with oppositely signed loadings from the bilateral cerebellar crus. There are minor loadings from the left parietal gyri and right paracentral lobule, and anticorrelated minor loadings from the right frontal inferior gyrus.

Structural elements. The precuneus is thought to be related to visuospatial imagery and mental visualization, episodic memory retrieval, and self-processing operations (perspective of the first-person, agency; Cavanna & Trimble, 2006). Hypothesized functions of the precuneus during at-rest states include continuous information gathering to develop and maintain perception of self, processing of episodic memory stores, and manipulation of information in planning and problem-solving (Gusnard, Akbudak, Shulman, & Raichle, 2001; Raichle et al., 2001).

The anterior portion of the dorsal precuneus has been shown to be related to motor execution and attention, while the posterior dorsal surface is associated with motor and visual imagery. The ventral portion of the precuneus is integral to developing representations of oneself and in referencing these conceptions during periods of internal dialog and perhaps metacognition (Zhang & Chiang-shan, 2012).

The cuneus processes visual information in connection with afferent attention, working memory, and rewards information, and is associated with inhibition (Shepherd, 1994).

The cerebellar crus are the white matter portion of the cerebellar peduncle containing the oculomotor and motor tracts, and are thought to provide timing and coordination information for cortical functions (McAfee, Liu, Sillitoe, & Heck, 2019).

The superior and inferior parietal gyri are associated with functions of visuomotor and visuoperceptual skills, spatial cognition, working memory, reasoning, attention, and recognizing and responding to salient environmental stimuli. These components of the parietal lobe together may act as an always-on sensory and perceptual processing area (Wang et al., 2015).

The paracentral lobule contains motor functions related to lower extremities and excretory functions; however, it is also speculated that the right paracentral lobule may have a role in mood disorder and suicidal behavior, and it shares connections with the limbic system and amygdala (Zhang et al., 2021).

Functional integration. Interpretation of this final factor is limited by the apparent heterogeneity of the loadings. The largest loadings appear to indicate a visual processing function, however such utility is well-represented already in other factors (Cingulate-Occipital and Occipital Factors), so the 5% of variance accounted for by this final factor may represent a miscellaneous factor of unknown correlations.

Thus the Parietooccipital-Cerebellar factor is understood to function as a housekeeping factor representing non-specific miscellaneous at-rest functions.

Higher Order Factors

As a part of the EFA, an examination of potential higher-order factors, as indicated by moderate to high inter-factor correlations, revealed several possible configurations of second-order factors as shown in the Results in Table 31. As discussed

in the results, the usefulness and meaning of these higher-order factors is dependent on the interpretation of the first-order factors just performed. Also, any of the second-order factor configurations reduces the amount of total variance accounted for by the factors (Table 31).

In view of the first-order interpretations, a single second-order factor interpretation (encompassing Factors 1-6, and discarding 7 and 8) accounting for 40% of variance (compared to 66% for the 8-factor first-order solution) makes little sense. The meaning of a single factor related to blood flow would appear to be simplistic- many of the brain areas correlated in blood flow does not lend itself to functional interpretation.

The two second-order factors solution (accounting for 51% of variance) postulates Factors 1-4 and 6 express one underlying construct, and Factor 5 as the second, and again 7 and 8 are discarded. Factor 5, the Cerebellar-Insular factor, would logically stand on its own as a higher-order construct as it represents somatic and emotional homeostasis maintenance, with ongoing salience monitoring and self-speech generation activities, a function that does not clearly overlap other factor functions. Additionally, it is the only factor representing the larger cerebellar areas and the insula as a primary loading. However, the meaning of a single construct combining Factors 1-4 and 6 is broad and somewhat meaningless, involving most brain regions and most at-rest functions.

The three second-order factor solution accounts for 62% of variance. The first construct is Factors 1-4 and 6, as in the two-construct solution above, and continues to have the same limitation in being too general for interpretive use.

The four second-order factor solution, accounting for 63% of variance, is roughly equivalent to the 8-factor single-order solution in explaining the common variance, and

consists of loadings from Factors 3, 4, 6; Factors 1 and 2; Factor 7; and Factors 5 and 8.

Spontaneous cognition (Factor$_2$ 1). Factors 3, 4, and 6 (labeled Factor$_2$ 1 for clarity) accounts for 27% of the variance and consists of the Cingulate-Occipital, Frontal-Basal, and Temporal-Caudal Factors.

Structurally, Factor$_2$ 1 consists of a combination of regions yielding a frontotemporal-occipital-subcortical brain description, describing loadings from the frontal gyri, gyrus rectus, and olfactory cortex from the frontal lobe; the cingulate and amygdala from the limbic system and the caudate and thalamus from the basal ganglia for subcortical components; the fusiform, temporal, parahippocampal, and hippocampal gyri from the temporal lobe; the cuneus, calcarine cortex, and occipital gyri from the occipital lobe; and the angular gyrus from the parietal lobe.

Functionally, Factor$_2$ 1 incorporates management or generation of spontaneous (stimulus-independent) higher-level conscious and unconscious cognition during rest, with complementary control of eye movement and visual processing, from the Cingulate-Occipital factor. It also encompasses the Frontal-Basal factor function of management of working memory, executive control, memory, and emotional salience of inner cognition at rest. From the Temporal-Caudal factor, emotionally valenced memory processing (storage and consolidation, retrieval), especially for faces, is included. Factor$_2$ 1 appears to encompass a significant explanatory construct: that of the DMN, found consistently in fMRI studies.

Integrating the functions above, the dimensions of spontaneous, unconscious and conscious, higher-level cognition involving processing and consolidation of memories, visualization, and determination of emotional valences, appears to be the major function

of $Factor_2$ 1. Minor correlated and anti-correlated functions include visual tracking and executive control that occur as background logistical processes supporting cognition.

The DMN found in fMRI research is characterized as the higher-level conscious resting state of the brain, representing stimulus-independent cognition (Greicius, Krasnow, Reiss, & Menon, 2003) and internal mentation, including spontaneous and largely involuntary activities such as daydreaming, mind-wandering, problem-solving, and planning, based on memory retrieval (Raichle, 2015). This descriptor is an apt summary for $Factor_2$ 1.

Control ($Factor_2$ 2): The second component ($Factor_2$ 2) of the four factor second-order solution consists of Factors 1 and 2, the Parietal and Motor/Sensory Factors. As noted in the factor interpretations (Table 34), these two factors are both loaded with similar sensorimotor, parietal, and basal ganglia components in complementary fashion; they are similar in components yet out-of-phase with one another as indicated by anticorrelations. Therefore, describing the 18% of common variance accounted for by $Factor_2$ 2 with these two factors makes logical and intuitive sense.

Structurally, $Factor_2$ 2 is composed of parietal (supramarginal, angular, and parietal gyri and the precuneus), motor/sensory (supplementary motor area, precentral and postcentral gyri, paracentral lobule and Rolandic operculum), and basal ganglia (pallidum, putamen, caudate) components, as well as minor loadings from the frontal superior gyrus and temporal gyrus.

Functionally, $Factor_2$ 2 incorporates attention, salience determination, cognitive control, filtering of perceptual information, monitoring and adjusting the motor/sensory system, and incorporation of this information into somatic consciousness or self-

conceptualization.

In comparison with fMRI findings for resting-state networks, $Factor_2$ 2 appears to represent both task-evoked (sensorimotor) and spontaneous networks (attention, salience, cognitive control, perception), with the basal ganglia and frontal components governing the switching between functions. $Factor_2$ 2 is most closely related to the well-replicated executive control, sensorimotor, and salience resting-state networks from fMRI research.

The emergence of this comprehensive factor in higher-order factor analysis is commensurate with the temporally defined differences between SPECT and fMRI imaging modalities. fMRI resting-state analyses rely on the detection of low-frequency (e.g., only 1 activation per 10 sec) occurrences of activity, measured over 15-30 min of imaging. SPECT, on the other hand, is a snapshot over a period of activity of up to a minute or possibly more. Therefore, low-frequency activations indicating independent resting-state networks may appear as a combined factor in the second-order EFA of SPECT.

Visuoperception ($Factor_2$ 3): The third component ($Factor_2$ 3) of the four factor second-order solution consists of Factor 7, the Occipital factor, alone, at 13% of variance.

Structurally, this factor is loaded by occipital components (calcarine, lingual, and occipital gyri) and minor loadings from anticorrelated frontal components (olfactory cortex and gyrus rectus) and the parietal gyri and posterior cingulate gyrus.

Functionally, $Factor_2$ 3 appears to function in task-based gathering, processing, and management of visuoperceptual (and possibly multimodal sensory) information, and salience determination.

$Factor_2$ 3 is similar in nature to the fMRI-derived visual resting-state network, a

task-activated network that appears to be functional with eyes open (perceptual activity) as well as eyes closed (visualization). The inclusion of the olfactory cortex and parietal cortex in the loadings for $Factor_2$ 3 indicates that multimodal processing may be incorporated into this factor.

Homeostasis ($Factor_2$ 4): The fourth component ($Factor_2$ 4) of the four factor second-order solution is composed of Factors 5 and 8, the Cerebellar-Insular and Parietooccipital-Cerebellar Factors. It represents 5% of the total common variance.

Structurally, $Factor_2$ 4 is loaded principally by the cerebellum (cerebellum, cerebellar crus, vermis), temporal cortex (Rolandic operculum, insula, Heschl's gyrus, temporal gyrus, fusiform gyrus, paracentral lobule), parietooccipital medial cortex (precuneus and cuneus), and with minor loadings from the parietal gyri and frontal inferior gyri.

Functionally, $Factor_2$ 4 appears to represent somatic and emotional homeostasis management including salience monitoring, self-speech, and visual representations and processing.

While noting that $Factor_2$ 4 accounts for little variance amongst the four second-order factors, it is the only component representing the effects of both the cerebellum and the insula. Notably, these two regions are among the least understood. This factor appears to be meaningful and valuable, and open to future exploration.

In summary, the second-order extraction of four higher-order factors appears to be meaningful and useful, particularly in aligning results with existing interpretations of resting-state networks in the literature derived primarily from fMRI research. Table 35 provides a summary of the second-order interpretations.

Table 35

Summary of Second-Order Factor Interpretations

Factor	Description
1: Spontaneous cognition	Spontaneous, unconscious or conscious, higher-level cognition involving processing and consolidation of memories, visualization, and determination of emotional valence
2: Control	Task-evoked (sensorimotor) and spontaneous networks (attention, salience, cognitive control, perception)
3: Visuoperception	Task-based gathering, processing, and management of visuoperceptual (and possibly multimodal sensory) information, and salience determination
4: Homeostasis	Somatic and emotional homeostasis management including salience monitoring, self-speech, and visual representations and processing

CHAPTER VI: DISCUSSION

Comparison to Expected Findings

The hypothesized results of this experiment were that factor analysis of at-rest SPECT rCBF in a clinical sample will reduce 67 measured ROI variables into a latent three-factor structure. Together, these three factors were predicted to describe 80% of the variance in rCBF blood flow at rest, with the remaining 20% of variance attributable to noise or error. In general terms, the three factors will represent higher integrative functions, emotional and salience functions, and input-output functions.

The first hypothesized factor, higher integrative functions, was expected to also include attention and executive control and be loaded by the prefrontal cortex, cingulate gyrus, medial temporal, parietal, and occipital areas. The second factor, emotional and salience functions, was expected to be loaded by the subcortical and insular regions. The third factor, input-output functions, was expected to be loaded by ROI variables from the occipital areas, auditory cortex, and sensorimotor areas.

Results of the second-order interpretation (Table 35) indicated a four-factor pattern. The first factor, Spontaneous Cognition, is loaded by the frontal lobe, the cingulate and amygdala from the limbic system, the basal ganglia, the temporal lobe, the occipital lobe, and the angular gyrus from the parietal lobe. The second factor, Control, is loaded by the parietal, motor/sensory, basal ganglia, and minor loadings from the frontal superior gyrus and temporal gyrus. The third factor, Visuoperception, is loaded by occipital components with minor loadings from frontal, parietal, and cingulate gyrus components. The fourth factor, Homeostasis, is loaded by the cerebellum, temporal cortex, parietooccipital medial cortex, and with minor loadings from the parietal gyri and

frontal inferior gyri.

In comparison to the hypothesized results (noting that EFA is not hypothesis driven; the hypothesis serves as a descriptive benchmark only), it appears that experimentally derived results resemble the hypothesized constructs in both structure and function, but vary significantly in how those functions and structures are distributed across factors. Notably, functions and their corresponding structurally associated brain areas were assumed in the analysis to be correlated (not orthogonal).

The hypothesized functions predicted uncorrelated functions, which in hindsight does not seem to have been an appropriate assumption, given the acceptance that rCBF is highly correlated due to shared vascular systems and tissues between ROI. However, all the hypothesized functions and contributory structural reasons are represented in the results, and therefore it is fair to say that the hypothesis has been met.

Understanding the Findings and Interpretation

Tables 33-35 show the factor loadings (of the structural ROI), first-order factor, and second-order factor interpretations, respectively. To summarize, we interpret the findings to signify the presence of eight underlying constructs characterized by blood flow patterns in brain tissue (Table 34), and further conceptualize these constructs by the assignment of functionality associated with the specific ROIs, in accordance with the magnitude and direction of specific ROI loadings.

We then noted the large intercorrelations of these eight constructs and therefore interpreted a second-order extraction of factors. This second extraction yielded the four constructs as shown in Table 35. These four constructs represent the first known characterization of brain activity patterns in the resting state using SPECT imaging.

These findings, as discussed earlier, align well with findings from fMRI imaging that show brain activation over a time series.

Relationship of current to previous findings. Szabo et al. (1992) found a limbic factor, characterized by frontal, temporal, limbic, and basal ganglia loadings, and a sensorimotor factor, loaded by parietal and occipital lobes and the cerebellum, in a PET study of small sample size.

Findings in fMRI resting-state research (Raichle, 2015) supported the existence of a resting-state DMN in the ventral and dorsal medial prefrontal cortices, posterior cingulate cortex, precuneus, lateral parietal cortex, and the entorhinal cortex, as well as the parahippocampal gyrus and hippocampal formation.

Zhang and Raichle (2010) found that in addition to the DMN, resting-state networks include attention, executive control, sensorimotor, visual, auditory, and salience; this work was replicated by Yeo et al. (2011). Doucet, Lee, and Frangou (2019) found replications of findings reliably support involvement of the cingulate, precuneus, medial PFC, and angular gyrus in the DMN, and that other resting-state networks (Table 9: Executive Control, Sensorimotor, Visual, and Salience) also have reliable findings.

The four-factor description from the present study does not contradict these previous findings. The Spontaneous Cognition factor resembles the DMN in function and structure. The Control factor incorporates the fMRI-determined Executive Control, Sensorimotor, and portions of the Salience factors. The Visuoperception factor is similar to the Visual factor in fMRI resting states. The Homeostasis factor is like the Salience network identified in fMRI findings.

What exactly is the resting state? Throughout this exposition, we have

addressed the neural behavior of the brain at rest, simply defined as spontaneous brain activity occurring when no active, conscious task has been required. In the current study, people are free to blink eyes, yawn, scratch, shift gaze, think, or tap fingers. Participants in resting-state imaging studies have reported engaging in a series of tasks including inner speech, musical experience, visual imagery, episodic recall, future planning, mental number manipulation, and heightened somatosensory awareness (Bandettini, 2019).

Although movement in fMRI studies is more restricted with the use of a head positioning cradle, and stricter instructions not to move to avoid artifacts in imaging, involuntary movement still occurs, and mental activity cannot be strictly limited. The scientific interest in the resting state does not exclude these voluntary and involuntary behaviors when the ultimate interest is in non-task-oriented activity, such as processing of perceptual information, consolidation of memory, planning, rumination, review, scheduling, and more. The resting state does not clearly differentiate between voluntary and involuntary, conscious or unconscious, aware or unaware, or the like; it is only necessary that the behavior not related to an experimentally assigned task.

The present results clearly show an integration of spontaneous and less-spontaneous activity in the resting state; however, due to the nature of SPECT imaging, it is not possible to determine if spontaneous and task-activated activity is occurring simultaneously or in an alternating (and non-overlapping) fashion.

The Spontaneous Cognition factor reflects automatic activities such as consolidation of memory, assignment of emotional valence, and visualization as in daydreaming. This is conflated with more voluntary cognitive processing such as planning the grocery list or debating whether participating in this study was a good use of

time.

The Control factor involves automatic functions such as attention and salience determination, perception, cognitive control, and sensorimotor control such as eye-blinking, however, each of these spontaneous tasks has inseparable voluntary correlates, such as the automatic motor response shifting gaze to a perceived movement in the room, followed by turning the head voluntarily to consciously investigate.

Similarly, the Visuoperception factor is automatically gathering perceptual information and determining salience, but these processes have an element of voluntary activity at times.

Of all the factors, perhaps Homeostasis has the most automatic or unconscious, spontaneous nature.

This lack of differentiation of spontaneous and task-driven activation is not necessarily a confound, but an experimental observation. In addition, much task related behavior is anticorrelated with automatic behavior in the resting state (Fox et al., 2006), indicating a schedule or switching that keeps one activity from intruding on the other. In practical applications of the data, such as in diagnosing or classifying pathology, the comparison is to blood flow patterns in a healthy brain in a resting state with the same characteristics, so the differentiation of automatic versus task-based in the resting-state activity may not be critical.

However, if the differential between automatic and task-based behavior is predictive of dysfunction (e.g. depressed people may spend more time or energy on automatic than task-based default functioning), it would likely go undetected with current technology and study methods.

We do not have a clear idea of how much perceptual or memory information processed during the resting state, and especially by the DMN, consists of stored, versus real-time, information. Margulies and others (2016) noted that brain function can be laid on a spectrum from spontaneous systems such as the DMN to task-activated networks such as the motor-sensory. From Margulies' point of view, there is little overlap or correlation, and the DMN functions independent of immediate perceptual information.

Empirically, we know that brain activity consumes up to 20% of bodily energy availability (at 2% of overall body weight), and local energy requirements are estimated to increase by as little as 5% during a defined task (Raichle, 2015). In other words, it is not clear why default cognitive processing takes place only at rest while awake, and not simultaneous with other task-based activity, or during sleep, but evidence suggests that default and resting-state networks attenuate when a task is begun (Greicius et al., 2003; Raichle, 2015; Margulies et al., 2016) while the corresponding task network increases in activation. (However, the same effects were not noted in sensory perceptual networks, which appear to co-function with DMN and resting-state networks without attenuation; Greicius et al., 2003.)

Whether this attenuation of the DMN or resting-state network is related to energy budgeting, neuronal capacity, or some other restrictive factor, is unknown. The attenuation may be carried out by the frontal gyri or basal ganglia in their known switching roles (Greicius et al., 2003).

Hemispheric differences in rCBF. An unexpected finding in the current study was the apparent absence of moderate to large differences in loadings between contralateral-equivalent regions (left versus right hemisphere). With very few exceptions,

most loadings above |.30| were similar bilaterally.

Larger differences were found in the Parietal factor (right precentral gyrus and right Rolandic operculum were more strongly loaded, indicating more contralateral motor activity was possibly occurring on the left than right); the Cingulate-Occipital factor (only in the left calcarine cortex); the Cerebellar-Insular factor (loadings from the right temporal gyri only); the Occipital factor (loadings from the right parietal gyri only); and the Parieto-Occipital factor (right frontal inferior gyrus only).

The limited predominance of right hemisphere ROI in these factors appears to be consistent with past findings of right- or non-dominant hemisphere predominance of social, emotional, visuospatial, nonverbal, and personality functionality.

Generalizability of the current findings. The marked strength of the present results is in reliability of the EFA results due to the methods used. The incorporation of robust EFA methods controlled for influential outliers and allowed for tolerance of possibly non-normal distributions. Use of bootstrapping methods in extraction and determination of loadings, in addition to the very large sample size, indicates that the EFA results are highly replicable.

However, although EFA results are likely to be generalizable to the population with neurological and psychological pathologies sampled, there is no assurance that pathological samples from other sources would not have different participant characteristics that could affect results. More importantly, the next step should be CFA examination of data. EFA is not intended to be a generalizable result.

Clinical significance. Resting-state studies are useful for several reasons. The present study provides the first step towards an empirically supported and standardized

template for expectations of blood flow in clinical patients (additional steps will follow with CFA studies). Measuring the resting state of blood flow in the brain allows the clinician to view the patient's physiological and mental functioning, because blood flow represents neuronal activity; it is analogous to the general practitioner assessing health with blood pressure and pulse rate.

Confirmatory analysis, standards, and norms are necessary to establish the range of healthy behavior and function, but patterns for unhealthy states are also needed. Comparing resting-state neuropathological or psychopathological rCBF may allow assessment of degree and type of pathology. Through the factor analysis of rCBF, this study provides a normative template for clinical outpatient rCBF to allow for these comparisons.

This study is also a step towards advancing the science beyond the at-rest healthy brain to the pathological brain's at-rest blood flow patterns. Without a process of model-building and testing, there is no way to study rCBF and diagnosis of pathology methodically.

Limitations

The overarching strength of this study is in the reliability of the results, based on replicability (using 1000 re-samples for factor extraction), generalizability (with a sample size of 12,217), minimizing of influence of outliers and missing data through robust analysis techniques, use of bootstrapped confidence intervals to determine significant loadings, and use of multiple methods of selecting factors to be extracted.

Weaknesses in this study include the lack of a healthy sample with which to make comparisons or draw inferences regarding normal resting-state network function.

A weakness inherent to the SPECT imaging used is the lack of temporally spaced slices that would allow observation of blood flow over time, for more direct comparison to fMRI.

An inherent weakness in the statistical analysis is that there is no previous EFA that would justify the use of confirmatory methods, thus limiting this study to exploratory information and results pending a subsequent CFA. Furthermore, factor scores, although obtainable in EFA, are not deemed reliable enough to draw conclusions.

Another weakness in the current study is the reliance of EFA on researcher assumption and interpretation. Although attempts have been made to examine possible alternatives, the opportunity for experimenter bias to influence EFA results was still present.

First, selection of extraction method was compared with other methods to ensure no significant difference in results. Second, the number of extracted factors was determined by experimenter selection of preferred outcome from many techniques; however, analysis and comparison of other factor extractions was made and compared for differences to minimize bias. Third, the selection of loaded variables to be interpreted in the factor descriptions was made with a liberal cutoff (|.30|) to minimize bias and loss of power in understanding the nature of the factors, however, doing so increased the opportunity for interpretation of spurious variable loadings.

On the other hand, the use of bootstrapped loadings maximized the reliability of those loadings.

The interpretation of the factors was based on an oblique rotation, and compared to the orthogonal rotation. Furthermore, a secondary extraction was made based on high

intercorrelations. There is no objective method to check or verify these choices; they are based on judgement of the distribution of variance and the ease of interpretation, a very subjective criteria. However, both solutions (orthogonal and oblique, and first- and second-order extractions) were included in case a reader wishes to draw different conclusions.

An additional threat of bias in interpretation comes from the translation of brain regions as loaded variables into functional descriptions of factor functions. We do not have empirical proof that any given brain region is 1) in the same location in every participant; 2) has the same delineated boundaries of function in each participant; or 3) has any defined purported function. Although much evidence supports the attribution of specific functions to fixed brain areas, iatrogenic variance is also common.

The best defense against this threat is the sample size and replication through bootstrapping. Further, interpretations appear to be commensurate with prior fMRI discoveries (although that does not rule out confirmation bias). Only with successive replication in CFA will results be accepted without qualification.

There is an additional risk in SPECT and fMRI error of capitalization on chance findings. Random data is known to generate apparent patterns that can be misinterpreted as underlying constructs (Osborne, 2014). It remains a possibility that random noise could be interpreted as a lower-level factor as an artifact of the data; the replicability of the same result may occur because there is a pattern in the noise.

Although this possibility cannot be excluded in the present study, its likelihood is decreased because results are (in general) like replicated fMRI results. However, overinterpretation of the lower-variance factors should proceed with caution.

A related limitation of fMRI and SPECT studies of resting-state networks is that noise specific to the imaging modality may obscure low-frequency and low-amplitude signals otherwise representative of resting-state networks. When imaging methodology is modified to filter noise, areas otherwise shown as non-active in fMRI have been shown to be active at low levels, and up to 95% of the whole brain demonstrates activity correlated with task-activated brain areas at very low signal levels (Gonzalez-Castillo, Saad, Handwerker, Inati, Brenowitz, & Bandettini, 2012).

As discussed previously, in the best-case generalizability of results should be quite good for a pathological population, but further work is needed before inferences can be made to a healthy population. Moreover, additional work is necessary to understand age and gender differences, and differences between pathologies and number of diagnoses, as indicated in the results.

Theoretical Challenges

In addition to intrinsic limitations due to methodology as discussed previously, there are some assumptions in the science of resting-state blood perfusion that are revisited here to clarify possible challenges to underlying theory. Of note, the use of resting-state analysis in this study may reduce possible effects from these challenges, but they are still germane to interpretation of results.

Assumptions. The assumption that blood flow is linear, normally distributed, and correlated with neural activity underlies the expected relationship between the SPECT results and neuronal activity. This underpinning assumption is not without controversy (past and present).

The neurovascular coupling hypothesis is a century-and-a-half old: Increased

neuronal activity demands increased metabolism that triggers increased blood flow (Sandrone et al., 2014). This was challenged by evidence from Fox and Raichle (1986) that blood oxygenation during neuronal activation exceeded demands, increasing, and then overshooting, requirements, as though the neurovascular coupling had decoupled.

In other words, long-held theory predicted that blood flow will increase while oxygenation and metabolic fuel supplies remain constant to meet neural demand, but the observation was that blood flow increased and supplied needed oxygen, but resulted in a surplus of unused oxygen (which is the basis of fMRI detection of activation). Thus, by measuring blood flow with SPECT, we assume that increased concentration of radiotracer in brain tissue (assuming we know the baseline concentration) indicates increased neuronal activity. However, we are measuring tissue deposits, and not the tracer remaining in the venous draining system.

Therefore, comparisons of relative blood flow (measuring deposited radiotracer as a correlate of metabolic increase due to neuronal activation) to fMRI activations (measuring increased blood oxygenation as a correlate of neuronal activation) is based on assumptions that are not well documented at this time, and may be revised as research progresses (Bandettini, 2019). We do not know why oxygenation overshoot occurs, and if it is purposeful (the human body is normally efficient). The answer to why this occurs may directly bear on interpretation of blood flow observations.

Further, we are measuring direction of change, but not magnitude of change; these are relative and not absolute comparisons. Although present EFA results rank factors in prominence based on accounting of variance, quantification of actual metabolic change still eludes us. Proposed use of SPECT imaging to differentiate psycho- and

neuropathology is like other neuropsychological assessment processes. Large, well-stratified normative data are needed for relative comparison, but there is no benchmark criterion value for pathology without comparison to the normal distribution, assuming blood flow response is indeed normally distributed.

Finally, experimental results have reliably documented the post-stimulus undershoot effect in fMRI (Bandettini, 2019). After oxygenation has decreased post-activation, oxygenation levels temporarily drop below baseline for up to 40 s. The reason is unknown, but one possibility is a brief reduction in blood flow due to neuronal inhibition mechanisms occurring post-activation. Although it appears unlikely that absorption of the injected bolus of radiotracer in SPECT would be affected during such a short interval, the unknown nonlinear dynamics of blood flow and neuronal habituation suggest an element of caution in interpretation.

Given the reported low frequency of some resting-state networks (a task-based network may activate just once every 10 s; Bandettini, 2019) combined with possible inhibitory or habituation effects acting to attenuate activity, the possibility exists that some resting-state networks could be missed entirely in SPECT imaging.

The pancake effect. As discussed previously, when we use SPECT measurement of blood flow, we are looking at a pancaked or collapsed temporal effect. It is unknown from examination of SPECT data whether metabolic demand changed in a linear fashion or, like the fMRI-oxygenation hemodynamic response curve, in a non-linear pattern. We only know that radiotracer deposits reached a certain level by the time of injection of the radiotracer bolus.

Thus, interpretation of results is based on comparison to expectations of final

results (again making this fundamentally a neuropsychological process) rather than knowledge of actual neuronal activity.

Correlation is not necessarily connectivity. The assumption that intercorrelated ROI that are labeled as *networks* in this, and other studies is not without peril. In fMRI methodology, correlation of activations has the added temporal dimension that sometimes allows co-activating areas to be more easily found, because the activation pattern repeats several times during the imaging period, allowing a built-in replicability check. In SPECT, particularly in an EFA, there is a single characterization of any co-activated ROI in the dataset, so this check is not available.

It is a broad assumption inherent in the EFA method that if ROI are correlated, then they must be connected (part of the same factor structure). In fMRI, specific artifacts in imaging due to such things as bulk movement, cardiac pulsation, and breathing, are associated with false correlations that are interpreted as connectivity (Bandettini, 2019).

In SPECT, it is also possible that biological artifacts may influence results, but such artifacts are not well studied. Because SPECT images are based on radiotracer deposits in tissue of moderate duration (up to several hours) rather than time-fluctuating oxygen activity that dissipates in up to 10 s, these specific confounds are not an issue. However, there may be other yet unknown conditions in SPECT that increase absorption of radiotracer, outside of blood flow rate.

Dynamic connectivity. There is evidence from diffusion tensor imaging studies that resting-state networks correspond to structural tracts within the brain from ROI to ROI in cases where ROI are not already contiguous (Margulies et al., 2016). Thus, some resting-state networks may exist as ROI and connective myelinated pathways, hardwired

and always present to perform certain tasks.

However, some ROI are members of several networks, and discrete ROI or submodules are repurposed when the brain is acting on different stimuli demands. Some resting-state networks are only present on a determinate frequency rate (for example, the anticorrelated Parietal and Motor-Sensory factors represent networks that may alternately be active and inactive).

In fMRI, this is known as the dynamic functional connectivity paradigm, and much like Schrödinger's cat, observing the active network requires one to be in the right place at the right time. In the case of SPECT, the time span of radiotracer absorption must coincide with the appearance of the resting-state network to the extent that tissue deposits will be detectable on later imaging.

There is current study of variations in *dwell time*, a measure of the duration of appearance of the network, and its relationship to schizophrenia, autism, and mild cognitive impairment (Bandettini, 2019).

Future Directions

In addition to confirmatory analysis to replicate and verify factor structure in persons with neurological and psychological pathology, data collection using SPECT imaging and analysis in those without known disorders is necessary to enable comparisons. Furthermore, examination of results using CFA with consideration of age, gender, and pathology will be of benefit.

Present results indicate significant differences in blood flow by age in select ROI (gyrus rectus, amygdala, parietal gyri, calcarine cortex, putamen) and in gender (all ROI except the gyrus rectus, paracentral lobule, fusiform gyrus, and calcarine cortex) as well

as interaction effects. Significant differences in blood flow between diagnostic groups were also shown in an a priori discriminant analysis. These conditions and effects all require additional study beyond the scope of the present experiment.

What results could be expected from future factor-based research of resting-state blood flow pattern differences between persons with diagnosed pathology and healthy controls? Factor scores, although likely to be unreliable when taken from an EFA (Gorsuch, 2015; Osborne, 2014), may be useful after a CFA, and allow comparison of individuals based on factor scores for each resting-state network (eight first-order scores and four second-order scores, for instance).

The ranking of factors may be found to be indicative of inter-participant differences; a person with the Parietal factor ranking third instead of first may have cognitive pathology, for example. Such standardized assessment results can then be compared to and combined with traditional paper-pen/computer-based neuropsychological assessment scores to establish correlations and relationships with specific pathologies for classification and diagnosis (and perhaps monitoring of progress and decline and treatment effects).

In fMRI studies, Shannon et al. (2011) found motor-planning regions were correlated with spatial attention and executive control networks in typical juveniles, while they were correlated with the default mode network in juveniles with impulse control problems. This points towards another possible measure: Comparison of correlations of default and resting-state networks with active networks to examine meaningful differences and possible associations with pathology; Raichle (2015) calls this the *balance* approach. A set of normative data based on expected ratios or correlations with

active condition blood flow patterns may offer an additional path to assessment of neuro- and psychopathology.

Psychopathology and blood flow. As presented earlier in the review of the literature, the study of resting-state networks and their relationship with pathology is a topic of current interest. In fMRI studies, the resting-state DMN has been shown to be hyperactivated and interconnected more heavily with other brain regions in persons with schizophrenia or depression in comparison to healthy fMRIs, and ability to suppress the DMN has been correlated with better attention (Whitfield-Gabrieli and Ford, 2012).

In view of the present study's results, the expectation for future studies of blood flow in healthy individuals using SPECT resting state is that healthy blood flow patterns would show differences in loading strengths within factors, and differences in factor order based on less activity in some areas. The expectation for future blood flow studies in pathological individuals is that (as anticipated based on ROI blood flow comparisons already made; see Results) persons with multiple diagnoses will have different blood flow patterns than those with single diagnosis, and there will be a difference in blood flow patterns between several diagnostic groups.

Conclusion

In the present study, we reliably established eight first-order and four second-order latent constructs explanatory of 66% of the total variance in regional cerebral blood flow in the resting state of a large sample of participants with clinical psychopathology and neuropathology. These factors were interpreted based on perceived functional contributions from 67 structural regions of the brain, and the interpretations were informed by and compared to expectations based on previous fMRI research into the

resting state. The resting state is fundamentally a new construct, studied extensively only since 2005, but a topic of interest in determining methods for diagnosis, classification, and treatment efficacy for neuropathology and psychopathology.

From these results, we drew conclusions that SPECT imaging is a viable resource in the determination of resting-state networks, with complementary findings to those already achieved in fMRI. Moreover, the both the eight first-order and the four second-order factor patterns obtained appear to be reliable and replicable due to the use of robust methods, a large sample size, and internal replicability processes such as bootstrapping and confidence intervals.

The resulting second-order interpretation included factors of Spontaneous Cognition, Control, Visuoperception, and Homeostasis, indicating that the human brain at rest performs meaningful cognitive, motor-sensory, and self-management processes. Because this study examined a participant group with diagnosed psychopathology and neuropathology, future work is needed to establish healthy and individual-diagnosis group factor structures for comparison.

Needs for future research to meet these goals were also presented, as well as examples of eventual clinical applications for SPECT technology in detection and monitoring of disorders, given SPECT's cost advantages, ubiquity, and versatility. It is hoped that future confirmatory replications and expansion to healthy comparison groups will allow this technology to increase affordable international healthcare access for psychological and neurological screening purposes.

REFERENCES

Abdi, H. (2007). Centroid, center of gravity, center of mass, barycenter. In N. Salkind (Ed.), *Encyclopedia of measurement and statistics.* Thousand Oaks, CA: Sage.

Abdi, H., & Williams, L. J. (2010). Barycentric discriminant analysis (BADIA). In N. Salkind (Ed.), *Encyclopedia of research design*, 64-75. Thousand Oaks, CA: Sage.

Achim, A. (2017). Testing the number of required dimensions in exploratory factor analysis. The Quantitative Methods for Psychology, 13(1), 64-74. https://doi.org/10.20982/tqmp.13.1.p064

Agarwal, S., Sair, H. I., Yahyavi-Firouz-Abadi, N., Airan, R., & Pillai, J. J. (2016). Neurovascular uncoupling in resting state fMRI demonstrated in patients with primary brain gliomas. *Journal of Magnetic Resonance Imaging*, *43*(3), 620-626. https://doi.org/10.1002/jmri.25012

Amen, D. G., Sarabi, M. S., Willeumier, K., Taylor, D., Raji, C., Meysami, S., & Raghavendra, C. (2017). Functional SPECT neuroimaging using machine learning algorithms distinguishes autism spectrum disorder from healthy subjects. *Journal of Systems and Integrative Neuroscience, 3*(3). https://doi.org/10.15761/JSIN.1000160

Amen, D. G., Trujillo, M., Newberg, A., Willeumier, K., Tarzwell, R., Wu, J. C., & Chaitin, B. (2011). Brain SPECT imaging in complex psychiatric cases: An evidence-based, underutilized tool. *The Open Neuroimaging Journal*, *5,* 40-48. https://doi.org/10.2174/1874440001105010040

Andreescu, C., Gross, J. J., Lenze, E., Edelman, K. D., Snyder, S., Tanase, C., &

Aizenstein, H. (2011). Altered cerebral blood flow patterns associated with pathologic worry in the elderly. *Depression and Anxiety*, *28*(3), 202-209. https://doi.org/10.1002/da.20799

Arora, G., Sharma, P., Sharma, A., Mishra, A. K., Hazari, P. P., Biswas, A., ... & Kumar, R. (2018). 99mTc-Methionine hybrid SPECT/CT for detection of recurrent glioma: comparison with 18F-FDG PET/CT and contrast-enhanced MRI. *Clinical Nuclear Medicine*, *43*(5), e132-e138. https://doi.org/10.1097/RLU.0000000000002036

Asenbaum, S., Brücke, T., Pirker, W., Pietrzyk, U., & Podreka, I. (1998). Imaging of cerebral blood flow with technetium-99m-HMPAO and technetium-99m-ECD: a comparison. *Journal of Nuclear Medicine*, *39*(4), 613-618. Retrieved from https://jnm.snmjournals.org/content/jnumed/39/4/613.full.pdf

Ashburner, J., & Friston, K. J. (1999). Nonlinear spatial normalization using basis functions. *Human Brain Mapping*, *7*(4), 254-266. https://doi.org/10.1002/(SICI)1097-0193(1999)7:4<254::AID-HBM4>3.0.CO;2-G

Ashby, F. G. (2015). An introduction to fMRI. In B. Forstmann & E. J. Wagenmakers (Eds.), *An introduction to model-based cognitive neuroscience* (pp. 91-112). New York, N.Y.: Springer. https://doi.org/10.1007/978-1-4939-2236-9_5

Attwell, D., Buchan, A. M., Charpak, S., Lauritzen, M., MacVicar, B. A., & Newman, E. A. (2010). Glial and neuronal control of brain blood flow. *Nature*, *468*(7321), 232-243. https://doi.org/10.1038/nature09613

Bandettini, P. A. (2020). *fMRI.* Cambridge, MA: MIT Press.

Beck, A. T., Steer, R. A., & Brown, G. (1996). *Beck Depression Inventory–II.* San Antonio, TX: Psychological Corporation.

Bijsterbosch, J., Smith, S. M., & Beckmann, C. F. (2017). *An introduction to resting state fMRI functional connectivity*. Oxford, U.K.: Oxford University Press.

Blefari, M. L., Martuzzi, R., Salomon, R., Bello-Ruiz, J., Herbelin, B., Serino, A., & Blanke, O. (2017). Bilateral Rolandic operculum processing underlying heartbeat awareness reflects changes in bodily self-consciousness. *European Journal of Neuroscience*, *45*(10), 1300-1312. https://doi.org/10.1111/ejn.13567

Blumenfeld, H. (2014). Neuroanatomy through clinical cases. Sunderland, MA.: Sinauer Associates.

Broyd, S. J., Demanuele, C., Debener, S., Helps, S. K., James, C. J., & Sonuga-Barke, E. J. (2009). Default-mode brain dysfunction in mental disorders: A systematic review. *Neuroscience & Biobehavioral Reviews*, *33*(3), 279-296. https://doi.org/10.1016/j.neubiorev.2008.09.002

Buckner, R. L., Andrews-Hanna, J. R., & Schacter, D. L. (2008). The brain's default network: Anatomy, function, and relevance to disease. https://doi.org/10.1196/annals.1440.011

Bushnell, D. L., Eastman, G., & Barnes, W. E. (1991). Comparison of IMP and HMPAO for SPECT Brain Imaging. *Journal of Nuclear Medicine Technology*, *19*(2), 70-74. Retrieved from https://tech.snmjournals.org/content/jnmt/19/2/70.full.pdf

Cabeza, R. (2002). Hemispheric asymmetry reduction in older adults: The HAROLD model. *Psychology and Aging*, *17*(1), 85. https://doi.org/10.1037/0882-7974.17.1.85

Cabeza, R., Ciaramelli, E., Olson, I. R., & Moscovitch, M. (2008). The parietal cortex and episodic memory: an attentional account. *Nature Reviews Neuroscience, 9*(8), 613-625. https://doi.org/10.1038/nrn2459

Camargo, E. E. (2001). Brain SPECT in neurology and psychiatry. *Journal of Nuclear Medicine*, *42*(4), 611-623.

Camargo, E. E., Szabo, Z., Links, J. M., Sostre, S., Dannals, R. F., & Wagner Jr, H. N. (1992). The influence of biological and technical factors on the variability of global and regional brain metabolism of 2-[18F] fluoro-2-deoxy-D-glucose. *Journal of Cerebral Blood Flow & Metabolism*, *12*(2), 281-290. https://doi.org/10.1038/jcbfm.1992.38

Carpenter, M. B. (1985). *Core text of neuroanatomy*. Baltimore: Williams & Wilkins.

Catafau, A. M. (2001). Brain SPECT in clinical practice. Part I: perfusion. *Journal of Nuclear Medicine*, *42*(2), 259-271. Retrieved from https://jnm.snmjournals.org/content/42/2/259.long

Cavanna, A. E., & Trimble, M. R. (2006). The precuneus: A review of its functional anatomy and behavioural correlates. *Brain*, *129*(3), 564-583. https://doi.org/10.1093/brain/awl004

Chang, L. T. (1978). A method for attenuation correction in radionuclide computed tomography. *IEEE Transactions on Nuclear Science*, *25*(1), 638-643. https://doi.org/10.1109/TNS.1978.4329385.

Chen, J., Venkat, P., Zacharek, A., & Chopp, M. (2014). Neurorestorative therapy for stroke. *Frontiers in Human Neuroscience*, *8*, 382. https://doi.org/10.3389/fnhum.2014.00382

Chenji, S., Jha, S., Lee, D., Brown, M., Seres, P., Mah, D., & Kalra, S. (2016). Investigating default mode and sensorimotor network connectivity in amyotrophic lateral sclerosis. *PLoS One*, *11*(6), e0157443. https://doi.org/10.1371/journal.pone.0157443

Cordes, D., Haughton, V. M., Arfanakis, K., Wendt, G. J., Turski, P. A., Moritz, C. H., ... & Meyerand, M. E. (2000). Mapping functionally related regions of brain with functional connectivity MR imaging. *American Journal of Neuroradiology*, *21*(9), 1636-1644. Retrieved from http://www.ajnr.org/content/21/9/1636.short

Corbetta, M., & Shulman, G. L. (2002). Control of goal-directed and stimulus-driven attention in the brain. *Nature Reviews Neuroscience, 3*(3), 201-215. https://doi.org/10.1038/nrn755

Costello, A. B., & Osborne, J. (2005). Best practices in exploratory factor analysis: Four recommendations for getting the most from your analysis. *Practical Assessment, Research, and Evaluation, 10*(1), 7. https://doi.org/10.7275/jyj1-4868

Craddock, R. C., James, G. A., Holtzheimer III, P. E., Hu, X. P., & Mayberg, H. S. (2012). A whole brain fMRI atlas generated via spatially constrained spectral clustering. *Human Brain Mapping, 33*(8), 1914-1928. https://doi.org/10.1002/hbm.21333

Craig A. D. (2009). How do you feel- now? The anterior insula and human awareness. *Nature Reviews Neuroscience, 10*(1), 59–70. https://doi.org/10.1038/nrn2555

Damasio, A. R. (1999). *The feeling of what happens: Body and emotion in the making of consciousness*. New York, NY: Houghton Mifflin Harcourt.

Damoiseaux, J. S., Beckmann, C. F., Arigita, E. S., Barkhof, F., Scheltens, P., Stam, C.

J., ... & Rombouts, S. A. R. B. (2008). Reduced resting-state brain activity in the "default network" in normal aging. *Cerebral Cortex*, *18*(8), 1856-1864. https://doi.org/10.1093/cercor/bhm207

De Cristofaro, M. T. R., Sessarego, A., Pupi, A., Biondi, F., & Faravelli, C. (1993). Brain perfusion abnormalities in drug-naive, lactate-sensitive panic patients: A SPECT study. *Biological Psychiatry*, *33*(7), 505-512. https://doi.org/10.1016/0006-3223(93)90004-W

Derogatis, L. R. (1994). SCL-90-R. Administration, Scoring, and Procedures Manual National Computer System, Minneapolis.

Devous, M. D. (2005). Single-photon emission computed tomography in neurotherapeutics. *NeuroRx*, *2*(2), 237-249. https://doi.org/10.1602/neurorx.2.2.237

Devous, M. D., Stokely, E. M., Chehabi, H. H., & Bonte, F. J. (1986). Normal distribution of regional cerebral blood flow measured by dynamic single-photon emission tomography. *Journal of Cerebral Blood Flow & Metabolism*, *6*(1), 95-104. https://doi.org/10.1038/jcbfm.1986.12

Di Martino, A., Scheres, A., Margulies, D. S., Kelly, A. M. C., Uddin, L. Q., Shehzad, Z., ... & Milham, M. P. (2008). Functional connectivity of human striatum: a resting-state FMRI study. *Cerebral Cortex, 18*(12), 2735-2747. https://doi.org/10.1093/cercor/bhn041

Dinno, A. (2009). Exploring the sensitivity of Horn's Parallel Analysis to the distributional form of random data. Multivariate Behavioral Research, *44*(3), 362–388. https://doi.org/10.1080/00273170902938969

Dickerson, B. C., & Sperling, R. A. (2005). Neuroimaging biomarkers for clinical trials of disease-modifying therapies in Alzheimer's disease. *NeuroRx*, *2*(2), 348-360. https://doi.org/10.1602/neurorx.2.2.348

Doucet, G. E., Lee, W. H., & Frangou, S. (2019). Evaluation of the spatial variability in the major resting-state networks across human brain functional atlases. *Human Brain Mapping, 40*(15), 4577-4587. https://doi.org/10.1002/hbm.24722

Duelli, R., & Kuschinsky, W. (2001). Brain glucose transporters: relationship to local energy demand. *Physiology*, *16*(2), 71-76. https://doi.org/10.1152/physiologyonline.2001.16.2.71

Eckert, T., & Eidelberg, D. (2005). Neuroimaging and therapeutics in movement disorders. *NeuroRx*, *2*(2), 361-371. https://doi.org/10.1602/neurorx.2.2.361

Efron, B., & Tibshirani, R. (1997). Improvements on cross-validation: The 632+ bootstrap method. *Journal of the American Statistical Association, 92*(438), 548-560. https://doi.org/10.1080/01621459.1997.10474007

Enders, Craig K. (2010). *Applied missing data analysis.* London, U.K.: The Guilford Press.

Eren, İ., Tükel, R., Polat, A., Karaman, R., & Ünal, S. (2003). Evaluation of regional cerebral blood flow changes in panic disorder with Tc99m-HMPAO SPECT. *Psychiatry Research: Neuroimaging*, *123*(2), 135-143. https://doi.org/10.1016/S0925-4927(03)00062-3

Fantini, S., Sassaroli, A., Tgavalekos, K. T., & Kornbluth, J. (2016). Cerebral blood flow and autoregulation: Current measurement techniques and prospects for noninvasive optical methods. *Neurophotonics*, *3*(3), 031411.

https://doi.org/10.1117/1.NPh.3.3.031411

Field, A. (2009). *Discovering statistics using SPSS, Third Edition.* London, U.K: SAGE Publications Ltd.

First, M. B., Spitzer, R. L., Gibbon, M., Williams, J. (1996). Structured Clinical Interview for DSM-IV Axis I Disorders (SCID-I). New York, N.Y.: Biometrics Research Department, New York State Psychiatric Institute.

Friston, K. J. (1994). Functional and effective connectivity in neuroimaging: A synthesis. *Human Brain Mapping*, *2*(1-2), 56-78. https://doi.org/10.1002/hbm.460020107

Friston, K. J., Frith, C. D., Liddle, P. F., & Frackowiak, R. S. J. (1991). Comparing functional (PET) images: the assessment of significant change. *Journal of Cerebral Blood Flow & Metabolism*, *11*(4), 690-699. https://doi.org/10.1038/jcbfm.1991.122

Fox, P. T., & Raichle, M. E. (1986). Focal physiological uncoupling of cerebral blood flow and oxidative metabolism during somatosensory stimulation in human subjects. *Proceedings of the National Academy of Sciences, 83*(4), 1140-1144. https://doi.org/10.1073/pnas.83.4.1140

Fox, M. D., Corbetta, M., Snyder, A. Z., Vincent, J. L., & Raichle, M. E. (2006). Spontaneous neuronal activity distinguishes human dorsal and ventral attention systems. *Proceedings of the National Academy of Sciences*, *103*(26), 10046-10051. https://doi.org/10.1073/pnas.0604187103

Grady, C. L., & Craik, F. I. (2000). Changes in memory processing with age. *Current Opinion in Neurobiology*, *10*(2), 224-231. https://doi.org/10.1016/S0959-

4388(00)00073-8

Graham, J. M., Guthrie, A. C., & Thompson, B. (2003). Consequences of not interpreting structure coefficients in published CFA research: A reminder. *Structural Equation Modeling, 10*(1), 142-153. https://doi.org/10.1207/S15328007SEM1001_7

Grahn, J. A., Parkinson, J. A., & Owen, A. M. (2008). The cognitive functions of the caudate nucleus. *Progress in Neurobiology, 86*(3), 141–155. https://doi.org/10.1016/j.pneurobio.2008.09.004

Greicius, M. D., Krasnow, B., Reiss, A. L., & Menon, V. (2003). Functional connectivity in the resting brain: A network analysis of the default mode hypothesis. *Proceedings of the National Academy of Sciences, 100*(1), 253-258. https://doi.org/10.1073/pnas.0135058100

Gonzalez-Castillo, J., Saad, Z. S., Handwerker, D. A., Inati, S. J., Brenowitz, N., & Bandettini, P. A. (2012). Whole-brain, time-locked activation with simple tasks revealed using massive averaging and model-free analysis. *Proceedings of the National Academy of Sciences, 109*(14), 5487-5492.

Gorsuch, R. L. (2015). *Factor analysis*. New York, NY: Routledge.

Gusnard, D. A., Akbudak, E., Shulman, G. L., & Raichle, M. E. (2001). Medial prefrontal cortex and self-referential mental activity: Relation to a default mode of brain function. *Proceedings of the National Academy of Sciences, 98*(7), 4259-4264. https://doi.org/10.1073/pnas.071043098

Gutchess, A. H., Welsh, R. C., Hedden, T., Bangert, A., Minear, M., Liu, L. L., & Park, D. C. (2005). Aging and the neural correlates of successful picture encoding: Frontal activations compensate for decreased medial-temporal activity. *Journal of*

Cognitive Neuroscience, *17*(1), 84-96. https://doi.org/10.1162/0898929052880048

Haines, D. E. (1995). *Neuroanatomy: An atlas of structures, sections and systems*. Baltimore: Williams & Wilkins.

Hair, J., Black, W., Babin, B., Anderson, R. and Tatham, R. (2006). *Multivariate data analysis, 6th Edition*. Upper Saddle River, NJ: Pearson-Prentice Hall.

Haldane, M., Cunningham, G., Androutsos, C., & Frangou, S. (2008). Structural brain correlates of response inhibition in bipolar disorder I. *Journal of Psychopharmacology, 22*(2), 138–143. https://doi.org/10.1177/0269881107082955

Harris, R. J. (2001). *A primer of multivariate statistics*. New York, NY: Psychology Press.

Harris, J. J., Jolivet, R., & Attwell, D. (2012). Synaptic energy use and supply. *Neuron*, *75*(5), 762-777. https://doi.org/10.1016/j.neuron.2012.08.019

Hermes, M., Hagemann, D., Britz, P., Lieser, S., Rock, J., Naumann, E., & Walter, C. (2007). Reproducibility of continuous arterial spin labeling perfusion MRI after 7 weeks. *Magnetic Resonance Materials in Physics, Biology and Medicine*, *20*(2), 103. https://doi.org/10.1007/s10334-007-0073-3

Horn, J. (1965) A rationale and test for the number of factors in factor analysis. *Psychometrika, 30*, 179-185. https://doi.org/10.1007/BF02289447

Hosford, P. S., & Gourine, A. V. (2019). What is the key mediator of the neurovascular coupling response? *Neuroscience & Biobehavioral Reviews*, *96*, 174-181. https://doi.org/10.1016/j.neubiorev.2018.11.011

Huettel, S. A., Song, A. W., & McCarthy, G. (2014). *Functional magnetic resonance imaging (vol. 3)*. Sunderland, Massachusetts: Sinauer Associates, Inc.

Jöreskog, K. G. (2003). Factor analysis by MINRES. To the memory of Harry Harman and Henry Kaiser. Retrieved from https://www.ssicentral.com/wp-content/uploads/2020/07/lis_minres.pdf

Jung, J. H., Choi, Y., Hong, K. J., Min, B. J., Choi, J. Y., Choe, Y. S., ... & Kim, B. T. (2009). Development of a dual modality imaging system: a combined gamma camera and optical imager. *Physics in Medicine & Biology*, *54*(14), 4547. https://doi.org/10.1088/0031-9155/54/14/011

Kaczkurkin, A. N., Moore, T. M., Calkins, M. E., Ciric, R., Detre, J. A., Elliott, M. A., ... & Satterthwaite, T. D. (2018). Common and dissociable regional cerebral blood flow differences associate with dimensions of psychopathology across categorical diagnoses. *Molecular Psychiatry*, *23*(10), 1981-1989. https://doi.org/10.1038/mp.2017.174

Kaczkurkin, A. N., Moore, T. M., Ruparel, K., Ciric, R., Calkins, M. E., Shinohara, R. T., ... & Satterthwaite, T. D. (2016). Elevated amygdala perfusion mediates developmental sex differences in trait anxiety. *Biological Psychiatry*, *80*(10), 775-785. https://doi.org/10.1016/j.biopsych.2016.04.021

Kaplan, D., Kim, J. S., & Kim, S. Y. (2009). Multilevel latent variable modeling: Current research and recent developments. *The Sage Handbook of Quantitative Methods in Psychology*, 592-612. https://dx.doi.org/10.4135/9780857020994.n24

Kennedy, K. M., & Raz, N. (2015). Normal aging of the brain. In A. W. Toga (Ed.), *Brain mapping: An encyclopedic reference, vol. 3* (pp. 603-617). Cambridge,

MA.: Academic Press.

Kety, S. S., & Schmidt, C. F. (1945). The determination of cerebral blood flow in man by the use of nitrous oxide in low concentrations. *American Journal of Physiology, 143,* 53-66. Obtained from http://ajplegacy.physiology.org/cgi/reprint/143/1/53.

Kiernan, J. A. (2012). Anatomy of the temporal lobe. *Epilepsy Research and Treatment*, *Volume 2012.* https://doi.org/10.1155/2012/176157

Kisler, K., Nelson, A. R., Montagne, A., & Zlokovic, B. V. (2017). Cerebral blood flow regulation and neurovascular dysfunction in Alzheimer disease. *Nature Reviews Neuroscience*, *18*(7), 419. doi:10.1038/nrn.2017.48

Knezevic, S. (1988). *Handbook of regional cerebral blood flow*. Hillsdale, N.J.: Psychology Press.

Kuzniecky, R. I. (2005). Neuroimaging of epilepsy: Therapeutic implications. *NeuroRx*, *2*(2), 384-393. https://doi.org/10.1602/neurorx.2.2.384

Lanciego, J. L., Luquin, N., & Obeso, J. A. (2012). Functional neuroanatomy of the basal ganglia. *Cold Spring Harbor Perspectives in Medicine, 2*(12), a009621. https://doi.org/10.1101/cshperspect.a009621

Lee, S. H., Choi, C. W., Kim, J. H., Rhee, C. H., & Lim, S. M. (1998). Increased uptake of 99mTc-HMPAO in necrotic brain tumors. *Journal of Korean Medical Science, 13*(5), 529–532. https://doi.org/10.3346/jkms.1998.13.5.529

Lee, B., & Newberg, A. (2005). Neuroimaging in traumatic brain imaging. *NeuroRx*, *2*(2), 372-383. https://doi.org/10.1602/neurorx.2.2.372

Leech, R., & Sharp, D. J. (2014). The role of the posterior cingulate cortex in cognition and disease. *Brain*, *137*(1), 12-32. https://doi.org/10.1093/brain/awt162

Leys, C., Klein, O., Dominicy, Y., & Ley, C. (2018). Detecting multivariate outliers: Use a robust variant of the Mahalanobis distance. *Journal of Experimental Social Psychology*, *74*, 150-156. http://dx.doi.org/10.1016/j.jesp.2017.09.011

Li, J., Yang, Y., Zhu, Y., Zhou, L., Han, Y., Yin, T., ... & Chen, J. (2018). Towards characterizing the regional cerebral perfusion in evaluating the severity of major depression disorder with SPECT/CT. *BMC Psychiatry*, *18*(1), 1-8. https://doi.org/10.1186/s12888-018-1654-6

Lindauer, R. J. L., Booij, J., Habraken, J., Van Meijel, E. P. M., Uylings, H. B. M., Olff, M., ... & Gersons, B. P. R. (2008). Effects of psychotherapy on regional cerebral blood flow during trauma imagery in patients with post-traumatic stress disorder: A randomized clinical trial. *Psychological Medicine*, *38*(4), 543. doi:10.1017/S0033291707001432

Lindauer, U., Megow, D., Matsuda, H., & Dirnagl, U. (1999). Nitric oxide: A modulator, but not a mediator, of neurovascular coupling in rat somatosensory cortex. *American Journal of Physiology-Heart and Circulatory Physiology*, *277*(2), H799-H811. https://doi.org/10.1152/ajpheart.1999.277.2.H799

Lindquist, M. A. (2008). The statistical analysis of fMRI data. *Statistical Science*, *23*(4), 439-464. https://doi.org/10.1214/09-STS282

Liu, F., Zhuo, C., & Yu, C. (2016). Altered cerebral blood flow covariance network in schizophrenia. *Frontiers in Neuroscience*, *10*, 308. https://doi.org/10.3389/fnins.2016.00308

Longden, T. A., Dabertrand, F., Koide, M., Gonzales, A. L., Tykocki, N. R., Brayden, J.

E., ... & Nelson, M. T. (2017). Capillary K+-sensing initiates retrograde hyperpolarization to increase local cerebral blood flow. *Nature Neuroscience*, *20*(5), 717-726. https://doi.org/10.1038/nn.4533

Lourenço, C. F., Ledo, A., Barbosa, R. M., & Laranjinha, J. (2017). Neurovascular-neuroenergetic coupling axis in the brain: Master regulation by nitric oxide and consequences in aging and neurodegeneration. *Free Radical Biology and Medicine*, *108*, 668-682. https://doi.org/10.1016/j.freeradbiomed.2017.04.026

Lourenço, C. F., Santos, R. M., Barbosa, R. M., Cadenas, E., Radi, R., & Laranjinha, J. (2014). Neurovascular coupling in hippocampus is mediated via diffusion by neuronal-derived nitric oxide. *Free Radical Biology and Medicine*, *73*, 421-429. https://doi.org/10.1016/j.freeradbiomed.2014.05.021

Luria, A. R. (1997). *The working brain: An introduction to neuropsychology*. London, U.K.: Basic Books.

Lusic, H., & Grinstaff, M. W. (2013). X-ray-computed tomography contrast agents. *Chemical Reviews*, *113*(3), 1641-1666. https://doi.org/10.1021/cr200358s

McAfee, S. S., Liu, Y., Sillitoe, R. V., & Heck, D. H. (2019). Cerebellar lobulus simplex and crus I differentially represent phase and phase difference of prefrontal cortical and hippocampal oscillations. *Cell Reports, 27*(8), 2328–2334.e3. https://doi.org/10.1016/j.celrep.2019.04.085

Magistretti, P. J., & Allaman, I. (2015). A cellular perspective on brain energy metabolism and functional imaging. *Neuron*, *86*(4), 883-901. https://doi.org/10.1016/j.neuron.2015.03.035

Mardia, K. V. (1970). Measures of multivariate skewness and kurtosis with applications.

Biometrika, 57(3), 519-530. https://doi.org/10.1093/biomet/57.3.519

Menon, V. (2015). Salience network. In A. W. Toga (Ed.), *Brain mapping: An encyclopedic reference, vol. 2* (pp. 597-611). Cambridge, MA.: Academic Press.

Molina, V., Gispert, J. D., Reig, S., Sanz, J., Pascau, J., Santos, A., ... & Desco, M. (2003). Cerebral metabolism and risperidone treatment in schizophrenia. *Schizophrenia Research*, *60*(1), 1-7. https://doi.org/10.1016/S0920-9964(02)00199-8

Molina, V., Tamayo, P., Montes, C., De Luxán, A., Martin, C., Rivas, N., ... & Domínguez-Gil, A. (2008). Clozapine may partially compensate for task-related brain perfusion abnormalities in risperidone-resistant schizophrenia patients. *Progress in Neuro-Psychopharmacology and Biological Psychiatry*, *32*(4), 948-954. https://doi.org/10.1016/j.pnpbp.2007.12.028

Müller-Vahl, K. R., Szejko, N., Wilke, F., Jakubovski, E., Geworski, L., Bengel, F., & Berding, G. (2019). Serotonin transporter binding is increased in Tourette syndrome with obsessive compulsive disorder. *Scientific Reports*, *9*(1), 1-10. https://doi.org/10.1038/s41598-018-37710-4

Nolte, J., & Angevine, J. B. (2007). *The human brain in photographs and diagrams*, *3rd edition*. Maryland Heights, MO.: Mosby.

O'Connor, B. P. (2000). SPSS and SAS programs for determining the number of components using parallel analysis and Velicer's MAP test. *Behavior Research Methods, Instruments, & Computers*, *32*(3), 396-402. https://doi.org/10.3758/BF03200807

Osborne, J. W. (2014). *Best practices in exploratory factor analysis*. Clearspace

Publishing. Retrieved from https://www.researchgate.net/publication/265248967

Østergaard, L., Engedal, T. S., Aamand, R., Mikkelsen, R., Iversen, N. K., Anzabi, M., ... & Rasmussen, M. (2014). Capillary transit time heterogeneity and flow-metabolism coupling after traumatic brain injury. *Journal of Cerebral Blood Flow & Metabolism*, *34*(10), 1585-1598. https://doi.org/10.1038/jcbfm.2014.131

Ota, M., Matsuo, J., Sato, N., Teraishi, T., Hori, H., Hattori, K., ... & Kunugi, H. (2018). Relationship between autistic spectrum trait and regional cerebral blood flow in healthy male subjects. *Psychiatry Investigation*, *15*(10), 956. https://doi.org/10.30773/pi.2018.07.27

O'Toole, A. J., Jiang, F., Abdi, H., Pénard, N., Dunlop, J. P., & Parent, M. A. (2007). Theoretical, statistical, and practical perspectives on pattern-based classification approaches to the analysis of functional neuroimaging data. *Journal of Cognitive Neuroscience, 19*(11), 1735-1752. https://doi.org/10.1162/jocn.2007.19.11.1735

Pagani, M., Salmaso, D., Jonsson, C., Hatherly, R., Jacobsson, H., Larsson, S. A., & Wägner, A. (2002). Regional cerebral blood flow as assessed by principal component analysis and 99m Tc-HMPAO SPET in healthy subjects at rest: Normal distribution and effect of age and gender. *European Journal of Nuclear Medicine and Molecular Imaging*, *29*(1), 67-75. https://doi.org/10.1007/s00259-001-0676-2

Payne, J. K., Trivedi, M. H., & Devous, M. D. (1996). Comparison of technetium-99m-HMPAO and xenon-133 measurements of regional cerebral blood flow by SPECT. *Journal of Nuclear Medicine*, *37*(10), 1735-1740. Retrieved from http://jnm.snmjournals.org/.

Pearson, R., Mundfrom, D., & Piccone, A. (2013). A comparison of ten methods for determining the number of factors in exploratory factor analysis. *Multiple Linear Regression Viewpoints, 39*(1), 1-15. Retrieved from http://www.glmj.org/archives/articles/Pearson_v39n1.pdf

Peterson, R.A. (2000). A meta-analysis of variance accounted for and factor loadings in exploratory factor analysis. *Marketing Letters, 11*, 261–275. https://doi.org/10.1023/A:1008191211004

Pian, K. L. H., van Megen, H. J., Ramsey, N. F., Mandl, R., den Boer, J. A., & Westenberg, H. G. (2005). Exacerbation of obsessive-compulsive symptoms increases blood flow in orbitofrontal cortex and putamen. In *The effects of serotonergic intervention on behavior and cerebral blood flow in obsessive-compulsive disorder* (pp. 67). The Hague, The Netherlands: University of Groningen.

Pison, G., Rousseeuw, P. J., Filzmoser, P., & Croux, C. (2003). Robust factor analysis. *Journal of Multivariate Analysis, 84*(1), 145-172. https://doi.org/10.1016/S0047-259X(02)00007-6

Delli Pizzi, S., Franciotti, R., Tartaro, A., Caulo, M., Thomas, A., Onofrj, M., & Bonanni, L. (2014). Structural alteration of the dorsal visual network in DLB patients with visual hallucinations: A cortical thickness MRI study. *PloS One, 9*(1), e86624. https://doi.org/10.1371/journal.pone.0086624

Prior, J.O. (2016). Imaging of brain perfusion. In: J. Hodler, R. Kubik-Huch, & G. von Schulthess (Eds.), *Diseases of the brain, head and neck, spine 2016-2019* (pp. 249-259). Zurich, Switzerland: Springer.

https://doi.org/10.1007/978-3-319-30081-8_28

Purves, D., Augustine, G.J., Fitzpatrick, D., Hall, W.C., Lamantia, A.S., McNamara, J.O., White, L.E. (2008). *Neuroscience, 4th edition.* Sunderland, MA: Sinauer Associates.

Rahmim, A., & Zaidi, H. (2008). PET versus SPECT: Strengths, limitations and challenges. *Nuclear Medicine Communications*, *29*(3), 193-207. https://doi.org/10.1097/MNM.0b013e3282f3a515

Raichle, M. E. (1998). Behind the scenes of functional brain imaging: A historical and physiological perspective. *Proceedings of the National Academy of Sciences*, *95*(3), 765-772. https://doi.org/10.1073/pnas.95.3.765

Raichle, M. E. (2001). Bold insights. *Nature*, *412*(6843), 128-130. https://doi.org/10.1038/35084300

Raichle, M. E. (2011). The restless brain. *Brain Connectivity, 1*(1), 3-12. https://doi.org/10.1089/brain.2011.0019

Raichle, M. E. (2015). The brain's default mode network. *Annual Review of Neuroscience*, *38*, 433-447. https://doi.org/10.1146/annurev-neuro-071013-014030

Raichle, M. E., MacLeod, A. M., Snyder, A. Z., Powers, W. J., Gusnard, D. A., & Shulman, G. L. (2001). A default mode of brain function. *Proceedings of the National Academy of Sciences, 98*(2), 676-682. https://doi.org/10.1073/pnas.98.2.676

Reuter-Lorenz, P. A. (2002). New visions of the aging mind and brain. *Trends in Cognitive Sciences*, *6*(9), 394-400.

https://doi.org/10.1016/S1364-6613(02)01957-5

Reuter-Lorenz, P. A., & Cappell, K. A. (2008). Neurocognitive aging and the compensation hypothesis. *Current Directions in Psychological Science, 17*(3), 177-182. https://doi.org/10.1111/j.1467-8721.2008.00570.x

Revelle, W. (2019). Scree plots of data or correlation matrix compared to random "parallel" matrices [Instruction set]. Retrieved from https://personality-project.org/r/psych/help/fa.parallel.html

Roberts, J. S., Vavilala, M. S., Schenkman, K. A., Shaw, D., Martin, L. D., & Lam, A. M. (2006). Cerebral hyperemia and impaired cerebral autoregulation associated with diabetic ketoacidosis in critically ill children. *Critical Care Medicine*, *34*(8), 2217-2223. https://doi.org/10.1097/01.ccm.0000227182.51591.21

Robinson, S., Basso, G., Soldati, N., Sailer, U., Jovicich, J., Bruzzone, L., ... & Moser, E. (2009). A resting-state network in the motor control circuit of the basal ganglia. *BMC Neuroscience, 10*(1), 1-14. https://doi.org/10.1186/1471-2202-10-137

Rousseeuw, P. J., & van Driessen, K. (1999). A fast algorithm for the minimum covariance determinant estimator. *Technometrics, 41*(3), 212-223. https://doi.org/10.2307/1270566

Sandrone, S., Bacigaluppi, M., Galloni, M. R., Cappa, S. F., Moro, A., Catani, M., ... & Martino, G. (2014). Weighing brain activity with the balance: Angelo Mosso's original manuscripts come to light. *Brain*, *137*(2), 621-633. https://doi.org/10.1093/brain/awt091

Schmitt, T. A. (2011). Current methodological considerations in exploratory and confirmatory factor analysis. *Journal of Psychoeducational Assessment*, *29*(4),

304-321. https://doi.org/10.1177/0734282911406653

Schwarz, G. (1978). Estimating the dimension of a model. *Annals of Statistics, 6*(2), 461-464. https://doi.org/10.1214/aos/1176344136

Seedat, S., Warwick, J., van Heerden, B., Hugo, C., Zungu-Dirwayi, N., Van Kradenburg, J., & Stein, D. J. (2004). Single photon emission computed tomography in posttraumatic stress disorder before and after treatment with a selective serotonin reuptake inhibitor. *Journal of Affective Disorders*, *80*(1), 45-53. https://doi.org/10.1016/S0165-0327(03)00047-8

Seeley, W. W., Menon, V., Schatzberg, A. F., Keller, J., Glover, G. H., Kenna, H., ... & Greicius, M. D. (2007). Dissociable intrinsic connectivity networks for salience processing and executive control. *Journal of Neuroscience*, *27*(9), 2349-2356. https://doi.org/10.1523/JNEUROSCI.5587-06.2007

Shannon, B. J., Raichle, M. E., Snyder, A. Z., Fair, D. A., Mills, K. L., Zhang, D., ... & Kiehl, K. A. (2011). Premotor functional connectivity predicts impulsivity in juvenile offenders. *Proceedings of the National Academy of Sciences, 108*(27), 11241-11245. https://doi.org/10.1073/pnas.1108241108

Shepherd, G. M. (1994). *Neurobiology*. New York, N.Y.: Oxford University Press.

Shi, Y., Thrippleton, M. J., Makin, S. D., Marshall, I., Geerlings, M. I., de Craen, A. J., ... & Wardlaw, J. M. (2016). Cerebral blood flow in small vessel disease: a systematic review and meta-analysis. *Journal of Cerebral Blood Flow & Metabolism*, *36*(10), 1653-1667. https://doi.org/10.1177/0271678X16662891

Shipp, S. (2017). The functional logic of corticostriatal connections. *Brain Structure & Function, 222*(2), 669–706. https://doi.org/10.1007/s00429-016-1250-9

Shirer, W. R., Ryali, S., Rykhlevskaia, E., Menon, V., & Greicius, M. D. (2012). Decoding subject-driven cognitive states with whole-brain connectivity patterns. *Cerebral Cortex, 22*, 158–165. https://doi.org/10.1093/cercor/bhr099

Silverstein, S. M., Berten, S., Olson, P., Paul, R., Williams, L. M., Cooper, N., & Gordon, E. (2007). Development and validation of a World-Wide-Web-based neurocognitive assessment battery: WebNeuro. *Behavior Research Methods*, *39*(4), 940-949. https://doi.org/10.3758/BF03192989

Small, B. J., Dixon, R. A., & McArdle, J. J. (2011). Tracking cognition–health changes from 55 to 95 years of age. *Journals of Gerontology Series B: Psychological Sciences and Social Sciences*, *66*(supplement 1), i153-i161. https://doi.org/10.1093/geronb/gbq093

Stevens, J. (2002). *Applied Multivariate Statistics for the Social Sciences (4th Edition*). Mahwah, NJ: Lawrence Erlbaum Associates.

Szabo, Z., Camargo, E. E., Sostre, S., Shafique, I., Sadzot, B., Links, J. M., ... & Wagner, H. N. (1992). Factor analysis of regional cerebral glucose metabolic rates in healthy men. *European Journal of Nuclear Medicine*, *19*(7), 469-475. https://doi.org/10.1007/BF00185851

Thompson, B. (2010). *Exploratory and confirmatory factor analysis: Understanding concepts and applications.* Washington, DC: American Psychological Association.

Tinsley, H. E., & Tinsley, D. J. (1987). Uses of factor analysis in counseling psychology research. *Journal of Counseling Psychology*, *34*(4), 414-424. https://doi.org/10.1037/0022-0167.34.4.414

Todorov, V., & Filzmoser, P. (2009). An Object-Oriented Framework for Robust Multivariate Analysis. *Journal of Statistical Software, 32*(3), 1 - 47. http://doi.org/10.18637/jss.v032.i03

Tomasi, D., & Volkow, N. D. (2012). Aging and functional brain networks. *Molecular Psychiatry*, *17*(5), 549-558. https://doi.org/10.1038/mp.2011.81

Tonkonogy, J., & Goodglass, H. (1981). Language function, foot of the third frontal gyrus, and Rolandic operculum. *Archives of Neurology*, *38*(8), 486-490. doi:10.1001/archneur.1981.00510080048005

Toth, P., Tarantini, S., Ashpole, N. M., Tucsek, Z., Milne, G. L., Valcarcel-Ares, N. M., ... & Ungvari, Z. (2015). IGF-1 deficiency impairs neurovascular coupling in mice: Implications for cerebromicrovascular aging. *Aging Cell*, *14*(6), 1034-1044. https://doi.org/10.1111/acel.12372

Traystman, R. J. (2004). The paper that completely altered our thinking about cerebral blood flow measurement. *Journal of Applied Physiology*, *97*(5), 1601-1602. https://doi.org/10.1152/classicessays.00023.2004

Van Audenhaege, K., Van Holen, R., Vandenberghe, S., Vanhove, C., Metzler, S. D., & Moore, S. C. (2015). Review of SPECT collimator selection, optimization, and fabrication for clinical and preclinical imaging. *Medical Physics*, *42*(8), 4796-813. https://doi.org/10.1118/1.4927061

Van Buuren, S., Brand, J. P., Groothuis-Oudshoorn, C. G., & Rubin, D. B. (2006). Fully conditional specification in multivariate imputation. *Journal of Statistical Computation and Simulation*, *76*(12), 1049-1064. https://doi.org/10.1080/10629360600810434

Van Der Linden, G., Van Heerden, B., Warwick, J., Wessels, C., Van Kradenburg, J., Zungu-Dirwayi, N., & Stein, D. J. (2000). Functional brain imaging and pharmacotherapy in social phobia: Single photon emission computed tomography before and after treatment with the selective serotonin reuptake inhibitor citalopram. *Progress in Neuro-Psychopharmacology and Biological Psychiatry*, *24*(3), 419-438. http://doi.org/10019.1/72143

van Dyck, C. H., Lin, C. H., Smith, E. O., Wisniewski, G., Cellar, J., Robinson, R., ... & Hoffer, P. B. (1996). Comparison of technetium-99m-HMPAO and technetium-99m-ECD cerebral SPECT images in Alzheimer's disease. *Journal of Nuclear Medicine*, *37*(11), 1749-1755. Retrieved from https://jnm.snmjournals.org/content/jnumed/37/11/1749.full.pdf

Van Heertum, R. L., Tikofsky, R. S., & Ichise, M. (2010). *Functional cerebral SPECT and PET imaging*. Philadelphia, PA: Lippincott Williams and Wilkins.

Velicer, W. F., Eaton, C. A., & Fava, J. L. (2000). Construct explication through factor or component analysis: A review and evaluation of alternative procedures for determining the number of factors or components. In R. Goffin & E. Helmes (Eds.), *Problems and solutions in human assessment.* Boston, MA: Springer. https://doi.org/10.1007/978-1-4615-4397-8_3

Venkat, P., Chopp, M., & Chen, J. (2016). New insights into coupling and uncoupling of cerebral blood flow and metabolism in the brain. *Croatian Medical Journal*, *57*(3), 223-228. https://doi.org/10.3325/cmj.2016.57.223

Wang, J., Yang, Y., Fan, L., Xu, J., Li, C., Liu, Y., ... & Jiang, T. (2015). Convergent functional architecture of the superior parietal lobule unraveled with multimodal

neuroimaging approaches. *Human Brain Mapping*, *36*(1), 238-257. https://doi.org/10.1002/hbm.22626

Warwick, J. M. (2004). Imaging of brain function using SPECT. *Metabolic Brain Disease*, *19*(1), 113-123. https://doi.org/10.1023/B:MEBR.0000027422.48744.a3

Wen, S. L., Cheng, M. H., Cheng, M. F., Yue, J. H., & Wang, H. (2013). Pharmacotherapy response and regional cerebral blood flow characteristics in patients with obsessive-compulsive disorder. *Behavioral and Brain Functions, 9*(1), 1-8. https://doi.org/10.1186/1744-9081-9-31

Wen-han, Y., Jin, J., Li-juan, X. I. U., Mu-hua, C., Xin, W., Peng, B., & Qing-xiong, W. (2011). Regional cerebral blood flow in children with autism spectrum disorders: A quantitative 99mTc-ECD brain SPECT study with statistical parametric mapping evaluation. *Chinese Medical Journal*, *124*(9), 1362-1366. https://doi.org/10.3760/cma.j.issn.0366-6999.2011.09.017

Whitfield-Gabrieli, S., & Ford, J. M. (2012). Default mode network activity and connectivity in psychopathology. *Annual Review of Clinical Psychology*, *8*, 49-76. https://doi.org/10.1146/annurev-clinpsy-032511-143049

Yamanaka, M., Otomi, Y., Terazawa, K., Ryota, B., Otsuka, H., & Harada, M. (2018). To compare diagnostic ability of thallium-201 SPECT for brain tumor between quantitative evaluation, semi-quantitative evaluation and ADC values upon MRI. *Journal of Nuclear Medicine*, *59*(supplement 1), 1434. Retrieved from https://jnm.snmjournals.org/content/59/supplement_1/1434.short

Yeo, B. T., Krienen, F. M., Sepulcre, J., Sabuncu, M. R., Lashkari, D., Hollinshead, M., ... & Buckner, R. L. (2011). The organization of the human cerebral cortex

estimated by intrinsic functional connectivity. *Journal of Neurophysiology*. https://doi.org/10.1152/jn.00338.2011

Zhang, D., & Raichle, M. E. (2010). Disease and the brain's dark energy. *Nature Reviews Neurology*, *6*(1), 15-28. https://doi.org/10.1038/nrneurol.2009.198

Zhang, R., Zhang, L., Wei, S., Wang, P., Jiang, X., Tang, Y., & Wang, F. (2021). Increased amygdala-paracentral lobule/precuneus functional connectivity associated with patients with mood disorder and suicidal behavior. *Frontiers in Human Neuroscience, 14*, 585664. https://doi.org/10.3389/fnhum.2020.585664

Zhang, S., & Chiang-shan, R. L. (2012). Functional connectivity mapping of the human precuneus by resting-state fMRI. *Neuroimage, 59*(4), 3548-3562. https://doi.org/10.1016/j.neuroimage.2011.11.023

Zhang, Y. Y. (2013). *An Object-Oriented Solution for Robust Factor Analysis* (Natural Science Foundation Project of CQ CSTC CSTC2011BB0058). Chongqing, China: Chongqing University. Retrieved from https://cran.r-project.org/web/packages/robustfa/vignettes/robustfa.pdf

Zygmont, C., & Smith, M. R. (2014). Robust factor analysis in the presence of normality violations, missing data, and outliers: Empirical questions and possible solutions. *The Quantitative Methods for Psychology, 10*, 1, 40-55. https://doi.org/10.20982/tqmp.10.1.p040